論文 / 著書情報
Article / Book Information

題目(和文)	
Title(English)	Elucidation of Dehydration and Rehydration Mechanisms of Pharmaceutical Hydrates by Activation Energy Analysis
著者(和文)	高橋美知子
Author(English)	Michiko Takahashi
出典(和文)	学位:博士(理学), 学位授与機関:東京工業大学, 報告番号:甲第12142号, 授与年月日:2021年12月31日, 学位の種別:課程博士, 審査員:植草 秀裕,江口 正,岡田 哲男,小松 隆之,河野 正規
Citation(English)	Degree:Doctor (Science), Conferring organization: Tokyo Institute of Technology, Report number:甲第12142号, Conferred date:2021/12/31, Degree Type:Course doctor, Examiner:,,,,
学位種別(和文)	博士論文
Type(English)	Doctoral Thesis

2019 Doctoral Dissertation

Elucidation of Dehydration and Rehydration Mechanisms of Pharmaceutical Hydrates by Activation Energy Analysis

Michiko Takahashi

Department of Chemistry, Tokyo Institute of Technology

Copyrights notification

Acknowledgement

I would like to express my sincere thanks to Associate professor Hidehiro Uekusa to adopt the research themes I wanted to work on for many years and express my appreciate for his constructive guidance and helpful discussion throughout the course of this study.

I would like to offer my special thanks to Dr. Akiko Sekine for her generous support and encouragements throughout my university life.

I gratefully acknowledge past and present members of the Uekusa's laboratory for their support and useful comments.

I appreciate Dr. Masaki Tsushima for cooperation in helping me to study in doctoral degree program and thank for Ms. Akiko Gyobu for her hearted support.

Finally, I give a huge thanks to my husband and son for their affectionate encouragement.

January 2020

Michiko Takahashi

Contents

1. General Introduction

In stoichiometric hydrates, the water molecule in a crystalline compound is considerably more constrained compared with water or aqueous solutions. Hydrates are molecular complexes that incorporate water molecules usually stoichiometrically in their crystals.[1] It is not known if any of water contents is water of constitution until hydrate crystal structure has been determined.[2]

Hydrate crystal is a pharmaceutically novel type of crystal form since one-third of drug substances are developed as pharmaceutical hydrates (**Figure 1-1**).[3]

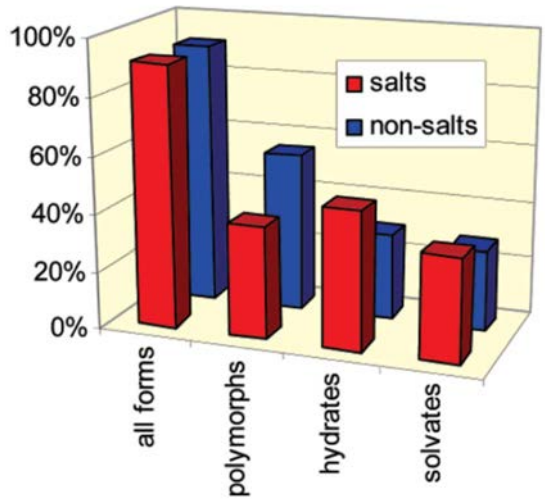

Figure 1-1Comparison of the propensity of salts and non-salts to occur in different solid forms.[3]

It is essential to investigate the thermal behavior of hydrate crystals in order to ensure the stability of the drug substance and drug product in the development process. When hydrate is selected as a drug substance form, the pathway between hydrate and anhydrate concerning temperature/humidity must be found out because of the risk of dehydration and phase transition in the pulverizing, granulating and tableting processes which should be excluded. Mostly, the water molecule accommodation in the host structure alters pharmaceutical properties such as solubility and stability,[4-6] and those in turn affect blood concentrations. As

a result of comparing the dissolution curves of tablets containing dihydrate and tetrahydrate of berberine chloride, a clear difference was observed in the dissolution rate of both hydrate tablets (**Figure 1-2**).[7]

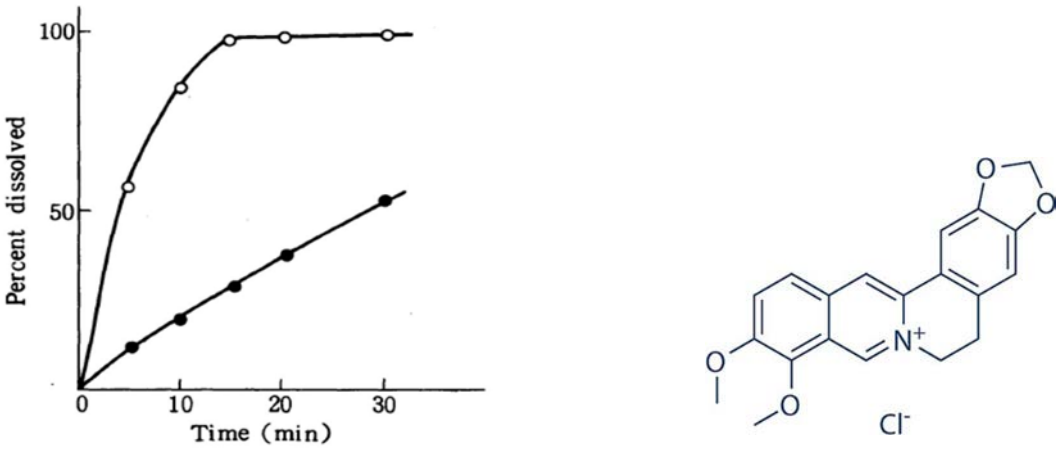

Figure 1-2 Dissolution curves of berberine chloride from tablet containing dihydrate (closed circle) and tetrahydrate (open circle) in water at 37℃, and chemical structure of berberine chloride. [7]

The example of tetracycline in which the solubility influences the blood concentration is shown in **Figure 1-3**. The administration of dihydrate gave higher plasma levels than those after the administration of trihydrate during actual absorption studies and the differences in the bioavailability are thought to be due to the differences in solubility of the two forms in aqueous solutions. This result indicates that dihydrate of tetracycline is more efficiently absorbed than trihydrate.[8]

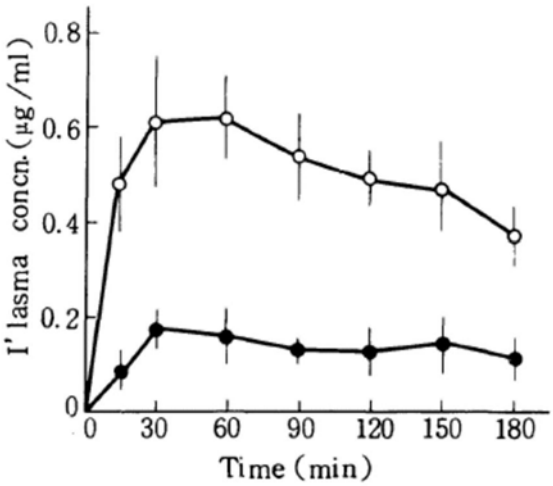

Figure 1-3 Plasma levels after intraduodenal administration of trihydrate (closed circle) and dihydrate (open circle) of tetracycline to rabbits.[8]

It has also been reported that there is a difference in absorption in the body between anhydrides and trihydrates with ampicillin.[9,10]

The crystal form of drug substance is the first issue to be decided in drug development. It is well known that the most crucial step in the drug substance manufacturing process is the final crystallization step in order to obtain the proper crystalline form. Especially for a hydrate form, stability strongly depends on the water molecule accommodation in the crystal lattice. Also, once a final crystal form has been selected as a hydrate, there remains the risk of phase transitions, which could be triggered by exposure to air in the manufacturing process of drug substance. For instance, if the drug substance is too dried, the undesired crystalline form such as anhydrate might be obtained in the industrial production. Limited vacuum drying methods may be used to prevent over drying and dehydration by controlling at constant pressure such as 430 mmHg on samples for a period of time.[11]

Even if the desired hydrate form is obtained for a drug substance in the final crystallization step, it may convert to another form in a subsequent formulation step to make drug products. The wet granulation method is a first choice and frequently used for oral drug production, because it is easy to mix uniformly with additives and to obtain higher content uniformity of the drug product. If wet granulation is not available for any reason, dry granulation[12] method is the second

choice. In a wet granulation process, water content, temperature, wet massing time, and drying conditions affect the degree of drug transformation. The transformation from the non-solvated form (anhydrate) to the amorphous and hemihydrate form of compound A was occurred in the granulation process including pre-blend, water addition and wet massing (**Figure 1-4)**.[13]

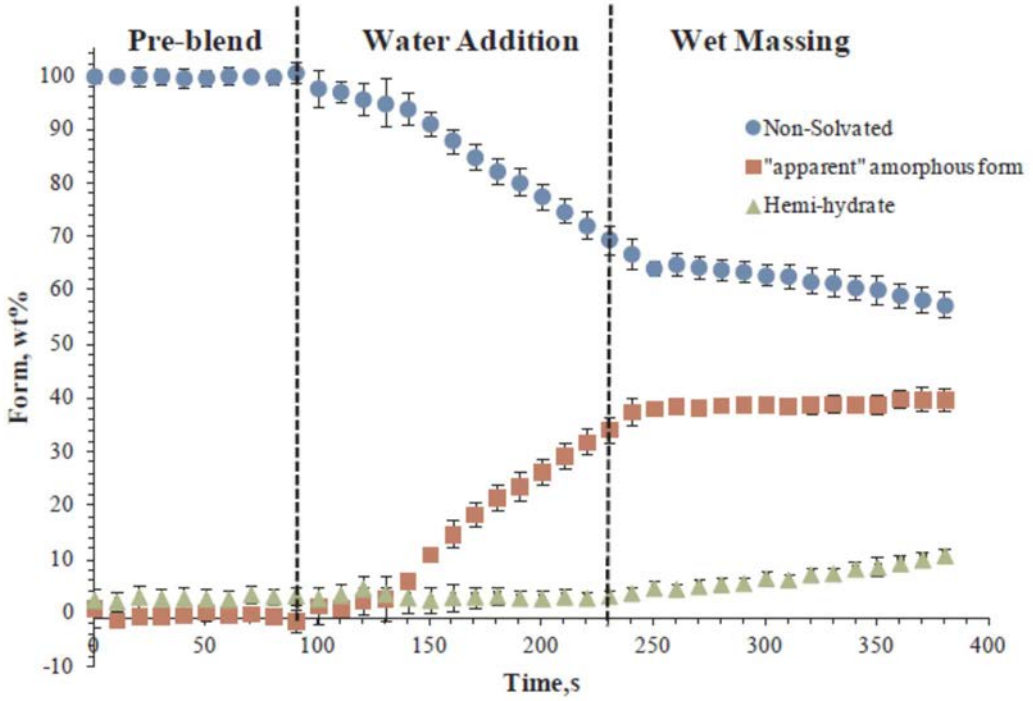

Figure 1-4 Transformation profile of compound A in the granulation process.[13]

Specifically, adding an aqueous solution of binder into active pharmaceutical ingredient induces hydration. The hydration of theophylline induced in wet granulation process affected solid state stability.[14] On the contrary, the drying process using hot air induces dehydration. Drying is one of the fundamental processes involved in a wet granulation process. In direct type tray-drier, the heated air is circulated by a fan. There must be a constant temperature and air flow over the granules being dried. The drying process was evaluated by monitoring temperature and moisture content of granules.[15] In these cases, it is also necessary to investigate whether the anhydride form can return to its initial hydrate form. Various diluents have been investigated to reduce incidence of cracking on tablet. Talc was shown to enhance the ability of the films to relax and this was related to the lower incidence of tablet film.[16] However, when the anhydrate formed by

dehydration in the drying process reverts to a hydrate form by moisture absorption, volume expansion of tablet may cause cracks on the surface during storage, which leads to the claims at medical facilities. Since the drying process of drug substance and formulation process are closely related to phase transformation, investigating dehydration and rehydration is demanded to supply stable medicine.

A schematic diagram composed of development of hydrates and factors of phase transformation for pharmaceutical tablets was shown in **Figure 1-5**. Actually, in each process of manufacturing, formulation, and market release of the drug, there is a possibility that the phase transformation due to dehydration and rehydration may occur due to the environmental change, and it is extremely important to quantitatively evaluate the easiness of crystal water removal and rehydration in order to prevent this risk.

There are two main reasons for the need to know the stability of hydrates. One is that solubility and bioavailability differ depending on the crystal form like hydrate and anhydrate, as described above. The other is that chemically unstable crystal forms may produce new degradation products with a risk of toxicity. Traditionally, the content of impurities in drugs has been limited by impurity safety thresholds in accordance with “International Council for Harmonisation of Technical Requirements for Pharmaceuticals for Human Use (ICH) guidelines”. However, new guidelines recently enacted requirement that the threshold should be reduced to one thousandth in order to reduce impurities with risk of toxicity. This allowable amount is so small that it cannot be quantified by a frequently used high performance liquid chromatography. From the above, it is clear how important it is in drug development to avoid the risk of phase transformation.

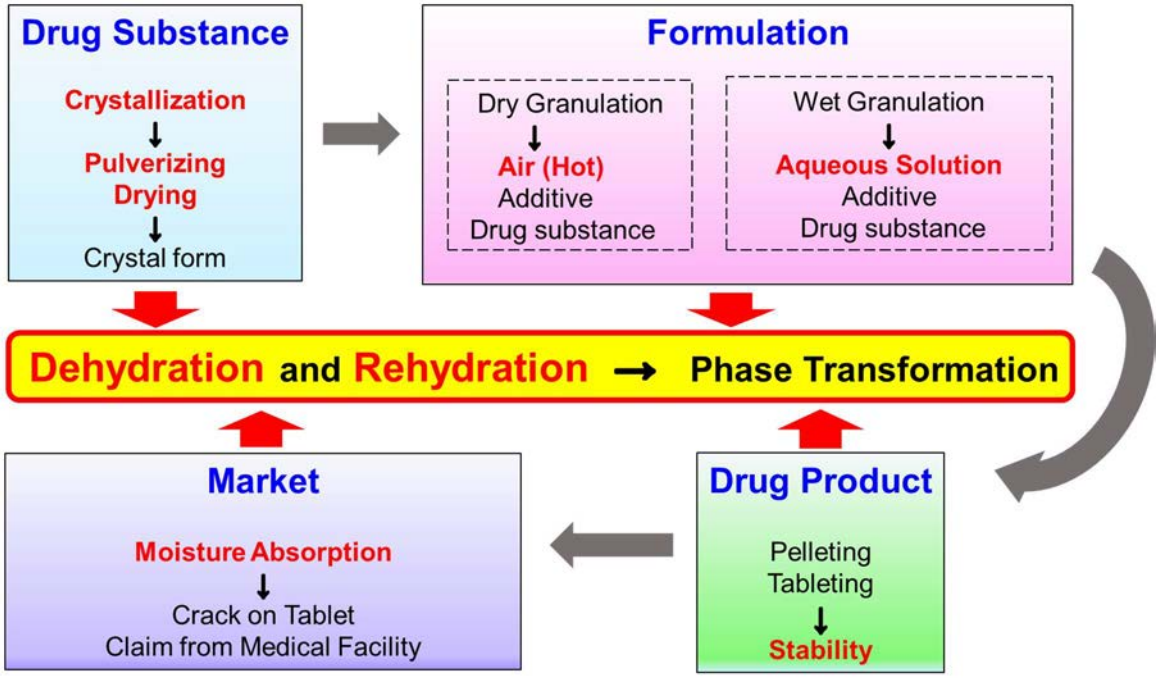

Figure 1-5 A schematic diagram composed of development of hydrates and factors of phase transformation for pharmaceutical tablets.

Drugs are broadly divided into original drugs and generic drugs. The development of an original drug generally takes as long as 10 to 20 years, and even if a new active pharmaceutical ingredient (API) is discovered, the development is often interrupted because the drug does not work well in the human body or is too toxic at the stage of development. On the other hand, the development process of generic drugs is quite different from that of original drugs. That development period is as short as 3 to 4 years, because API whose efficacy and safety have already been confirmed are used. In order to develop both original and generic drug, elucidation of dehydration and rehydration mechanisms that influences phase transformation is urgently required at an early stage in order to bring pharmaceuticals to the market quickly. It is also necessary to make short-term predictions of hydrate stability data that require a long period of time in a conventional manner.

At present, the conventional method used to predict the possibility of dehydration is the dehydration temperature. Actual dehydration ease cannot be evaluated only by dehydration temperature, which hardly reflected the features of water molecules accommodation in crystal structure sufficiently. Therefore, we need to find a suitable parameter which indicates how tightly the water molecule

is bound to host molecules in the crystal lattice. Such parameter allows us to predict actual propensities of dehydration and rehydration transition in the manufacturing process, and also to classify the crystals by the parameters. However, the dehydration process is complicated because of great diversity in the strength of intermolecular interactions, and in the number of water molecules in their crystal. To the best of our knowledge, for these reasons, there has not been systematic research to compare hydrate crystals based on the binding force between crystal water and host molecules. Therefore, the classification rule of hydrates using specific comparison parameters has not been reported.

To quantitatively evaluate the ease of dehydration and rehydration, we investigated whether activation energies (E_a) could be used. A schematic diagram of phase transition and potential energy between hydrate and anhydrate was shown in **Figure 1-6**. Since the activation energy corresponds to the energy required to excite the starting material of the reaction from the ground state to the transition state, it has been used in various fields. In this study, activation energy was applied as the physical property values indicating the magnitude of the energy barriers of dehydration and rehydration.

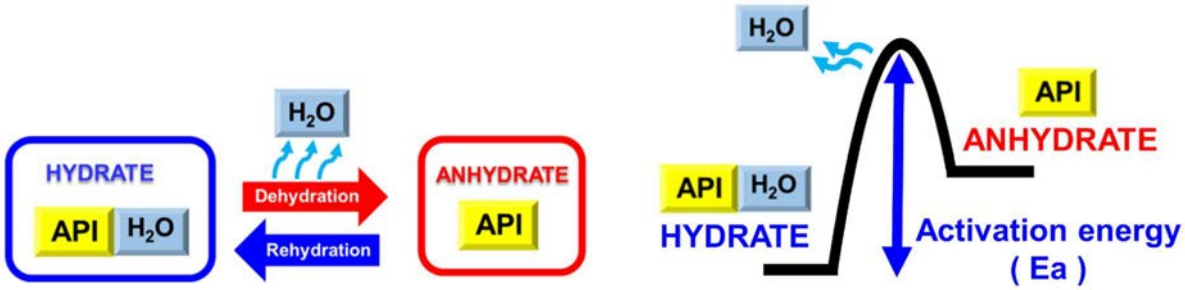

Figure 1-6 A schematic diagram of the relationship between hydrate and anhydrate through dehydration and rehydration processes (left side) and potential energy (right side). API indicates active pharmaceutical ingredient.

In the first of this study, for the purpose of establishing the evaluation system, the E_a measurement method which does not depend on the model by the noniso-thermal method instead of the conventional method was examined focuses on quantitative evaluation using of E_a. Further, the dependence of the noniso-thermal method measurement on the particle states including particle size and particle aggregation and the sample history were examined.

In the second of this study, the phase transition behavior of eleven kinds of pharmaceutical hydrates was investigated. After that, we set out to classify eleven pharmaceutical hydrate crystals by using dehydration E_a as well as rehydration propensities as comparison parameters. The former was evaluated through non-isothermal analyses performed by differential scanning calorimetry, and the latter was investigated through dehydration-hydration cycling test under controlled humidity condition. Also, rehydration E_a was also estimated as another parameter of classification to evaluate the ability to revert to its initial hydrate form through isothermal analyses performed by dynamic vapor sorption.

As pharmaceutical hydrates, solid-state of antibacterial agents, spectinomycin dihydrochloride, meropenem, acrinol, pipemidic acid, enoxacin, amoxicillin, nitrofurantoin, piperacillin, cefminox sodium, and β-lactamase inhibitor tazobactam were used for the classification of hydrates in this study.

In the third of this study, for hydrate crystals of unknown crystal structure, single crystal X-ray structure analysis revealed the packing of water in the crystals, then the relation between this classification and the features of the crystal structure was also examined. Furthermore, the dehydration E_a estimated in this study were compared to dehydration temperatures with the crystal packing of the corresponding hydrates, and the usefulness of classification by activation energy was examined.

2. Establishment of Evaluation Method of Dehydration Activation Energy

2.1. Introduction

Activation energy (E_a) is one of the most essential kinetic parameter, and thermal analysis is a very useful tool for investigating the kinetics of dehydration process. Two methods, namely iso-thermal and noniso-thermal methods, are applied for thermal analysis.[17] Generally, an iso-thermal measurement takes longer than a noniso-thermal measurement. An isothermal method has been conventionally used, because iso-thermal experiment data can be interpreted by Johnson-Mehl-Avrami equation.[18] In order to measure the dehydration E_a of hydrates by iso-thermal method, it is necessary to calculate the energy by fitting the weight change to an arbitrary model equation for each crystal. Furthermore, there is a possibility that the calculated energy cannot be used for comparison between a plurality of crystals owing to different model equation and different dehydration temperature of each crystal, and the stability of the sample is influenced by the necessity of measurement for a long time. On the other hand, a noniso-thermal measurement is rather simple and quick. Therefore, the application of the noniso-thermal method to calculate E_a from the endothermic peak temperature of differential scanning calorimetry was examined. The Kissinger equation utilizes a model-independent relationship in which the logarithm of the ratio between the heating rate and the square of the temperature at the maximum of the endothermic peak is proportional to the reciprocal of the temperature.[19] This equation is derived with the assumption that the reaction rate, here dehydration rate is maximum at the temperature at which the endothermic peak reaches a maximum.[20]

The magnitude of the rate constant, k, is determined by the temperature and is given by the Arrhenius equation

$$k = A\exp(-E_a/RT)$$

where R is the gas constant, T is the Kelvin temperature, A is the frequency factor, and E_a is the activation energy. According to Kissinger, the following equation of the same type as Arrhenius equation holds when the reaction consisted of a single elementary reaction

$$dx/dt = A(1-x) \cdot \exp(-E_a/RT)$$

$$dx/dt = A\exp(-E_a/RT) - A\ x\exp(-E_a/RT) \qquad (1)$$

x is the fraction of material decomposed. In this study, dx/dt corresponds to the dehydration rate constant. When both sides of this equation are differentiated with t the following equation is obtained.

$$d/dt(dx/dt) = A(E_a/RT^2)\exp(-E_a/RT)dT/dt - A\exp(-E_a/RT)dx/dt - Ax(E_a/RT^2)\exp(-E_a/RT)dT/dt$$

The following equation is derived by summarizing common terms and from equation (1).

$$d/dt(dx/dt) = dx/dt\{E_a/RT^2 \cdot dT/dt - A\exp(-E_a/RT)\}$$

Here, the reaction rate is maximized when the right side of the equation is 0, and when the temperature at that time is T_m, defined by

$$E_a/RT_m^2 \cdot dT/dt = A\exp(-E_a/RT_m)$$

When the heating rate component is input by substituting $\varphi = dT/dt$,

$$E_a\varphi/RT_m^2 = A\exp(-E_a/RT_m)$$

Taking its natural logarithm,

$$\ln E_a/R + \ln\varphi/T_m^2 = \ln A - E_a/RT_m$$

When differentiated with $1/T_m$,

$$d \ln(\varphi/T_m^2) /d(1/T_m) = - E_a/R$$

This is the Kissinger equation and it is the same type equation as the Arrhenius equation containing the heating rate components. In other words, when the ratio between the heating rate and the square of the temperature is plotted on the logarithmic axis and the reciprocal of the temperature is plotted on the horizontal axis, a linear relationship is established, and the activation energy is obtained from the slope of this straight line.

It has long been known that the particle size and crystal form[21] of the drug substance used in solid pharmaceutical preparations affect the dissolution rate, bioavailability, and stability.[22] In the case of poorly soluble drugs, a significant effect of particle size is often observed and is particularly important. Because the particle size can have major impact on the dissolution of poorly soluble drugs and thus the clinical performance.[23,24] The plasma profiles obtained after dosing showed that dosing of smaller particles led to faster uptake of solute than after dosing of larger particles.[23] It strongly indicates that the rate of dissolution is the rate limiting step to absorption, because of the difference in specific surface area. When the methods of dissolution and particles size are set in the specification for of drug substance, ensuring suitable clinical performance is often required. The simulations were performed using a certain drug substance batch with a particle size distribution at the limit of the proposed specification for particle size. Such a batch is anticipated to be bioequivalent to clinical reference, demonstrating that the proposal specification limits for particle size distribution would give products bioequivalent to the pivotal clinical batches.[25] Uncontrolled drug particle size distribution may show a significant variation, side effect during clinical development.[26]

Thus, the relationship between the API and the particle diameter is close. The particle size not only influences the solubility and the absorption of the drug, but also influences the thermal behavior. As an influencing factor used for the thermal measurement, the possibility that the particle size of the sample crystal influences

the dehydration E_a has been pointed out in the past. Tendency toward lower activation energy with decreasing particle size for dehydration of theophylline monohydrate was reported (**Table 2-1**).[27]

Table 2-1 The relationship between particle size and dehydration activation energy of theophylline monohydrate, and chemical structure of theophylline.[27]

Particle size (μm)	<150	<500	Intact	
Dehydration activation energy (kJ/mol)	73.2	75.7	76.3	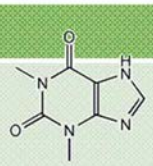

In another literature, the dehydration E_a of hemihydrate of 4-hydroxynicotinic acid changed from 90.5 kJ/mol to 111.7 kJ/mol with the increase of the particles size range from 177 μm to >707 μm (**Table 2-2**).[28]

Table 2-2 The relationship between particle size and dehydration activation energy of hemihydrate of 4-hydroxynicotinic acid, and chemical structure of 4-hydroxynicotinic acid.[28]

Particle size (μm)	177-250	250-354	>707	
Dehydration activation energy (kJ/mol)	90.5	97.1	111.7	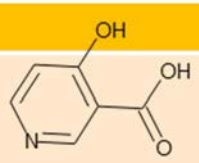

In the case of mildronate dihydrate, the dehydration E_a was 75±3 kJ/mol for particles with a diameter below 350 μm but it decreased for lager particles (**Figure 2-1**). Not only E_a but also the kinetic model differed depending on the particle size.[29]

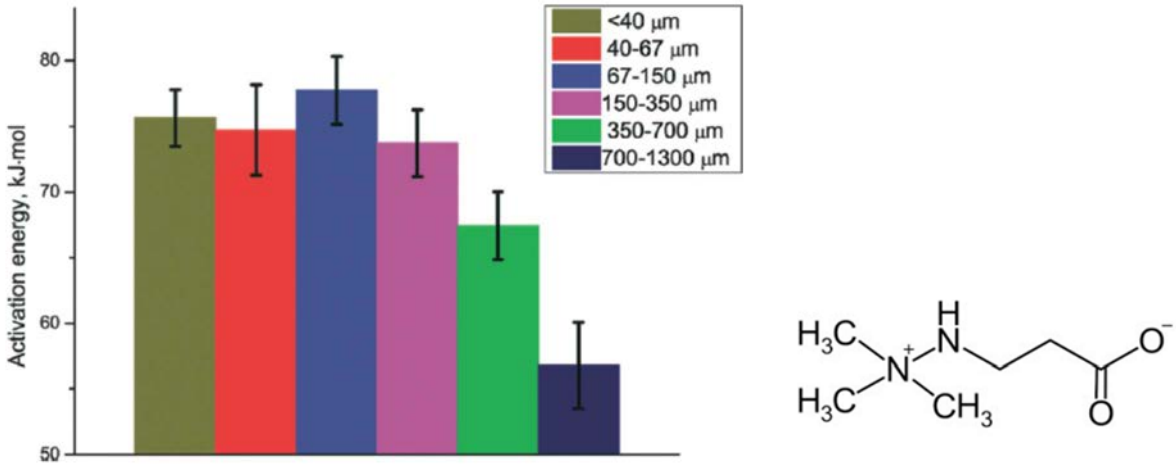

Figure 2-1 Dehydration activation energy for different fraction of mildronate dihydrate and chemical structure of mildronate.[29]

In order to establish the method of dehydration E_a, it was considered necessary to specify factors that may affect E_a such as the sample aggregation and the pulverization method in addition to the particle size. A grinding process often affects particle size of drug substance and phase transformation. Cefalexin has monohydrate form and this form decreased with increasing grinding time; after 10 min it was about 20%, and after 2h it was 0%, that was, monohydrate form had been converted to a completely amorphous phase (**Figure 2-2**).[30]

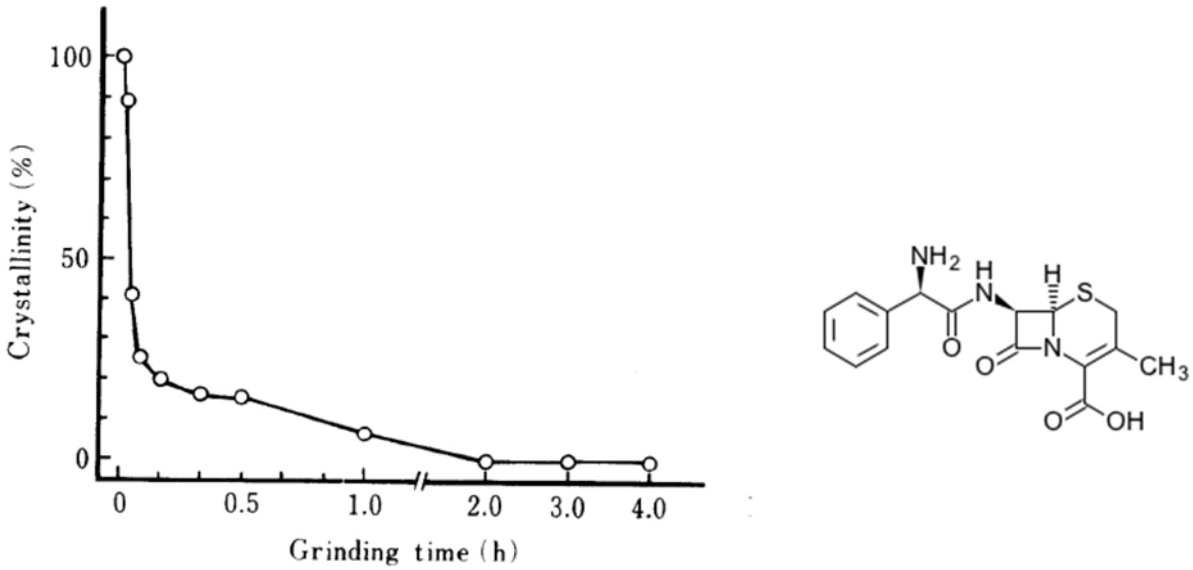

Figure 2-2 Effect of grinding on crystallinity of cefalexin monohydrate and chemical structure of cefalexin.[30]

The milling process also affects to physico-chemical properties of sample. Maillard reaction between metoclopramide hydrochloride and lactose increased with milling time owing to increasing surface area and creation of defects.[31]

Furthermore, the excessive pulverizing can also cause secondary agglomeration of particles in the manufacturing process. Therefore, not only the size of each particle but also the influence of the aggregation of the particles on the pharmaceutical hydrates becomes important in the pharmaceutical production. Because drug particle properties are critical for the therapeutic efficiency of a drug delivery system.[32] Particle size and agglomeration also affect thermal behavior.

Effective thermal conductivity in the field of polymeric materials, including epoxy resins, has been investigated for the case where the particle diameters are uniformly randomly dispersed.[33] Studies on the effect on the effective thermal conductivity of polymeric materials have shown that particle sizes of several micrometers or more are not affected by thermal conductivity.[34-36] However, if the particle size forms a powder region by aggregation, the thermal conductivity increases as the particle size decreases.[37] This is considered to be because in the case of the powder region, the particles tend to agglomerate, the continuous body of the particles tends to form, and the dispersion state tends to change, so that the thermal conductivity increases. It is considered that the difference in the dispersion state formed by the particle aggregation affects the thermal conductivity. Conversely, in the case of high crystalline graphite, which is required to have high thermal conductivity in the field of electronic equipment, a compressed powder of graphite powder pulverized by using a jet mill is produced, and the thermal conductivity is evaluated. The thermal conductivity is improved as the particle diameter is increased. When performing thermal analysis, it is necessary to consider thermal conductivity due to particle size and its aggregation, because they may affect the amount of dehydration E_a.

It is also important to evaluate the particle size accurately as part of the investigation of the effect on E_a. There are many different types of instruments used for measuring particle size distribution, sieving analysis, image analysis and laser diffraction. Laser diffraction has been widely accepted as one of powder size distribution techniques, used to estimate properties of the entire ensemble and not individual particles.[38-40] Particle size distribution measurement utilizes the fact that the intensity pattern of diffracted and scattered light when a laser beam is applied to particles suspended in a dispersion medium depends on the size of the

particles. Particles are translocated through a diffracted light beam in a flowing stream of liquid or air, former is wet and latter is dry dispersion style.

As an examination of the dependence of the particle state on E_a, the history of the sample should not be forgotten. When a drug substance as hydrate crystal is produced, the drying process is selected to be a limited vacuum drying or a ventilation drying. The former is a mechanism for controlling the degree of decompression by opening the leak valve for a short time when the vacuum is likely to be higher than a predetermined pressure, and the latter is a mechanism for drying by flowing a gas whose humidity is controlled. If it is not a suitable drying condition for the hydrate form, the desired water content cannot be incorporated in the crystal and the dehydration or rehydration will be repeated unexpectedly to obtain desired hydrate phase. Therefore, the effect of dehydration history on E_a was also investigated and untreated samples were used if not specifically noted to distinguish them from historical samples.

The aim of this study was to investigate a noniso-thermal model-independent method for measuring E_a instead of the conventional method; isothermal method. Moreover, the effect of sample aggregation, particle size and repeated dehydration process on the magnitude of dehydration E_a were determined to establish the noniso-thermal method of dehydration E_a. Because, to my knowledge, there was no report of the effect of aggregation and dehydration history on E_a, and this study was considered important to estimate E_a accurately.

2.2. Experimental

2.2.1. Materials

Spectinomycin dihydrochloride (SPE) pentahydrate, meropenem (MEPM) trihydrate, cefminox sodium (CEF) heptahydrate, tazobactam (TAZ) hemihydrate were used without any further purification and **Figure 2-3** shows their chemical structures. CEF heptahydrate, TAZ hemihydrate were provided by Meiji Seika Pharma Co., Ltd.

Separately, MEPM trihydrate was sieved, and four range of particle fractions (less than 75 μm, 75-125 μm, 125-212 μm and more than 212 μm) were obtained. Since the intact sample of CEF heptahydrate had large crystals of 100 μm, the powder sample of particle size of less than 50 μm by sieving, the ground sample by grinding in a mortar for 30 seconds, and fine sample by pulverization for 30 seconds were prepared. Labo Milser LN-Plus (Osaka chemical) was used for pulverization.

The purities of the hydrate samples before and after evaluation the activation energies were measured by high performance liquid chromatography or gas chromatography, and it was confirmed that the residual ratio with respect to intact sample was 95% or more.

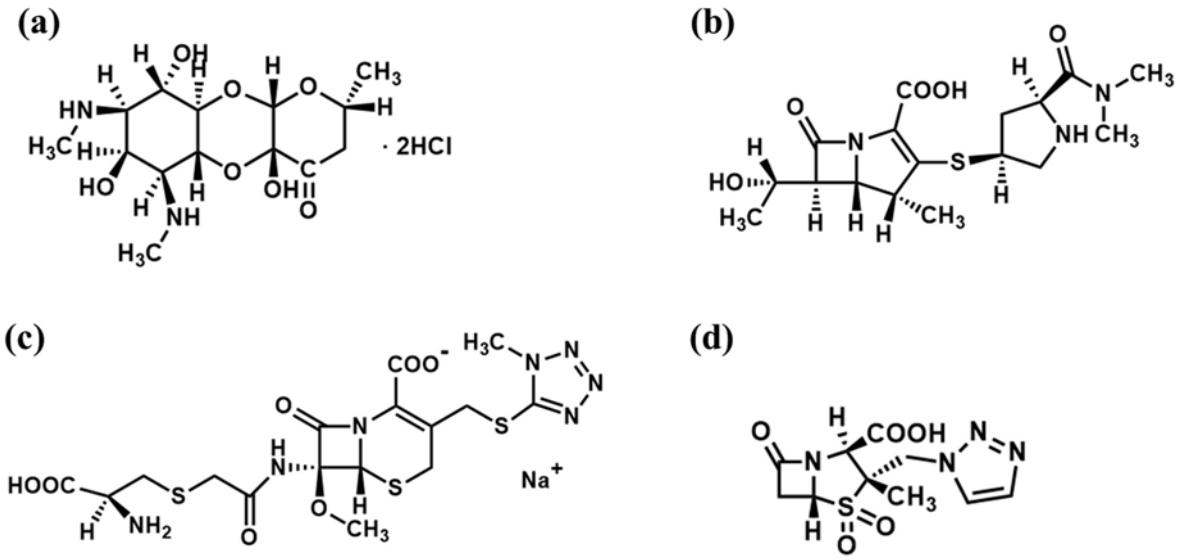

Figure 2-3 Chemical structure: (a) Spectinomycin dihydrochloride (SPE), (b) Meropenem (MEPM), (c) Cefminox Sodium (CEF), (d) Tazobactam (TAZ).

2.2.2. Differential Scanning Calorimetry (DSC)

TA Q200 DSC (TA Instruments) was used for the non-isothermal analyses. The hydrate samples were heated in Aluminum open pans at heating rates of 2, 5, 10, 20 and 30K /min under nitrogen purge (50 mL/min). Temperature was calibrated using indium. The activation energy (E_a) for dehydration of each hydrate was estimated using the Kissinger equation:[19]

$$d\ln(\varphi/T_m^2)/d(1/T_m) = -E_a/R$$

where T_m is the temperature at the maximum of endothermic peak measured at a heating rate of φ, and R is the gas constant. E_a was obtained from the slope of a plot of $\ln(\varphi/T_m^2)$ against $1/T_m$.

2.2.3. Thermogravimetric Analysis (TGA)

TGA was performed using TA Q500 TGA (TA Instruments) by two methods. One was raising temperature method, heating rate of 5K/min, and it was used to search for the early stage temperature regions of dehydration process. The other was holding temperature method, at five fixed temperatures covering the early stage temperature region estimated above, and it was used for iso-thermal dehydration study. The measurements were conducted under a nitrogen gas flow rate of 100 mL/min, with platinum pans.

The fraction dehydrated, α, at time t was firstly fitted to Hancock-Sharp equation[41] for inferring some mathematical models, then fitted to the known solid-state kinetic equations.[42] Finally, dehydration activation energy, E_a, was calculated from the slope of Arrhenius plot.

2.2.4. Particle Size Distribution analysis (PSD)

Particle size distribution analysis (PSD) was performed using Laser scattering particle size distribution LA-950 (Horiba) with dry measure unit. In this study, a dry method was used for particle size distribution analysis in order to avoid secondary agglomeration of particles. The schematic block diagram of laser scattering particle size distribution and its main body were shown in Figure 2-4.

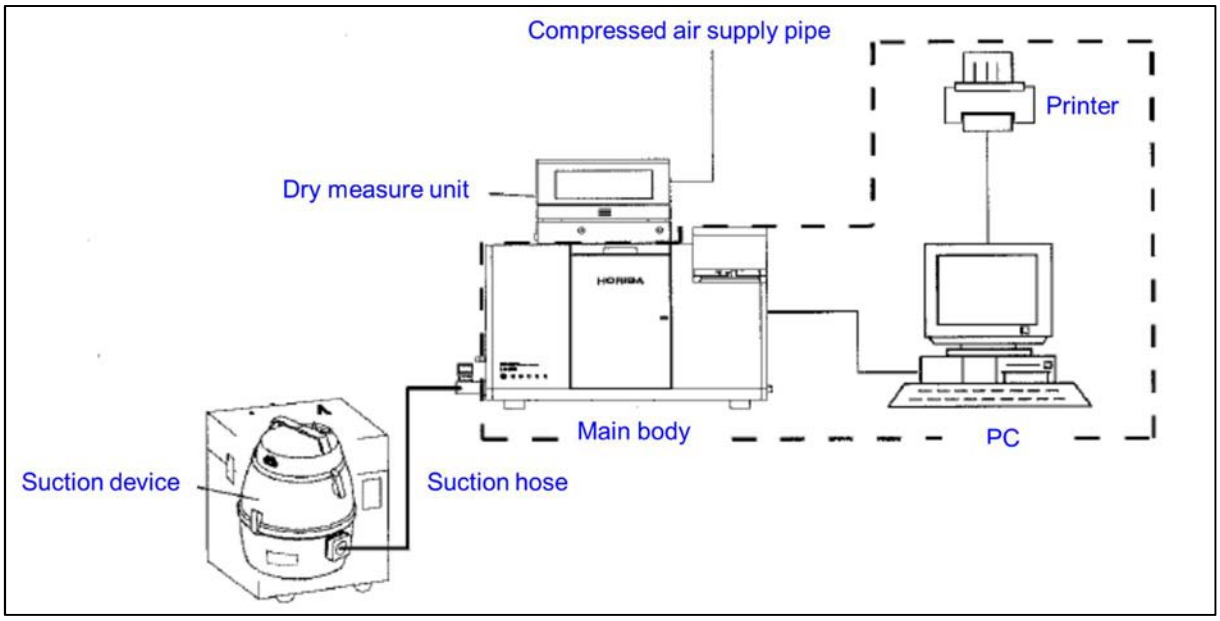

Figure 2-4 Schematic block diagram of laser scattering particle size distribution.

2.2.5. Scanning Electron Microscope (SEM)

Scanning Electron Microscope (SEM) images of MEPM trihydrate and CEF heptahydrate were collected using S-3400N (Hitachi) operated at an excitation voltage of 25 kV. The samples were mounted on an aluminum metal stub with double-sided adhesive carbon tape, and sputter coated with platinum-palladium using a sputter coater.

2.2.6. Powder X-Ray Diffraction (PXRD)

PXRD measurements were performed at room temperature on SmartLab 3 kW (Rigaku) using Cu Kα radiation at 1.54186Å at a voltage of 40 kV and a current of 30 mA. Data were collected at a scan rate of 4°/min.

2.2.7. Dehydration History

A series of the dehydration, rehydration, and dehydration operations were performed using the same sample, and the results obtained in the second dehydration were compared with those obtained in the first dehydration. MEPM trihydrate and SPE pentahydrate were used. DSC and PXRD measurements were

performed in order to compare dehydration E_a and diffraction peak width between first and second cycle samples.

2.3. Results and Discussion

2.3.1. Iso-thermal Activation Energy

MEPM trihydrate exhibited the early dehydration stage at 50-60°C (**Figure 2-5 (a)**), corresponding to the loss of 3 mol of water. The iso-thermal measurements of α versus t were obtained at 50.0, 52.5, 55.0, 57.5 and 60.0°C. SPE pentahydrate exhibited two successive early dehydration stages at 40-50°C and 90-100°C, each corresponding to the loss of 3 mol and 2 mol of water, respectively (**Figure 2-5 (b)**). The iso-thermal measurements were conducted at 40.0, 42.5, 45.0, 47.5 and 50.0°C for the first stage, and at 90.0, 92.5, 95.0, 97.5 and 100.0°C for the second stage. CEF heptahydrate exhibited the early dehydration stage at 40-50°C (**Figure 2-5 (c)**), corresponding to the loss of 7 mol of water. The iso-thermal measurements were conducted at 40.0, 42.5, 45.0, 47.5 and 50.0°C. TAZ hemihydrate exhibited the early dehydration stage at 100-110°C (**Figure 2-5 (d)**), corresponding to the loss of 0.5 mol of water. The iso-thermal measurements were conducted at 100.0, 102.5, 105.0, 107.5 and 110.0°C. The iso-thermal measurements are performed in triplicate for all of hydrate samples.

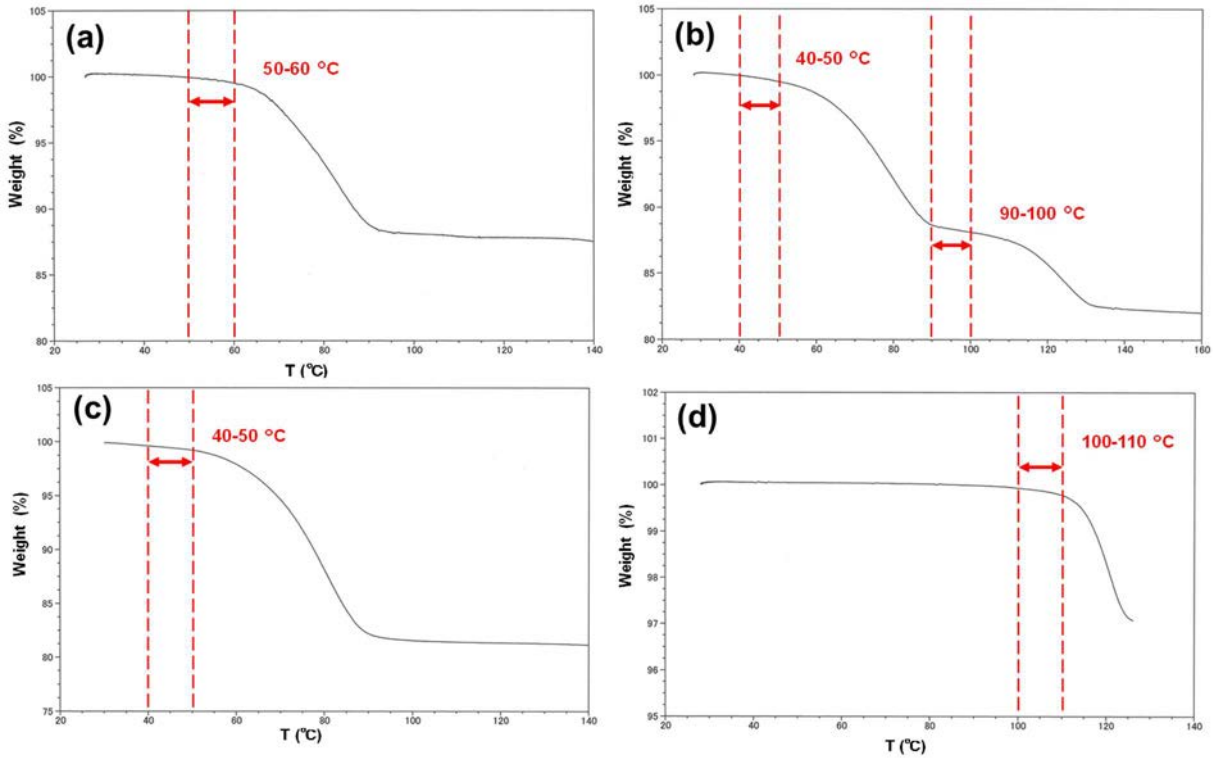

Figure 2-5 TGA curve of (a) MEPM trihydrate, (b) SPE pentahydrate, (c) CEF heptahydrate and (d) TAZ hemihydrate.

Iso-thermal dehydration curves of SPE pentahydrate, MEPM trihydrate, CEF heptahydrate and TAZ hemihydrate were shown in **Figure 2-6-Figure 2-10**.

Their sigmoidal curves showed dehydration rates increased with increasing temperature. Especially for SPE pentahydrate for the second dehydration step, the weight loss at each temperature after dehydration of 3 moles of water molecules was observed.

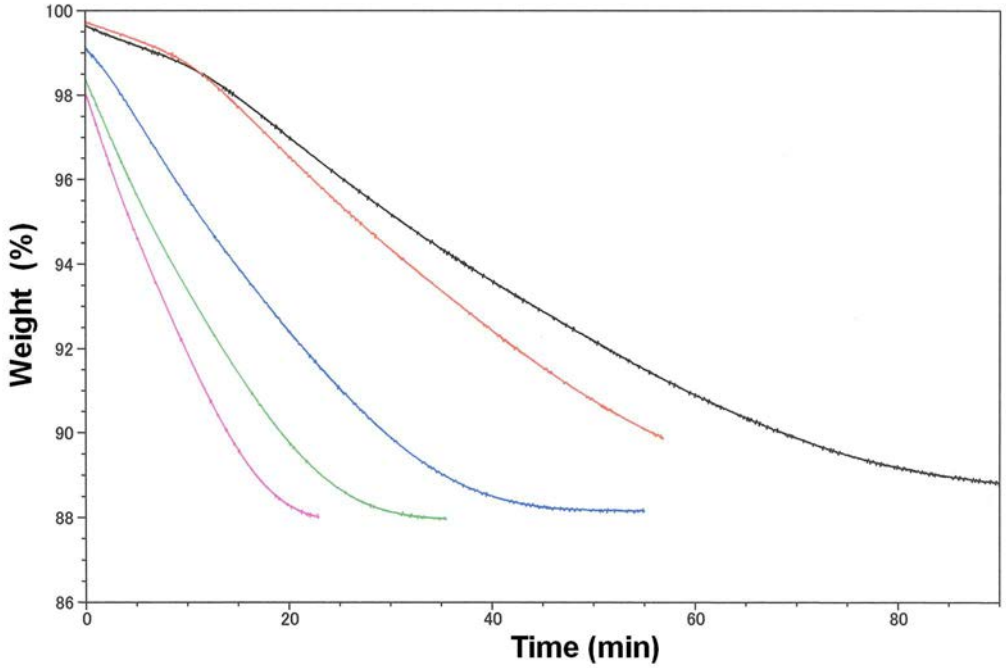

Figure 2-6 Iso-thermal dehydration curves of MEPM trihydrate, 50.0 °C (black), 52.5 °C (red), 55.0 °C (blue), 57.5 °C (green) and 60.0 °C (pink).

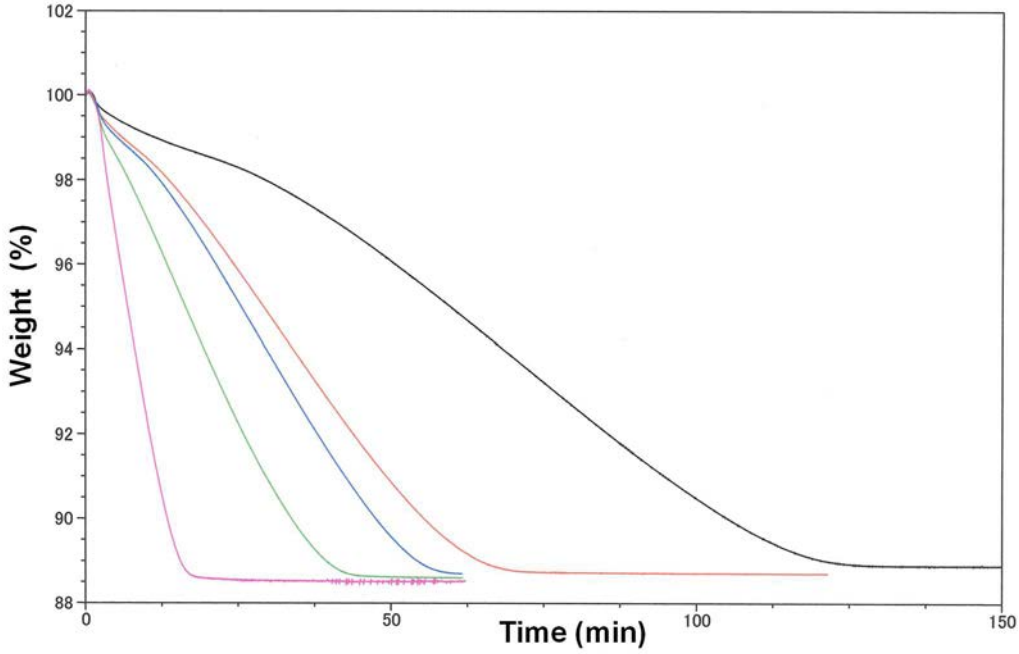

Figure 2-7 Iso-thermal dehydration curves of SPE pentahydrate for the first dehydration step, 40.0 °C (black), 42.5 °C (red), 45.0 °C (blue), 47.5 °C (green) and 50.0 °C (pink).

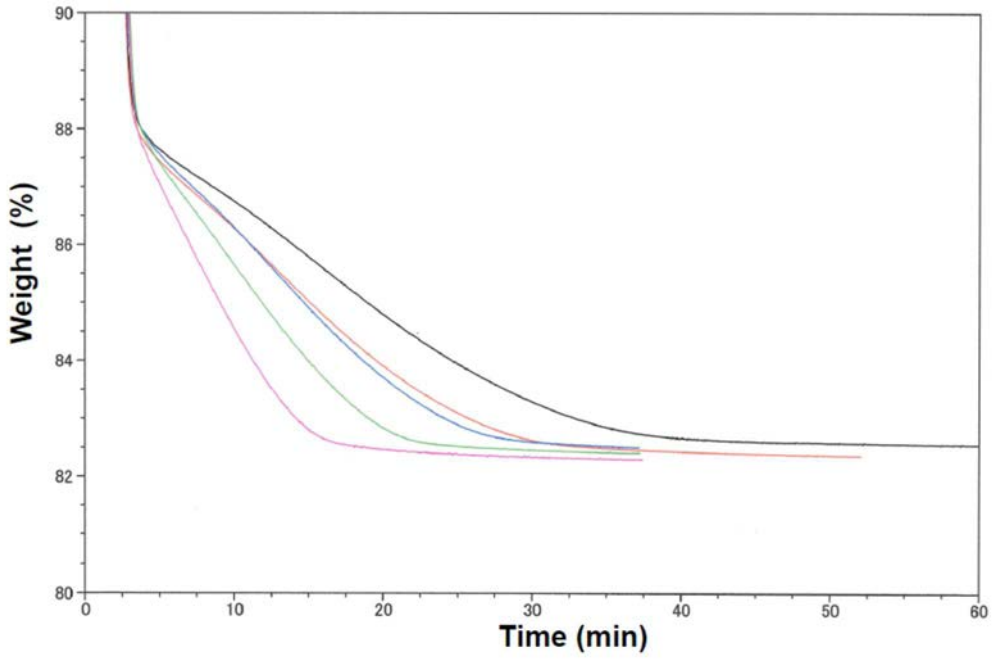

Figure 2-8 Iso-thermal dehydration curves of SPE pentahydrate for the second dehydration step, 90.0 °C (black), 92.5 °C (red), 95.0 °C (blue), 97.5 °C (green) and 100.0 °C (pink).

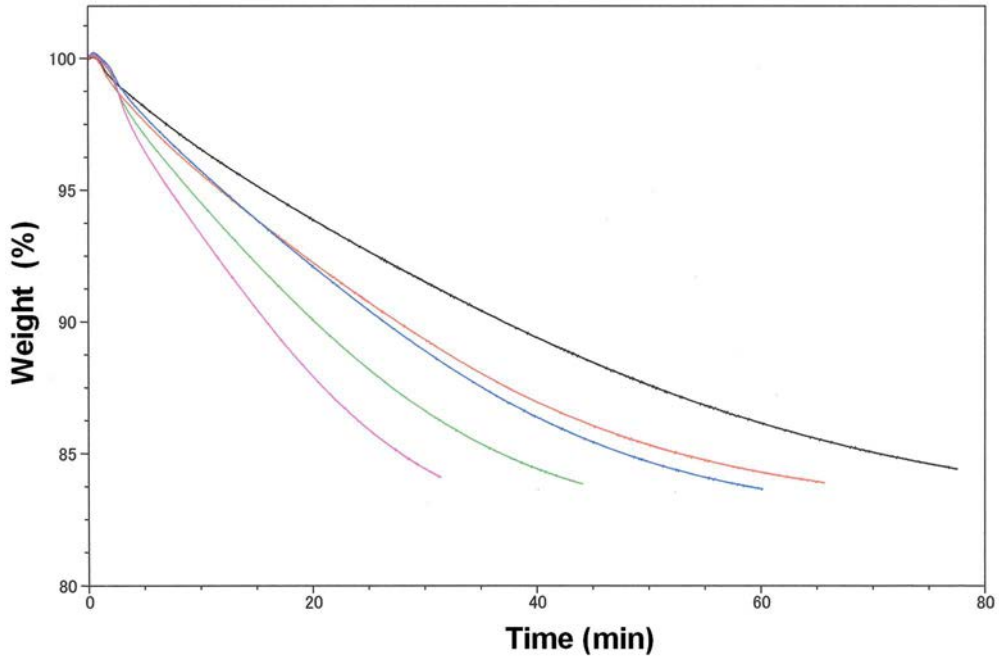

Figure 2-9 Iso-thermal dehydration curves of CEF heptahydrate, 40.0 °C (black), 42.5 °C (red), 45.0 °C (blue), 47.5 °C (green) and 50.0 °C (pink).

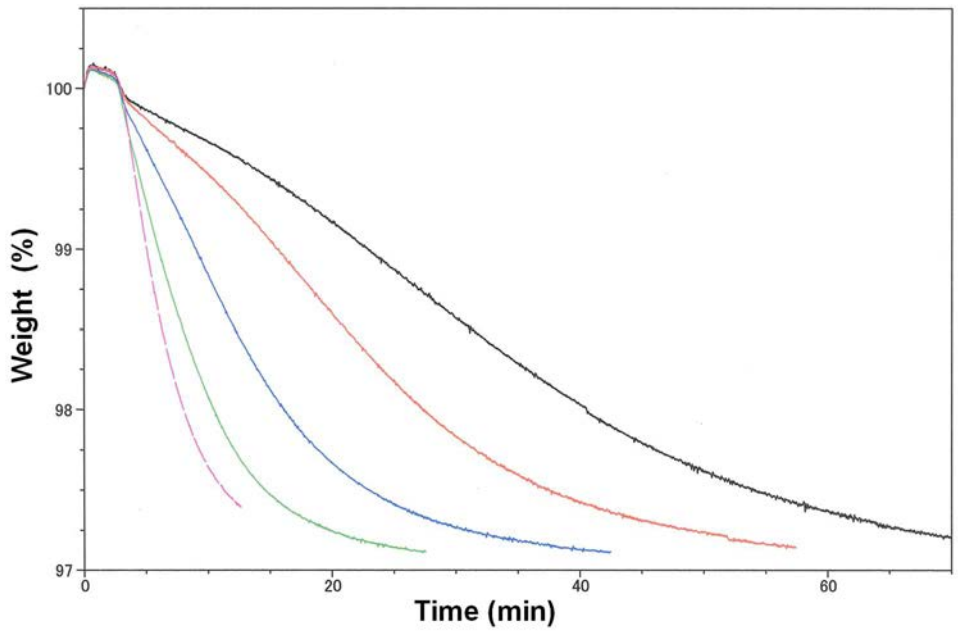

Figure 2-10 Iso-thermal dehydration curves of TAZ hemihydrate, 100.0 °C (black), 102.5 °C (red), 105.0 °C (blue), 107.5 °C (green) and 110.0 °C (pink).

The values in the range of 0.2-0.8 fraction dehydrated (α) of MEPM trihydrate were fitted to the Hancock-Sharp equation to determine the mathematical model. Hancock-Sharp plot at 50 °C was shown in **Figure 2-11**, and *m* was calculated to be 1.1 from the slope of the line. The values of *m* at five fixed temperatures were listed in **Table 2-3**.

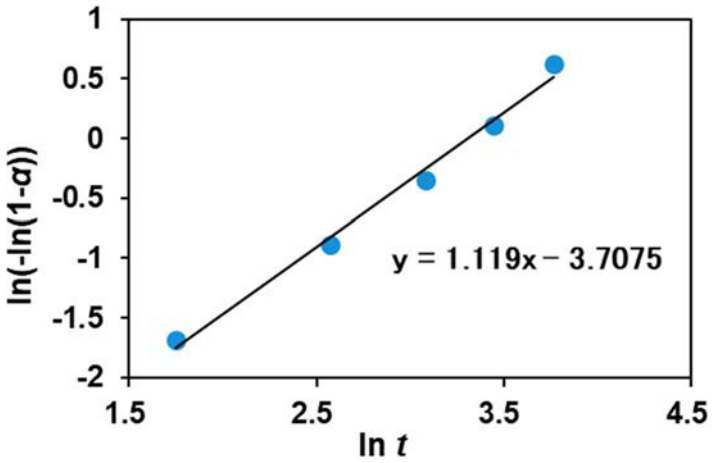

Figure 2-11 Hancock-Sharp plot for dehydration of MEPM trihydrate at 50 °C.

Table 2-3 The dehydration mechanism (*m*) of MEPM trihydrate at fixed temperatures.

Temperature (°C)	*m*		
	1	2	3
50.0	1.11	1.17	1.46
52.5	1.11	1.58	1.63
55.0	1.16	1.47	1.23
57.5	0.81	1.09	0.98
60.0	0.86	0.73	0.93

Six kinds of kinetic equations were selected from m values of 0.73-1.63, then fraction dehydrated (α) and time (t) was fitted to them to examine the linearity, and correlation coefficients were obtained (**Table 2-4**). The best *m*, 1.11, allowed us to predict that the best mathematical model of MEPM trihydrate was "Contracting area R2 model" by referring to *m* for solid-state reaction rate

equations, and R2 model fitting was shown in **Figure 2-12.** The dehydration rate constants were calculated from the slope of the line. Those of at five fixed temperature were tabulated in **Table 2-5**. Besides, dehydration rate constants of other hydrate crystals were also obtained in the same way (**Table 2-6 -Table 2-8**), and model equations of SPE, CEF and TAZ are A2, R3 and R2, respectively. The dehydration rate constants also increased by increasing temperature.

Table 2-4 Correlation coefficients by fitting to kinetic equations

m	Kinetic equation	Correlation coefficient					
		50.0°C	52.5°C	55.0°C	57.5°C	60.0°C	av.
0.62	$\alpha^2 = kt$	0.9948	0.9942	0.9982	0.9980	0.9973	0.9963
1.00	$-\ln(1-\alpha) = kt$	0.9897	0.9889	0.9905	0.9897	0.9883	0.9897
1.07	$1-(1-\alpha)^{1/3} = kt$	0.9980	0.9977	0.9976	0.9973	0.9965	0.9977
1.11	$1-(1-\alpha)^{1/2} = kt$	0.9997	0.9996	0.9994	0.9993	0.9988	0.9995
1.24	$\alpha = kt$	0.9954	0.9957	0.9976	0.9978	0.9984	0.9966
2.00	$[-\ln(1-\alpha)]^{1/2} = kt$	0.9995	0.9997	0.9994	0.9993	0.9988	0.9995

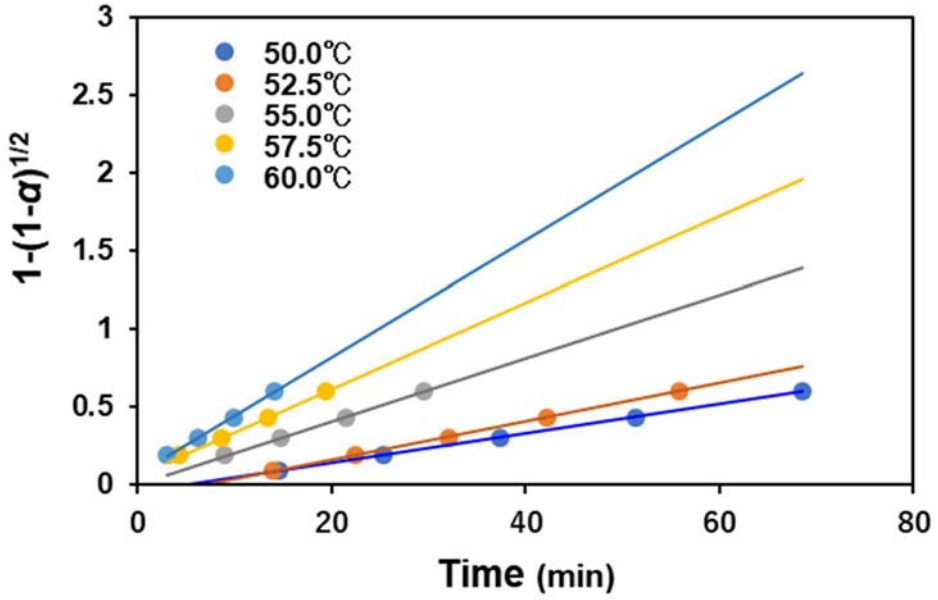

Figure 2-12 Contracting area R2 model fitting of MEPM trihydrate.

Table 2-5 Dehydration rate constants of MEPM trihydrate.

Temperature	k (min^{-1})			
(°C)	1	2	3	av.
50.0	0.0095	0.0095	0.0095	0.0095
52.5	0.0123	0.0128	0.0169	0.0140
55.0	0.0202	0.0170	0.0203	0.0192
57.5	0.0279	0.0291	0.0353	0.0308
60.0	0.0376	0.0379	0.0368	0.0374

Table 2-6 Dehydration rate constants of SPE pentahydrate and dihydrate.

Temperature	Pentahydrate k (min^{-1})			
(°C)	1	2	3	av.
40.0	0.0259	0.0247	0.0187	0.0231
42.5	0.0299	0.0314	0.0251	0.0288
45.0	0.0420	0.0372	0.0395	0.0396
47.5	0.0483	0.0481	0.0571	0.0512
50.0	0.0672	0.0539	0.0586	0.0599
Temperature	Dihydrate k (min^{-1})			
(°C)	1	2	3	av.
90.0	0.0312	0.0324	0.0433	0.0356
92.5	0.0422	0.0567	0.0547	0.0512
95.0	0.0652	0.0620	0.0610	0.0627
97.5	0.0697	0.0839	0.0795	0.0777
100.0	0.0757	0.0968	0.1127	0.0951

Table 2-7 Dehydration rate constants of CEF heptahydrate.

Temperature	k (min^{-1})			
(°C)	1	2	3	av.
40.0	0.0058	0.0053	0.0058	0.0056
42.5	0.0079	0.0077	0.0076	0.0077
45.0	0.0088	0.0102	0.0088	0.0093
47.5	0.0113	0.0138	0.0120	0.0124
50.0	0.0150	0.0133	0.0169	0.0151

Table 2-8 Dehydration rate constants of TAZ hemihydrate.

Temperature (°C)	k (min^{-1})			
	1	2	3	av.
100.0	0.0132	0.0127	0.0116	0.0125
102.5	0.0194	0.0212	0.0175	0.0194
105.0	0.0323	0.0337	0.0305	0.0322
107.5	0.0539	0.0455	0.0529	0.0508
110.0	0.0777	0.1073	0.1259	0.1036

The Arrhenius plot of MEPM trihydrate was shown in **Figure 2-13**, and the dehydration E_a was estimated from the slope of the line. The average value of E_a, standard deviation and relative standard deviation were estimated to be 126.5 kJ/mol, 2.7 kJ/mol and 2.1%, respectively (**Table 2-9**). The dehydration E_a of other hydrate crystals were also obtained in the same way, and the results were tabulated in **Table 2-10**. The average value of E_a of SPE pentahydrate were 83.9 kJ/mol for the first dehydration step and 107.4 kJ/mol for the second dehydration step. Those of CEF heptahydrate and TAZ hemihydrate were 81.7 kJ/mol and 245.0 kJ/mol, respectively.

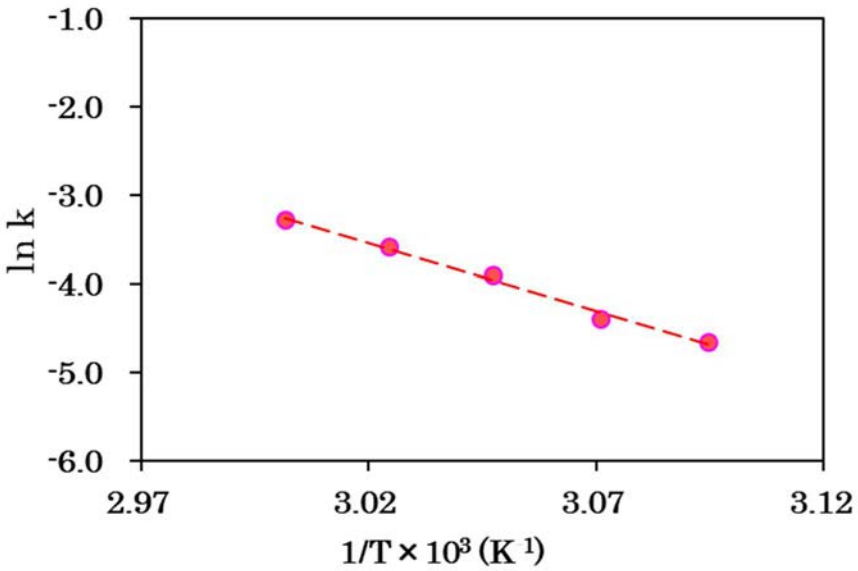

Figure 2-13 Arrhenius plot from the best fitting dehydration mechanism (R2 model) for MEPM trihydrate.

Table 2-9 Iso-thermal dehydration E_a and statistical parameters of MEPM trihydrate.

Number of repetition	Dehydration E_a (kJ/mol)	Average value	Standard deviation	Relative standard deviation (%)
1	127.6			
2	128.4	126.5	2.7	2.1
3	123.4			

Table 2-10 Iso-thermal dehydration E_a of all hydrate crystals.

Hydrate sample	Hydrate type	Fraction dehydrated	Mathematical model	Dehydration E_a (kJ/mol)			
				Iso-thermal			
				1	2	3	av.
SPE	Penta	0.3 - 0.9	A2	104.6	80.2	66.9	83.9
	Di	0.2 - 0.9	A2	102.9	116.3	102.9	107.4
MEPM	Tri	0.2 - 0.8	R2	127.6	128.4	123.4	126.5
CEF	Hepta	0.1 - 0.8	R3	76.1	81.6	87.4	81.7
TAZ	Hemi	0.1 - 0.9	R2	217.1	238.9	279.1	245.0

The above is the method of procedure for obtaining the iso-thermal E_a for dehydration.

2.3.2. Noniso-thermal Activation Energy

The dehydration E_a of SPE pentahydrate, MEPM trihydrate, CEF heptahydrate and TAZ hemihydrate were derived via the Kissinger equation. The advantage of using the Kissinger equation for estimating E_a is the unnecessity of assuming kinetic model in the dehydration process. Therefore, it is possible to evaluate individual E_a of hydrate samples on the same measurement condition. From this reason, the dehydration E_a of these samples can be compared to each other in spite of they had own dehydration mechanisms. DSC curves of CEF at heating rates (φ) of 2, 5, 10, 20, 30°C/min were shown in **Figure 2-14**, and maximum temperatures of endothermic peak (T_m) corresponding to heating rates were given in **Table 2-11**.

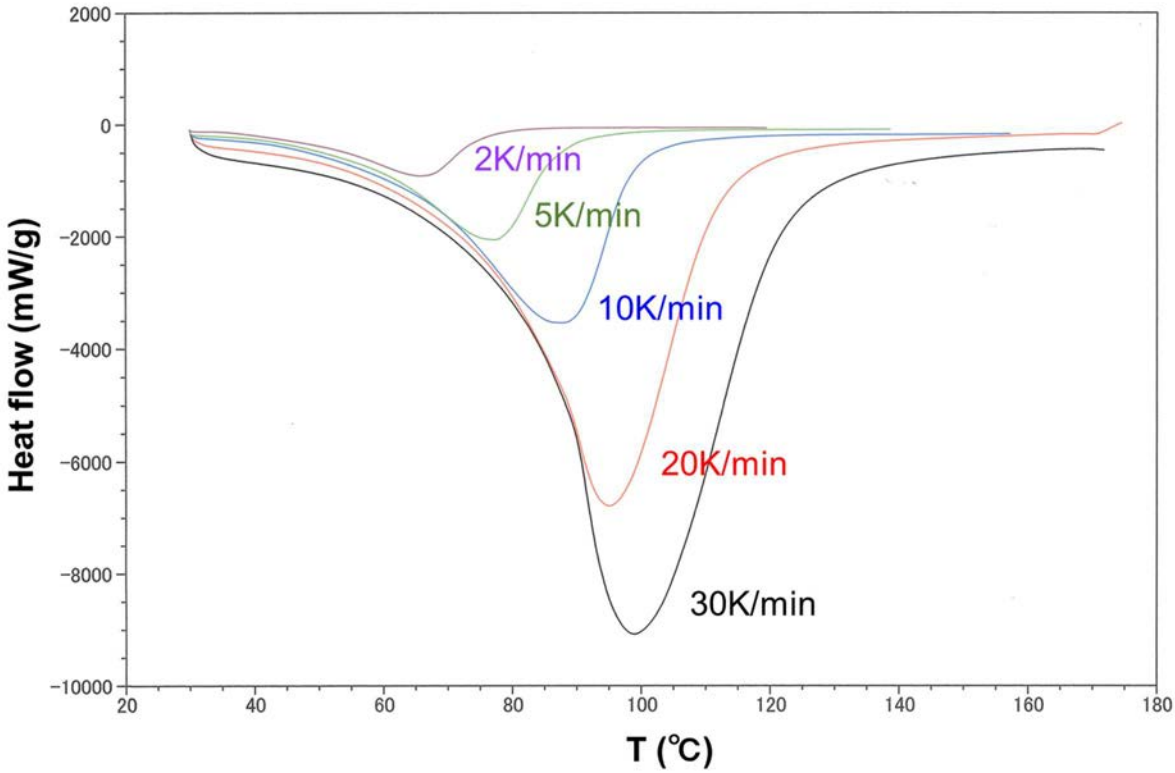

Figure 2-14 DSC curves of CEF at heating rates of 2, 5, 10, 20, 30K/min.

Table 2-11 Maximum temperatures of endothermic peak of CEF heptahydrate corresponding to heating rates.

Heating rate φ (K/min)	Maximum temperature of endothermic peak Tm (K)
2	339.1
5	350.5
10	360.9
20	368.2
30	372.1

Kissinger plot of $\ln(\varphi/T_m^2)$ against $1/T_m$ was shown in **Figure 2-15**. E_a of CEF heptahydrate was estimated to be 78.2 kJ/mol from the line's slope and the correlation coefficient R was 0.9958.

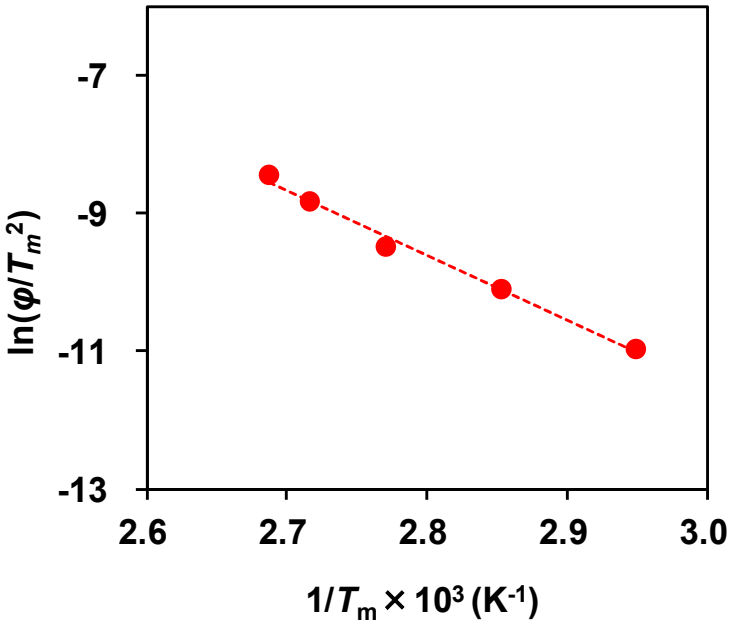

Figure 2-15 Kissinger plot of $\ln(\varphi/T_m^2)$ against $1/T_m$ for CEF heptahydrate.

The dehydration E_a of SPE was determined for the dehydration process from pentahydrate to dihydrate which is the first dehydration step, and from dihydrate to anhydrate which is the second dehydration step. The values of dehydration E_a of SPE, MEPM and TAZ were also obtained in the same way, and tabulated in Table 2-12. The above is the method of procedure for obtaining the noniso-thermal E_a for dehydration.

Table 2-12 Dehydration E_a calculated by iso-thermal and noniso-thermal method.

Hydrate sample	Hydrate type	Dehydration E_a (kJ/mol)					
		Iso-thermal			Noniso-thermal		
		1	2	3	1	2	3
SPE	Penta	104.6	80.2	66.9	71.1	68.3	68.2
	Di	102.9	116.3	102.9	90.2	89.8	90.5
MEPM	Tri	127.6	128.4	123.4	71.6	72.2	71.6
CEF	Hepta	76.1	81.6	87.4	78.2	84.6	79.5
TAZ	Hemi	217.1	238.9	279.1	158.2	156.3	157.4

2.3.3. Comparison of E_a by Iso-themal and Noniso-thermal Method

The dehydration E_a by iso-thermal and noniso-thermal method for SPE pentahydrate, MEPM trihydrate, CEF heptahydrate and TAZ hemihydrate were made into graph (**Figure 2-16**). Iso-thermal E_a was related to noniso-thermal E_a, and noniso-thermal ones were lower than iso-thermal ones by comparison of them. There is a possibility that weakening of H-bonding strength in heating process bring about increasing lattice vibration. The noniso-thermal E_a happens to show lower value as a result.

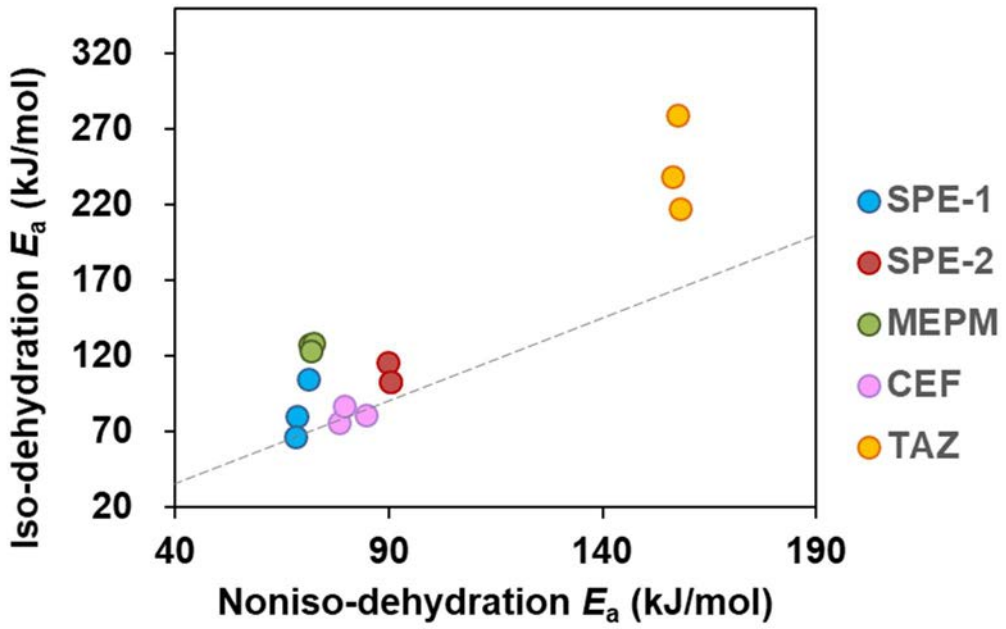

Figure 2-16 The relationship between iso-thermal and noniso-thermal dehydration E_a of SPE for the 1st dehydration (blue), SPE for the 2nd

dehydration (red), MEPM (green), CEF (pink) and TAZ (orange). The ratio of noniso and iso-dehydration E_a is 1 on the dashed line.

From the above, the comparison between the noniso-thermal E_a and the conventional iso-thermal E_a showed a certain correlation, hydrates which have higher noniso-E_a showed higher iso-E_a, and hydrates which have lower noniso-E_a showed lower iso-E_a. It was clarified that the noniso-thermal method can be used for the comparison of dehydration E_a among a plurality of hydrate crystals.

In the process of obtaining E_a by the iso-thermal method, the following approximation is performed. The measurement temperature is selected from a narrow temperature range in the initial stage of dehydration. The mathematical model is chosen to assume a dehydration mechanism. The dehydration rate constants are evaluated by fitting to the chosen kinetic equation. Here, if the straight line obtained by fitting to this equation does not pass through the origin, it means that the reliability of the rate constant itself is not high, and the selected model cannot be said to be sufficiently appropriate, as shown in the **Figure 2-12**. Finally, Arrhenius plotting is performed to calculate E_a. As described above, many approximations are included for the iso-thermal method since this method is based on the estimation model.

On the other hand, in the process of determining E_a by the noniso-thermal method, only the process of fitting to the Kissinger equation was approximated since the same five different heating rates were applied to every hydrate sample. Naturally, the assumption of the kinetic model in the dehydration process is unnecessary in noniso-thermal method. Therefore, the approximations to noniso-dehydration E_a was very few.

Comparing the E_a variations obtained by the iso-thermal and the noniso-thermal method, the relative standard deviation was 2.1% to 22.7% by the iso-thermal method, while it was 0.4% to 4.2% by the noniso-thermal method, and the variation by the iso-thermal method was larger (**Table 2-13**). In the iso-thermal method, there were many approximations in the process of obtaining E_a, and it can be inferred that the variation became large. From the above, the noniso-thermal method in which the variation of E_a was reduced by the minimum approximation would have a high advantage in order to uniformly evaluate E_a of a plurality of hydrates with different dehydration mechanisms.

Table 2-13 The dehydration E_a variations obtained by iso-thermal and noniso-thermal method.

Hydrate sample	Hydrate type	Iso-thermal		Noniso-thermal	
		av.	RSD (%)	av.	RSD (%)
SPE	Penta	83.9	22.7	69.0	2.4
	Di	107.4	7.2	90.0	0.4
MEPM	Tri	126.5	2.1	71.8	0.5
CEF	Hepta	81.7	6.9	80.8	4.2
TAZ	Hemi	245.0	12.8	157.3	0.6

2.3.4. Influencing factor on noniso-E_a

2.3.4.1.Sample Aggregation

The purpose of this study was to investigate the effect of sample aggregation on dehydration E_a. Therefore, PSD and SEM measurements were performed to confirm the particle size of the intact sample and the sample passing through the sieves, respectively. Particle size distribution of MEPM trihydrate performed by dry laser diffraction was shown in **Figure 2-17**. MEPM trihydrate had a sharp distribution, and the mass median diameter was estimated to be 28 μm. SEM image of MEPM of two fractions, smaller particle fraction; <75 μm and larger particle fraction; >212μm, were shown in **Figure 2-18**. The size of each particle in the intact sample, smaller and larger particle fractions showed almost same, around 25 μm, but the particles were only agglomerated.

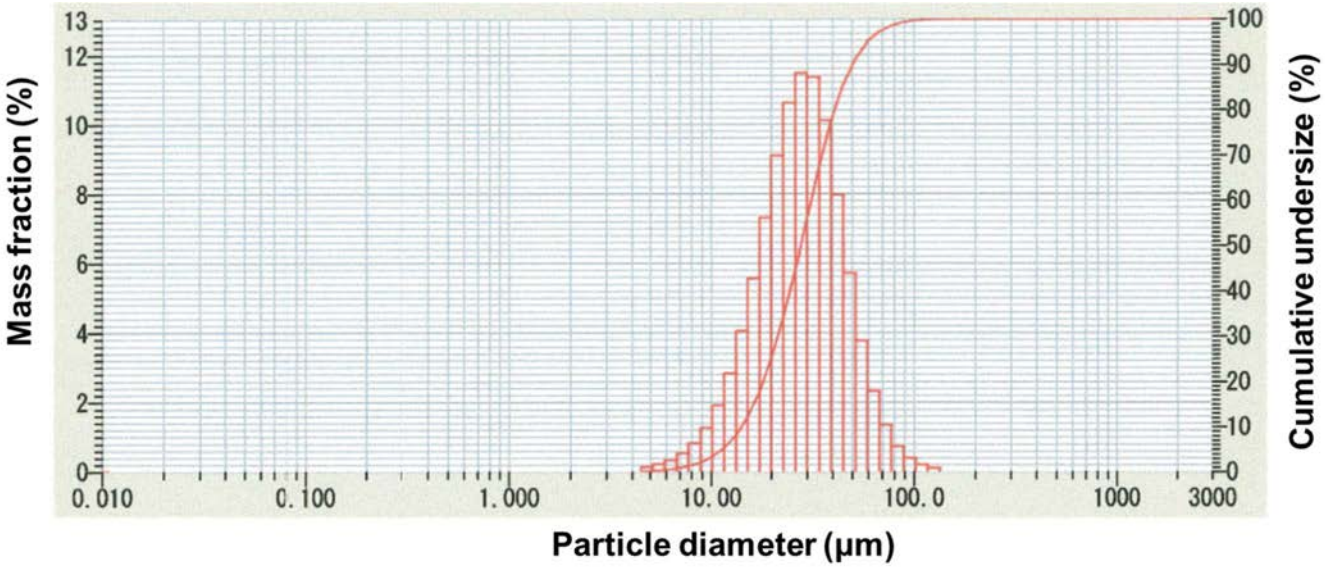

Figure 2-17 Particle size distribution of MEPM trihydrate.

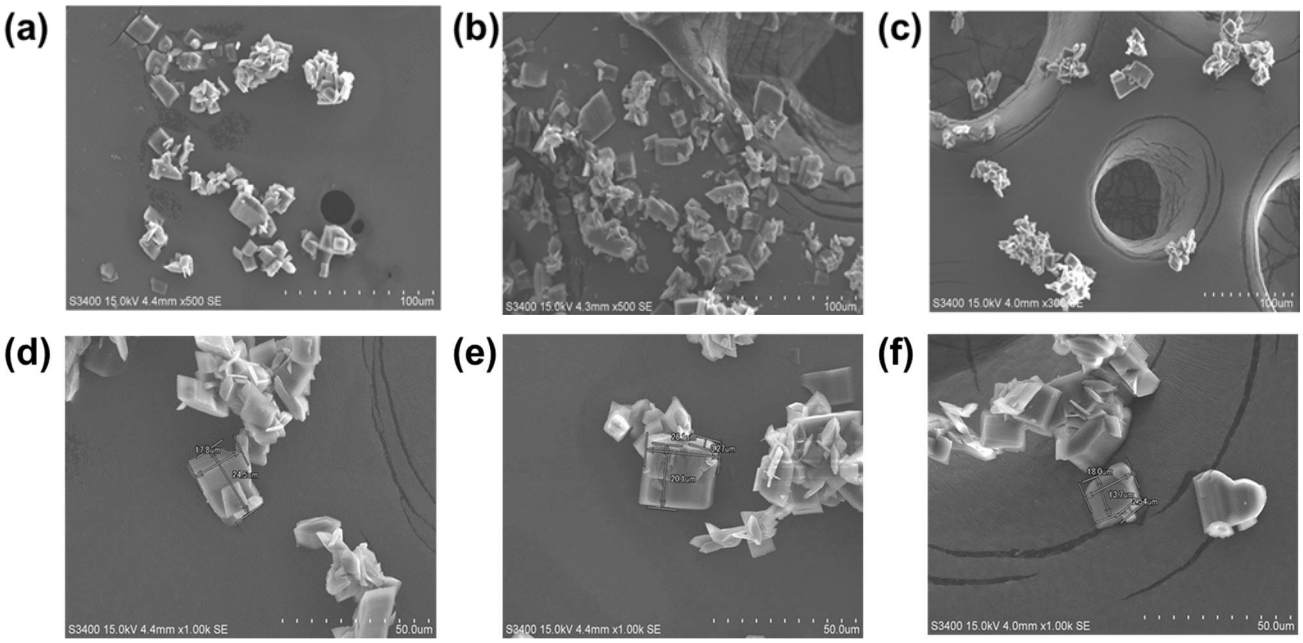

Figure 2-18 SEM image of MEPM trihydrate, (a)smaller particle fraction (<75 μm), (b) larger particle fraction (>212 μm) and (c)intact sample. (d), (e) and (f) indicate enlarged figures of (a), (b) and (c), respectively.

The noniso-thermal study was conducted using these samples. The maximum temperatures of endothermic peak corresponding to heating rates and dehydration

E_a of different particle fractions were given in **Table 2-14**. The dehydration E_a changed from 71.5 to 77.7 kJ/mol in four fractions and intact sample. Neither maximum temperatures of endothermic peak nor dehydration E_a did not show a constant trend with respect to the particle fraction, they simply showed the almost same values. These results revealed that the aggregation in the 75-212 μm range did not affect the magnitude of E_a.

Table 2-14 The maximum temperatures of endothermic peak corresponding to heating rates and dehydration E_a of different particle fractions for MEPM trihydrate.

Heating rate	Maximum temperature of endothermic peak T_m (K)				
φ (K/min)	<75 μm	75-125 μm	125-212 μm	>212 μm	intact
2	342.3	342.5	344.4	341.7	341.9
5	354.2	353.7	354.6	354.4	354.2
10	364.5	364.3	364.2	363.2	362.8
20	374.6	373.8	372.5	372.5	374.2
30	379.0	379.2	379.8	380.1	379.3
E_a (kJ/mol)	71.9	72.7	77.7	71.5	71.5

2.3.4.2.Size of Particle

The purpose of this study was to investigate the effect of particle size on dehydration E_a. SEM image of sieved sample (<50 μm), ground sample, fine sample and intact sample for CEF heptahydrate were shown in **Figure 2-19**. The particles of sieved sample were seen almost uniformly distributed throughout with size of approximately 50 μm, whereas the ground sample consisted of much smaller particles with ununiform shape. Besides, fine sample had tiny particles (approximately 10 - 20μm) and intact sample had various sizes (approximately 10 -100 μm) of particles.

The maximum temperatures of endothermic peak and dehydration E_a of these samples were given in **Table 2-15**. Maximum temperatures of endothermic peak were almost the same and dehydration E_a changed from 84.6 to 87.7 kJ/mol. These results revealed that particle size of approximately 10-100 μm and the treatment of grinding in a mortar and milling did not affect the magnitude of E_a.

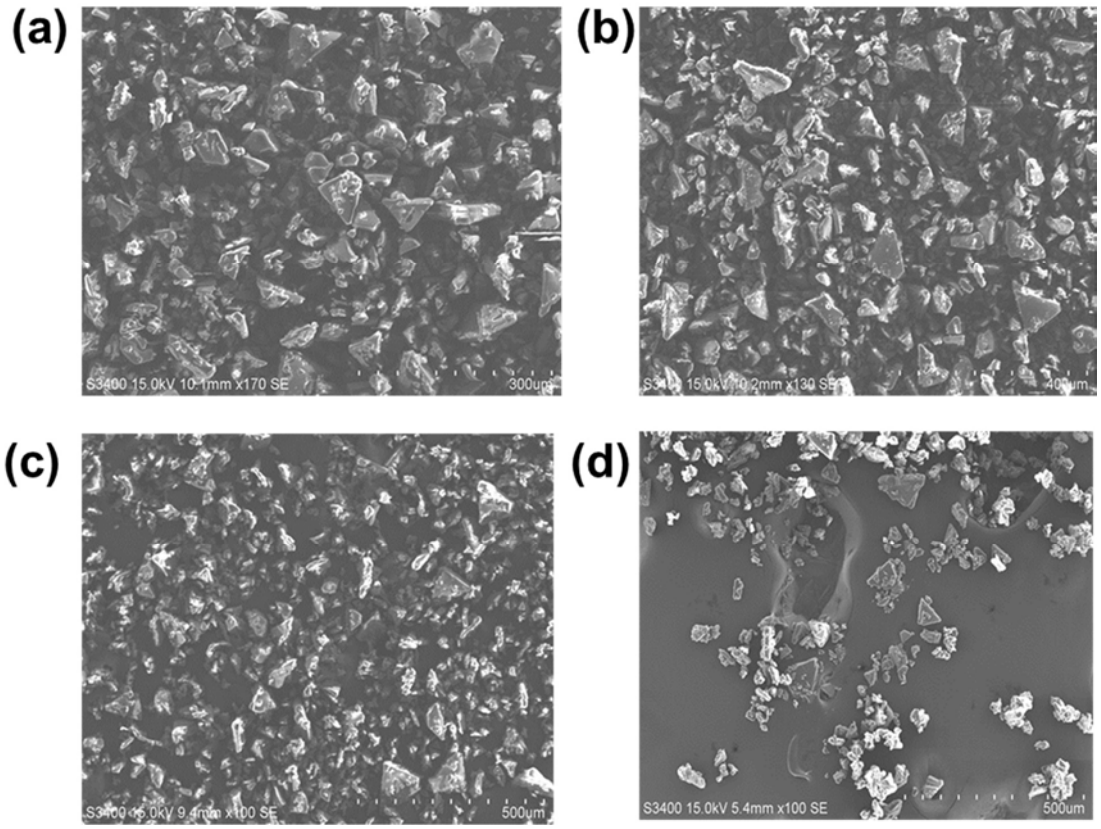

Figure 2-19 SEM image of CEF heptahydrate, (a)sieved sample (<50 μm), (b)ground sample, (c)fine sample and (d)intact sample.

Table 2-15 Maximum temperatures of endothermic peak and dehydration E_a of different particle size samples for CEF heptahydrate.

Heating rate	Maximum temperature of endothermic peak T_m (K)			
φ (K/min)	<50 μm	Ground	Fine	intact
2	340.4	341.6	340.0	339.9
5	352.2	352.4	352.1	350.5
10	360.0	362.6	358.6	360.7
20	366.9	366.7	367.6	366.8
30	370.9	370.2	369.3	370.4
E_a (kJ/mol)	86.9	87.7	87.7	84.6

2.3.4.3. Dehydration History

The purpose of this study was to investigate the effect of the sample history, such as repeated dehydration processes, on E_a. The dehydration E_a obtained by the first and the second measurement of MEPM trihydrate and SPE heptahydrate were given in **Table 2-16**. The 1st-dehydration as used herein means the first dehydration process using an intact sample, and 2nd-dehydation means the process of dehydrating after rehydrating the sample used for the first dehydration. The 2nd dehydration E_a of them were lower than those of 1st dehydration.

Table 2-16 Dehydration E_a obtained by 1st and 2nd measurement of MEPM trihydrate and SPE heptahydrate.

Hydrate sample	Hydrate type	Dehydration E_a (kJ/mol)			
		1st-dehydration			2nd-dehydration
MEPM	Tri	71.6	72.2	71.6	62.6
SPE	Penta	71.1	68.3	68.2	64.6

XRD patterns and characteristic peak angle of the samples prior to use for 1st and 2nd dehydrations for SPE pentahydrate were shown in **Figure 2-20** and **Table 2-17**, respectively.

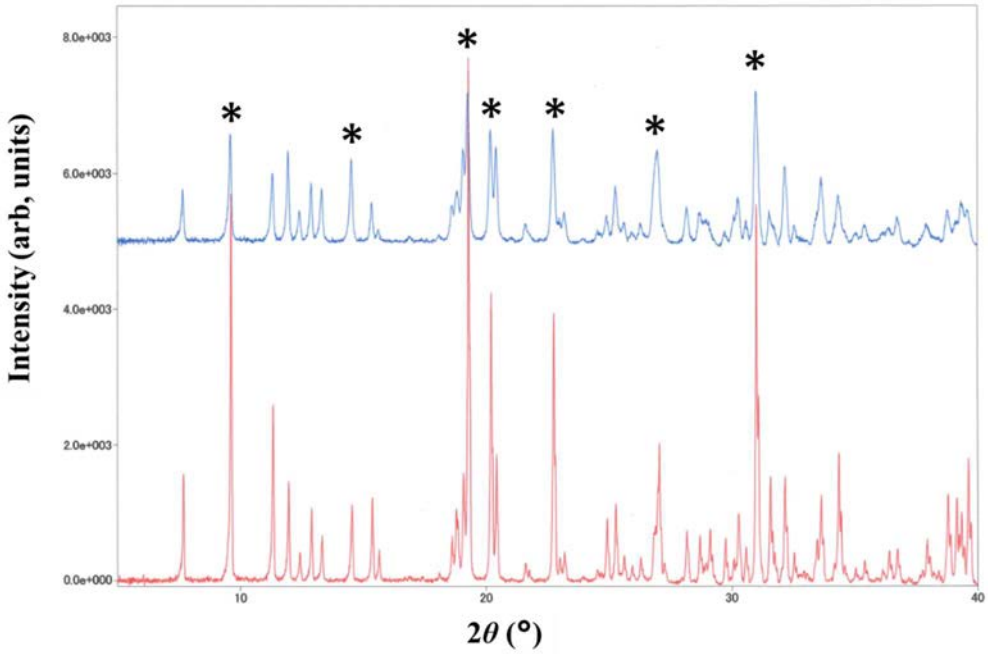

Figure 2-20 XRD patterns of SPE pentahydrate before 1st (red) and 2nd (blue) dehydration. * indicates characteristic peaks.

Table 2-17 The characteristic peak angle of SPE pentahydrate before 1st and 2nd dehydration.

Sample	2θ (°)						
Before 1st dehydration	9.631	15.650	19.307	20.224	22.766	27.054	31.017
Before 2nd dehydration	9.630	15.364	19.267	20.191	22.732	26.998	30.976

The samples prior to use for 1st and 2nd dehydration indicate the intact sample and the rehydrated sample, respectively. Although the patterns were the same between 1st and 2nd, the diffraction peaks of 2nd were broader and shifted to lower angle. This means that due to the dehydration, the lattice spacing widened and the ordered lattice arrangement collapsed slightly, although its crystal form was not changed. It was concluded that repeated dehydration process lowered dehydration E_a and considering the dehydration history of hydrate crystals are important for evaluating E_a.

2.4. Concluding Remarks

In order to measure the dehydration E_a of hydrate crystals, an iso-thermal method has been conventionally used, but it is necessary to calculate the energy by fitting the weight change curve to an arbitrary model equation for each crystal, and there is a possibility that the calculated energy cannot be used for comparison between a plurality of crystals, and the stability of the sample is influenced by the necessity of a long time-measurement.

Therefore, the application of the noniso-thermal method to calculate E_a from the endothermic peak temperature of DSC was examined. This method utilizes a model-independent relationship in which the logarithm of the ratio between the heating rate and the square of the peak temperature is proportional to the reciprocal of the temperature.

Comparison of E_a obtained from this measurement with the value obtained by the conventional iso-thermal method revealed that there was a certain correlation between both, and that the noniso-thermal method can be used for comparison of E_a among a plurality of crystals. In the iso-thermal method, there were many approximations in the process of obtaining E_a, and it can be inferred that the E_a variation became large. The noniso-thermal method in which the E_a variation was reduced by the minimum approximation would have a high advantage in comparing the E_a of hydrates with each other.

As an influencing factor used for the thermal measurement, the possibility that the particle diameter of the sample crystal influences E_a has been pointed out in the past. Therefore, agglomerated samples, samples of various particle size, samples obtained by changing the grinding method and samples which had different dehydration history were prepared. When E_a measurements for their samples were performed by the noniso-thermal method, agglomeration in the range of 75 - 212 μm and sample size in the range of 10 - 100 μm did not affect E_a, but E_a depended on only dehydration history. Therefore, intact samples should be used for the classification of hydrates.

From the above, it was clarified that E_a using a non-isothermal method should be used instead of the conventional method in order to uniformly evaluate a plurality of crystals with different dehydration mechanisms.

3. Elucidation of Phase Transition Behavior and Classification of Hydrate Crystals

3.1. Introduction

The solid-state phase transformation of active ingredient in medicine often dramatically change the pharmaceutical properties including stability, solubility, dissolution rate, bioavailability and tableting behavior.[43-45] Therefore, identifying and characterizing crystalline forms is important for pharmaceutical development.[46-48] Almost of drug substances are known to crystallize with solvent molecules including water. As a result, the frequency of formation of solvates and hydrates increases. When the solvent or water is removed from these crystals, another crystal form is formed. It is well known that the water content in the solid state of drugs can have significant effects on a variety of physical and chemical properties of drug. In other words, defining the conditions under which phase transformation occur leads to control of the efficacy and side effects of the drug.

The common techniques for clarifying phase transition behavior are powder X-ray diffraction,[49,50] differential scanning calorimetry,[51,52] thermogravimetry,[53,54] dynamic vapor sorption and infrared and Raman spectroscopy.[55,56] In particularly, thermal analysis, dynamic vapor sorption and powder X-ray diffraction-differential scanning calorimetry provide useful information about the change in weight while changing the temperature and humidity, heat flow and solid state during the dehydration process. It is possible to understand dehydration and rehydration processes by combining these techniques.

As far as we know, there were past examples in which activation energy (E_a) of each sample was compared among the same compounds in different sample preparation methods, but there were no examples in which E_a was compared among different compounds (active pharmaceutical ingredient). Kissinger plot of the noniso-thermal crystallization of amorphous lactose was shown in **Figure 3-1**. The crystallization kinetics of amorphous lactose in the presence and absence of seed crystals were investigated at 57.5% relative humidity, and crystallization E_a were determined by measuring peak crystallization temperature (T_p) at several

heating rates (β). The noniso-thermal E_a with and without seed crystals were evaluated from the slopes, 71.0 kJ/mol for with seeds and 80.9 kJ/mol for without seeds. The E_a with seeds suggested that crystallization was occurring by growth from a fixed number of preexisting nuclei.[57]

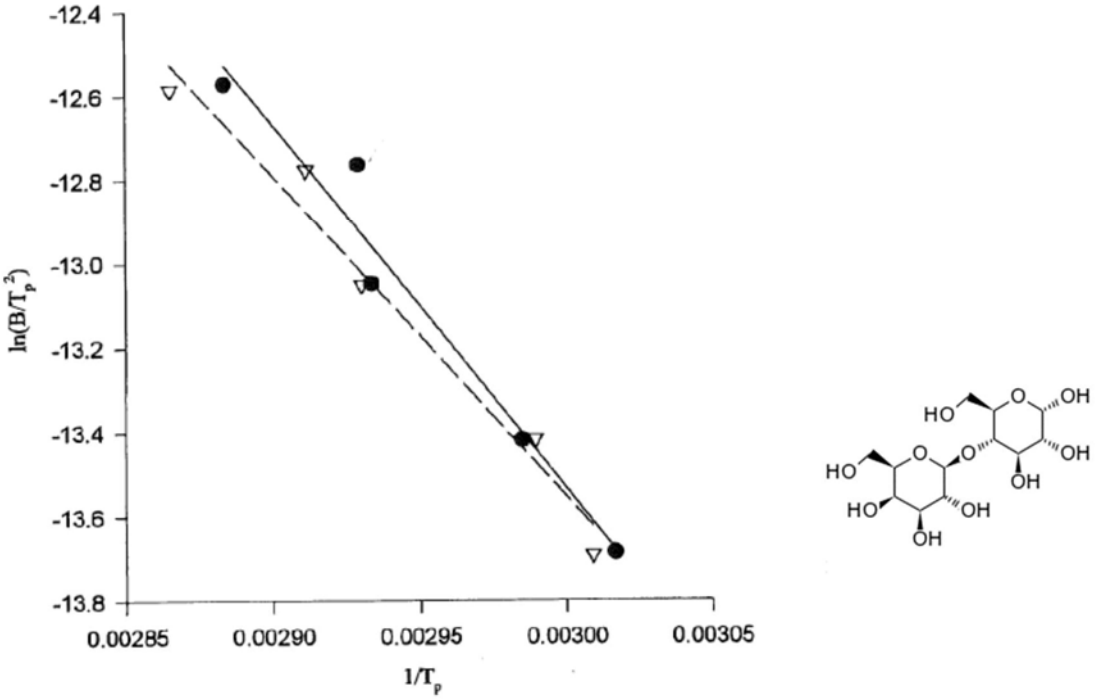

Figure 3-1 Kissinger plot of the noniso-thermal crystallization of amorphous lactose equilibrated at 57.5%RH without seeds (circle, solid line) and with seeds (triangle, dashed line), T_p and B denote a peak top of crystallization temperature and a heating rate, respectively, and chemical structure of lactose.[57]

In the hydrate example, for eprosartan mesylate dihydrate samples prepared from anhydrate by three kinds of different methods by slurry, exposing to 98%RH and granulating in the presence of 3% corn starch and 10% water. Then, E_a of the first and second dehydration steps were calculated from the Kissinger plots of differential scanning calorimetry data and were listed in **Table 3-1**. The dehydration E_a depended on the method of preparation.[20] The dependence of dehydration E_a like this may reflect properties of the crystals.

Table 3-1 The E_a from Kissinger plots for the first and second dehydrations of eprosartan mesylate dihydrate samples from various preparation methods, and chemical structure of eprosartan mesylate.[20]

Dehydration step	Preparation methods			
	98%RH	Slurry	Granulating	
First E_a (kcal/mol)	19.6	11.8	13.6	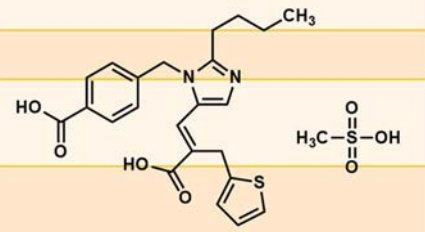
Second E_a (kcal/mol)	31.4	18.7	38.9	

The aim of this study was to clarify the transition behaviors of eleven hydrates by using of thermal analysis, dynamic vapor sorption and powder X-ray diffraction-differential scanning calorimetry.

Since it is necessary to consider the ease of rehydration for the classification of hydrates, the evaluation system of rehydration E_a was also examined. For this purpose, a change in weight in the process of returning the dehydrated sample to the original hydrate under a constant humidity condition was observed.

Then we attempted to classify them by the dehydration E_a, rehydration behavior and rehydration E_a.

3.2. Experimental

3.2.1. Materials

Spectinomycin dihydrochloride (SPE) pentahydrate, meropenem (MEPM) trihydrate, acrinol (ACR) monohydrate, pipemidic acid (PIPM) trihydrate, enoxacin (ENO) sesquihydrate, amoxicillin (AMO) trihydrate and nitrofurantoin (NF) anhydrate were purchased from commercial source. Piperacillin (PIPC) hydrate, cefminox sodium (CEF) heptahydrate, tazobactam (TAZ) anhydrate and its hemihydrate were provided by Meiji Seika Pharma Co., Ltd. They were used without any further purification and **Figure 3-2** shows their chemical structures. Other solvents were methanol and acetone of guaranteed grade.

The purities of the hydrate samples before and after evaluation the activation energies were measured by high performance liquid chromatography or gas chromatography, and it was confirmed that the residual ratio with respect to intact sample was 95% or more.

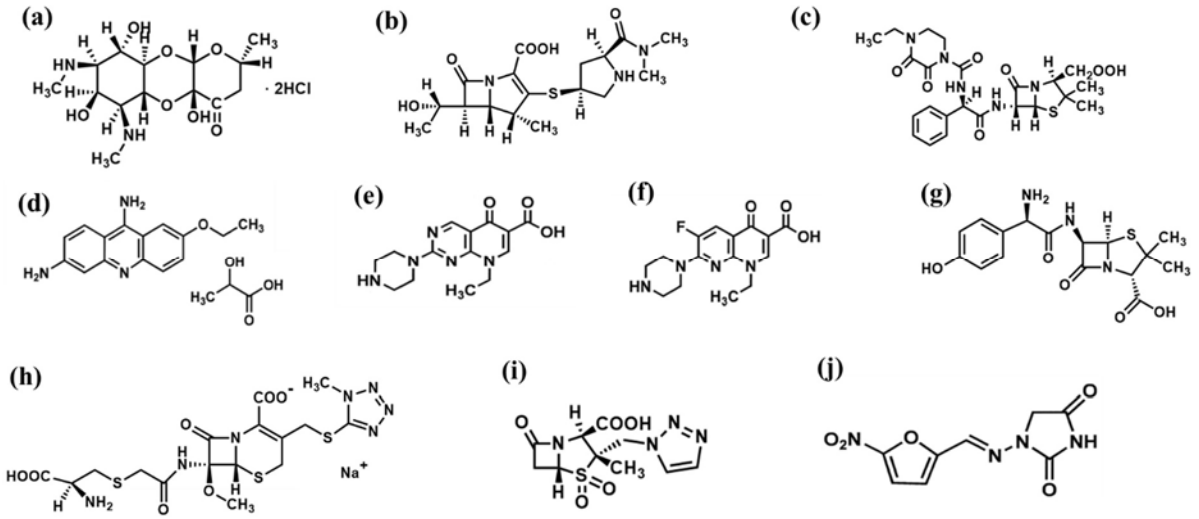

Figure 3-2 Chemical structure: (a) Spectinomycin dihydrochloride (SPE), (b) Meropenem (MEPM), (c) Piperacillin (PIPC), (d) Acrinol (ACR), (e) Pipemidic acid (PIPM), (f) Enoxacin (ENO), (g) Amoxicillin (AMO), (h) Cefminox Sodium (CEF), (i) Tazobactam (TAZ), (j) Nitrofrantoin (NF).

3.2.2. Preparation of Powderly Hydrates

Powderly crystals of NF monohydrate were obtained by dissolving NF (0.5 g) in 100 mL of acetone-water solution (volume ratio 1:1) at 55°C, followed by cooling to room temperature, and needle-shaped crystal appeared within 2 hours. Crystals were separated by filtration and dried overnight under ambient conditions. Exposure to direct light was prevented during the entire work.

Powderly crystals of ENO trihydrate were obtained by dissolving ENO sesquihydrate in methanol at 40°C, followed by cooling overnight in the refrigerator (2-8°C). The solid phase was collected by filtration and dried under ambient conditions.

3.2.3. Differential Scanning Calorimetry (DSC)

TA Q200 DSC (TA Instruments) was used to estimate phase transition temperature between two anhydrate forms of ACR, anhydrate I, and anhydrate II, ACR monohydrate was measured at a heating rate of 5K/min under a nitrogen purge of 50 mL/min.

3.2.4. Thermogravimetric Analysis (TGA)

TGA was performed using TA Q500 TGA (TA Instruments) by dynamic mode, in which the heating rate is continuously modified in response to weight change of the sample, sensitivity of 1, resolution of 5°C and heating rate of 50°C /min, with platinum pans. The measurements were conducted under a suitable nitrogen gas flow rate (60-100 mL/min) depending on hydration number of corresponding hydrates. Temperature calibration were carried out using nickel.

3.2.5. Powder X-Ray Diffraction (PXRD)

PXRD measurements were performed at room temperature on SmartLab 3 kW (Rigaku) using Cu Kα radiation at 1.54186Å at a voltage of 40 kV and current of 30 mA. Data were collected at a scan rate of 4°/min.

3.2.6. Powder X-Ray Diffraction-Differential Scanning Calorimetry (XRD-DSC)

Simultaneous measurements of powder X-ray diffraction data and differential scanning calorimetry (XRD-DSC) were performed on SmartLab 3 kW (Rigaku) using Cu Kα radiation at 1.54186Å at a voltage of 40 kV and current of 30 mA,

and a DSC attachment at a heating rate of 5°C /min with aluminum pans under a nitrogen gas flow of 200 mL/min. X-ray diffraction data were collected at a scan rate of 20°/min.

3.2.7. Storage of dehydrated sample under controlled relative humidity environment

Dehydrated samples were prepared by heating to dehydration temperature in the TGA instrument prior to storage in a desiccator containing a saturated salt solution of sodium chloride (75%RH). Samples were collected at one day of storage, then checked whether dehydrated samples revert to its original hydrate forms under the controlled relative humidity environment.

3.2.8. Dynamic Vapor Sorption (DVS)

Dynamic Vapor Sorption Advantage (Surface Measurement Systems) was used for the isothermal analyses. The hydrate samples were mounted on a balance, preheated to obtain dehydrated samples, and absorbed in controlled relative humidity air which was selected individually to suit reverting to original hydrates. The dehydrated sample masses were monitored at 25, 30 and 35°C during rehydration. The rehydration process from dihydrate to pentahydrate was investigated regarding SPE. In rehydration studies, fraction un-rehydrated (1-α) was calculated from the following equation:

$$1-\alpha = (m_0-m_t)/w_c$$

where α is the fraction rehydrated, m_0 is the mass of the sample before preheating, m_t is the mass of the rehydrated sample at time t, and w_c is the theoretical water content as hydrate in the sample used. Hancock-Sharp equation[41] was used to perform kinetic analyses:

$$\ln[-\ln(1-\alpha)] = m \ln t + \beta$$

where β is a constant which depends on the rate constant k, m is a characteristic value of the rehydration mechanism. The value of m was calculated from a slope of the plot of ln[-ln(1-α)] against ln t. In order to estimate the degree of suitability of the model, the known solid-state kinetic equations[42] which should be selected

based on the value *m* determined above were used, then correlation coefficients were calculated.

3.3. Results and Discussion

3.3.1. Phase Transition Behavior

The dehydration and rehydration cycling behavior using hydrate samples and dehydrated samples stored under the controlled humidity were characterized by TGA, PXRD, XRD/DSC. The phase transition behavior of reverting to the corresponding hydrate form from its anhydride form was observed in SPE, MEPM, ACR, PIPM, ENO and PIPC. PIPM and ACR were found to have two anhydrous forms, anhydrous I and anhydrous II. Anhydrate I transformed to anhydrate II at around 176-187°C by XRD/DSC (**Figure 3-3**) and around 190-200°C by DSC (**Figure 3-4**), respectively. Thus, the dehydration-rehydration cycling test of PIPM and ACR were determined between anhydrate I and the corresponding hydrate in this study.

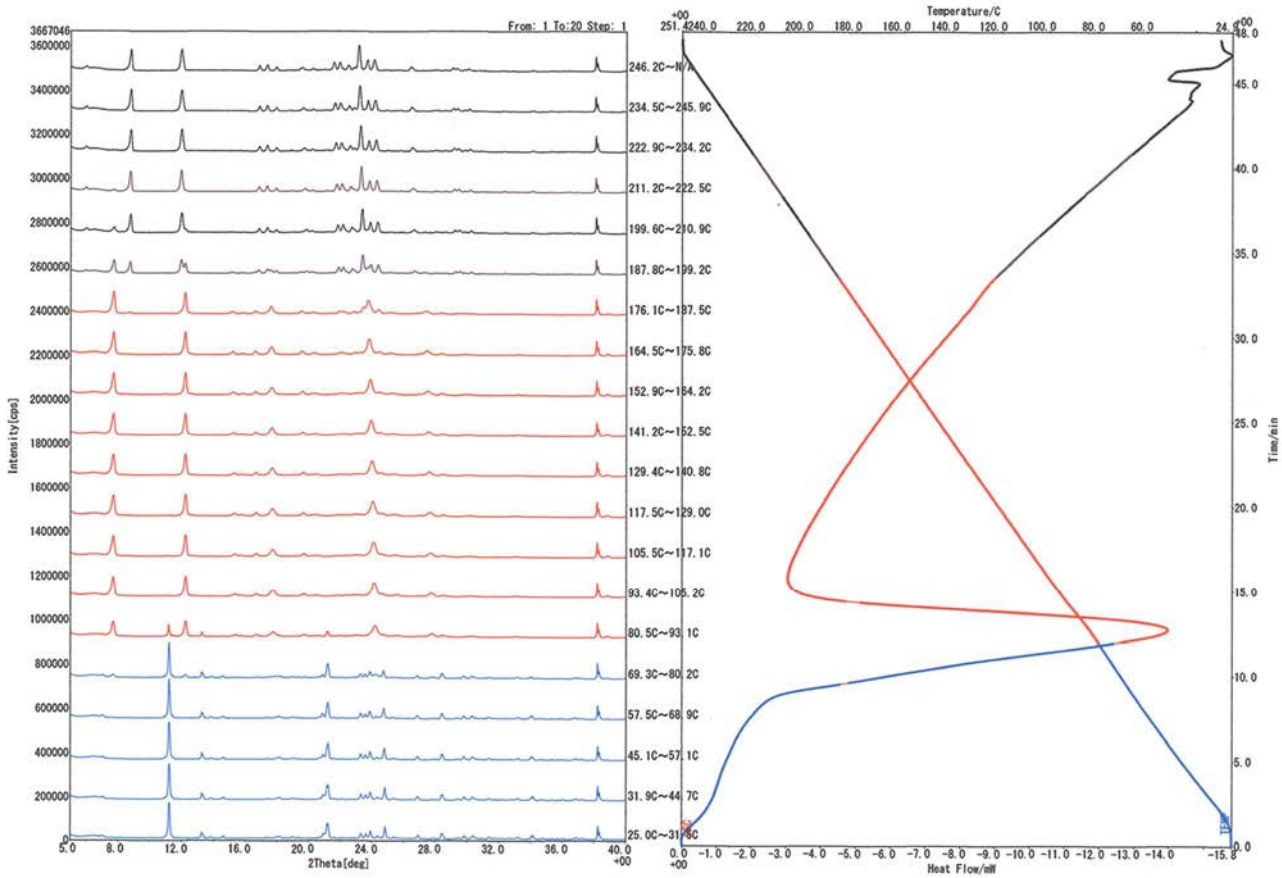

Figure 3-3 XRD/DSC results of PIPM trihydrate (blue), anhydrate I (red) and anhydrate II (black).

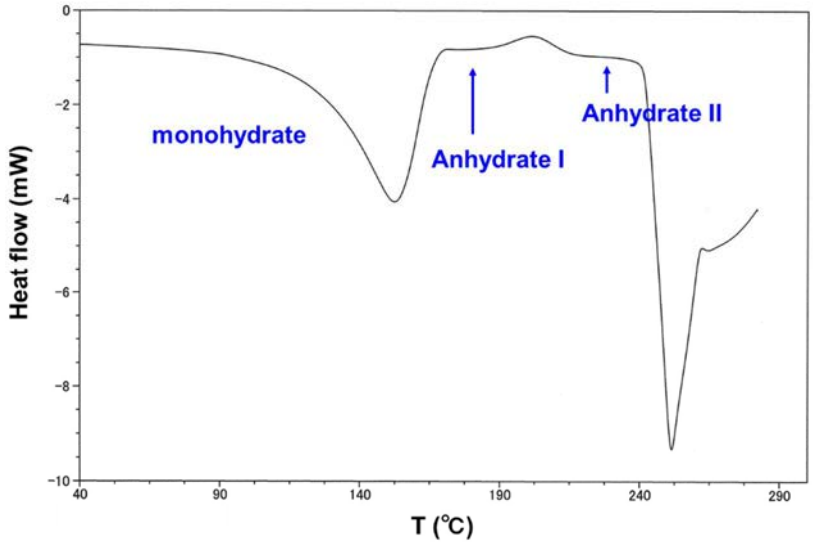

Figure 3-4 DSC curve of ACR monohydrate at heating rates of 5°C /min.

SPE pentahydrate was found to dehydrate in two steps, corresponding to the loss of three water molecules in the first step (lower temperature) and two water molecules in the second step (higher temperature) from TGA measurement performed in advance (**Figure 3-5**). Specifically, the process of rehydration from both of dihydrate and anhydrate to pentahydrate for SPE, from anhydrate I to trihydrate for PIPM, from anhydrate I to monohydrate for ACR and from anhydrate to trihydrate for ENO sesquihydrate were observed.

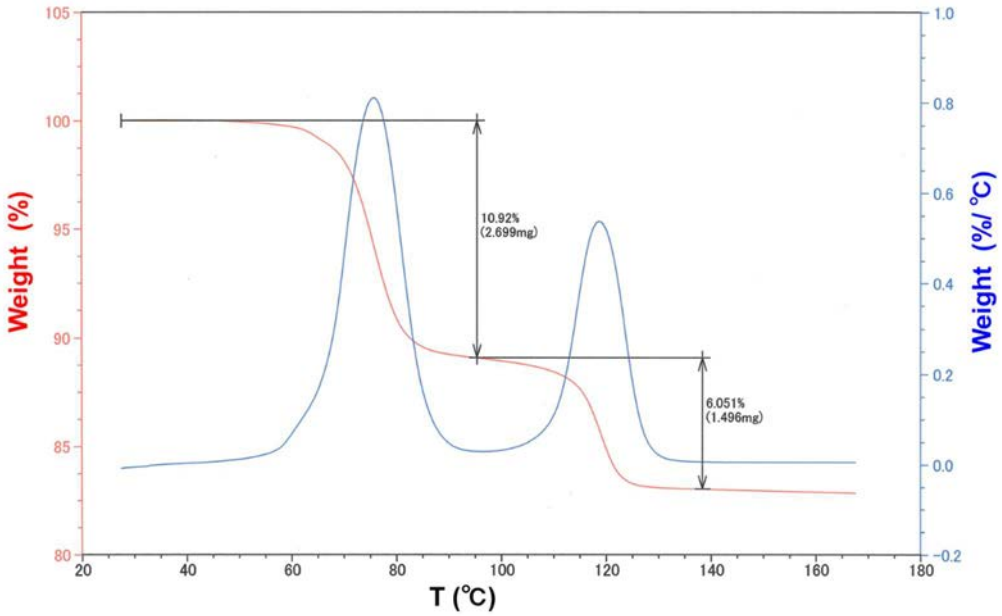

Figure 3-5 TGA curve (red) and derivative curve (blue) for intact sample of SPE pentahydrate.

Regarding whether to rehydrate or not, the results of TGA and PXRD measurements of intact samples were confirmed to dehydrated samples stored in 75%RH desiccator for one day. The results of TGA and PXRD of SPE were shown in **Figure 3-6** and **Figure 3-7** , respectively. The TGA curves of SPE dihydrate stored in 75%RH condition, and the intact sample showed a weight loss of 10.7%, which is equivalent to three water molecules in SPE pentahydrate (calc. 10.8%). Moreover, XRD patterns of dihydrate and anhydrate, which were once dehydrated and stored in 75%RH condition, were nearly identical to that of pentahydrate. These results suggested that dihydrate and anhydrate, which were metastable forms, gained moisture from the controlled humidity environment air, in order to form pentahydrate, which was the stable form. Similarly, the phase transition behavior from dehydrated to hydrate form was observed in MEPM, ACR, PIPM, ENO and PIPC.

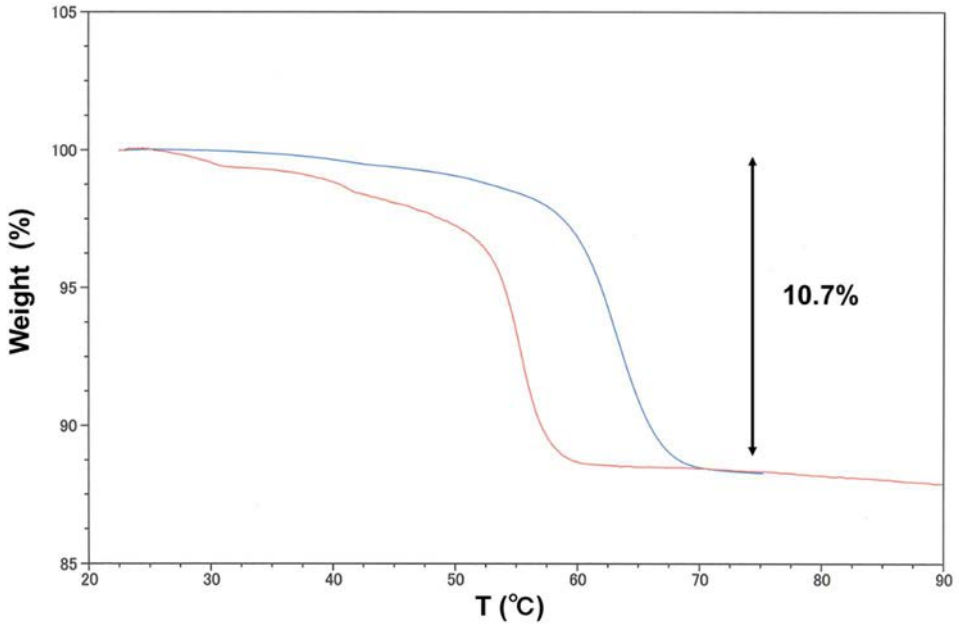

Figure 3-6 TGA curves of SPE pentahydrate, intact (blue) and dihydrate stored in 75%RH desiccator (red).

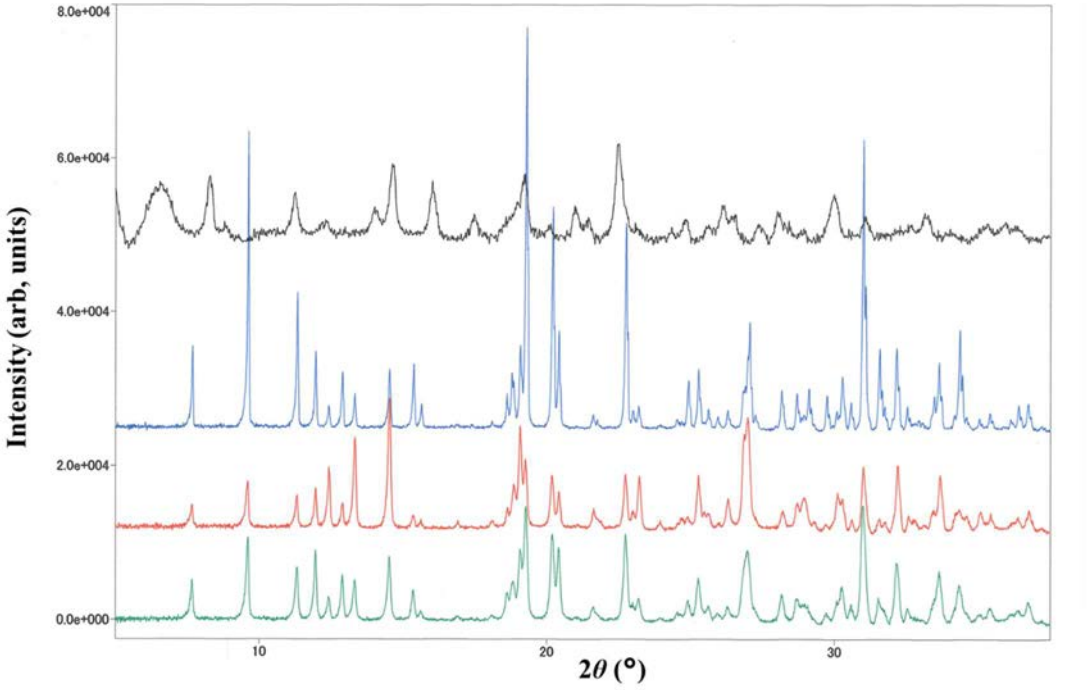

Figure 3-7 XRD patterns of SPE, dihydrate (black), pentahydrate (blue) and dihydrate stored in 75%RH desiccator (red), anhydrate stored in 75%RH desiccator (green).

On the other hand, the dehydrated forms of CEF, AMO, TAZ and NF stored in 75%RH condition were not reverted to initial hydrate forms. The results of TGA and PXRD measurements of CEF and TAZ were shown in **Figure 3-8 -Figure 3-11**. TGA curve of the intact sample of CEF heptahydrate showed a weight loss of 18.5% which was equivalent to five water molecules in CEF heptahydrate (calc. 18.5%). However, the result of the TGA measurement of the dehydrated sample stored in 75%RH condition showed a gentle curve, which is due to the removal of not crystal water but free water. The dehydrated CEF stored in 75%RH condition was found to transform into an amorphous phase because Bragg peaks almost disappeared, and only a diffuse halo was present on the XRD pattern.

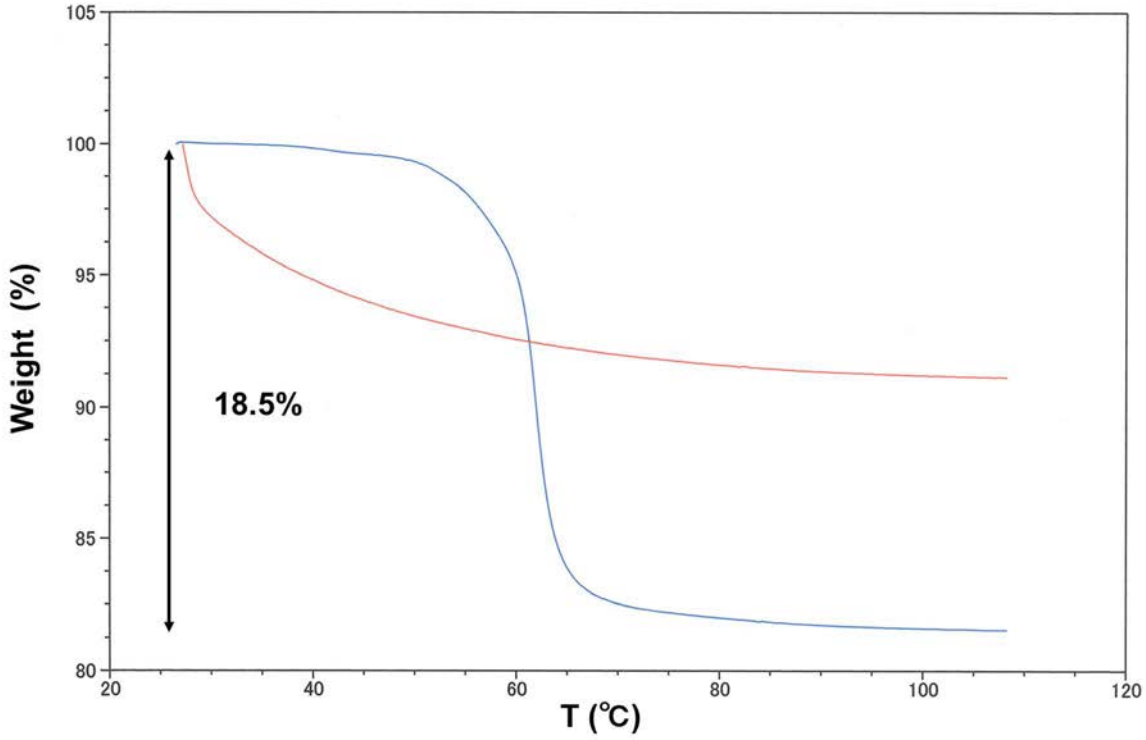

Figure 3-8 TGA curves of CEF heptahydrate, intact (blue) and dehydrated sample stored in 75%RH desiccator (red).

The transformation from dehydrated to hydrate form of CEF could not be triggered in the rehydration process by exposure to humid air. The results of TGA and PXRD measurements of AMO suggested similar behavior.

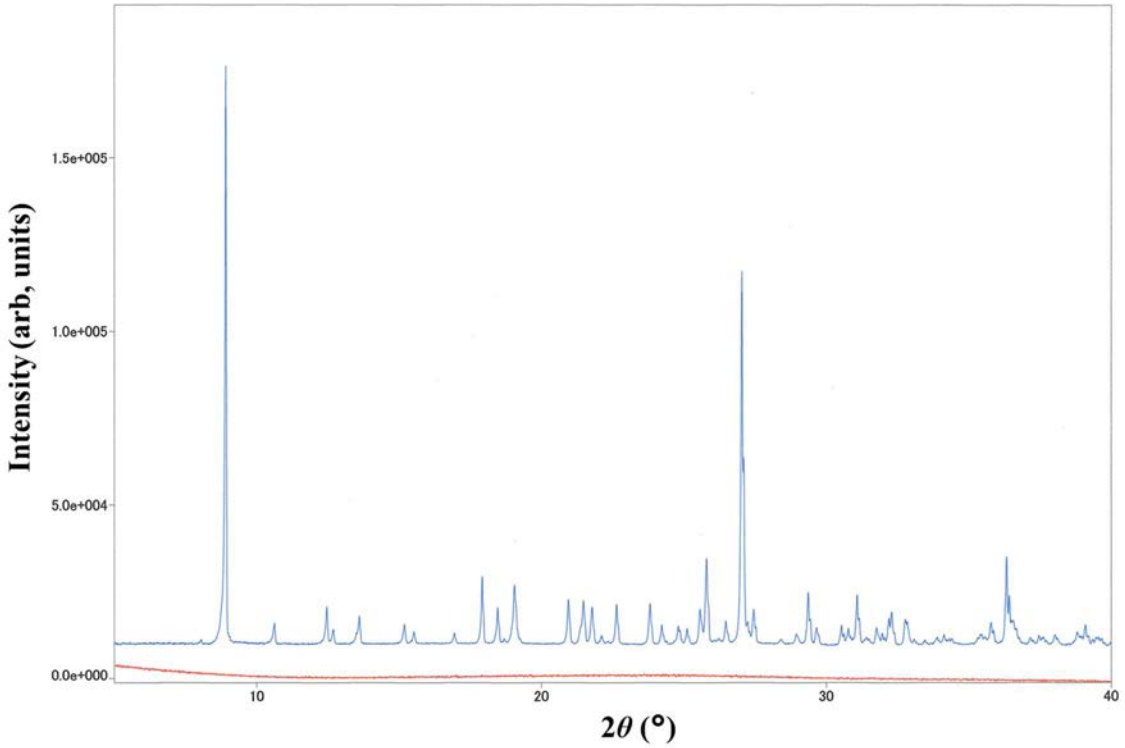

Figure 3-9 XRD patterns of CEF, heptahydrate (blue) and dehydrated sample stored in 75%RH desiccator (red).

In the case of TAZ hemihydrate, the TGA curve of the intact sample showed weight loss of 2.97%, which was equivalent to 0.5 molecules of the water molecule in TAZ hemihydrate (calc. 2.91%), although of the dehydrated sample stored in 75%RH condition showed no weight loss in contrast with the intact sample (**Figure 3-10**). Besides, the XRD pattern of the dehydrated sample stored in 75%RH condition was the same as that of anhydrate form (**Figure 3-11**). Thus, dehydrated TAZ showed no signs of rehydration and was still in anhydride form under higher relative humidity conditions. A similar result was provided in NF. NF anhydrate obtained after dehydration was clarified to be anhydrate β form[72] from its XRD patten.

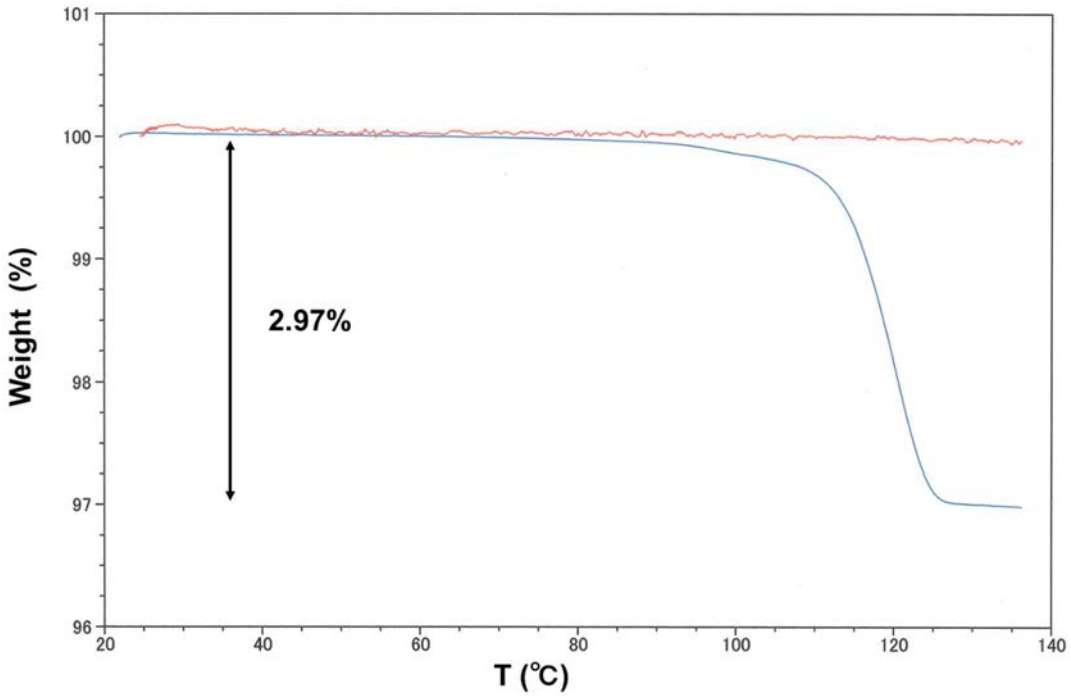

Figure 3-10 TGA curves of TAZ hemihydrate, intact (blue) and anhydrate stored in 75%RH desiccator (red).

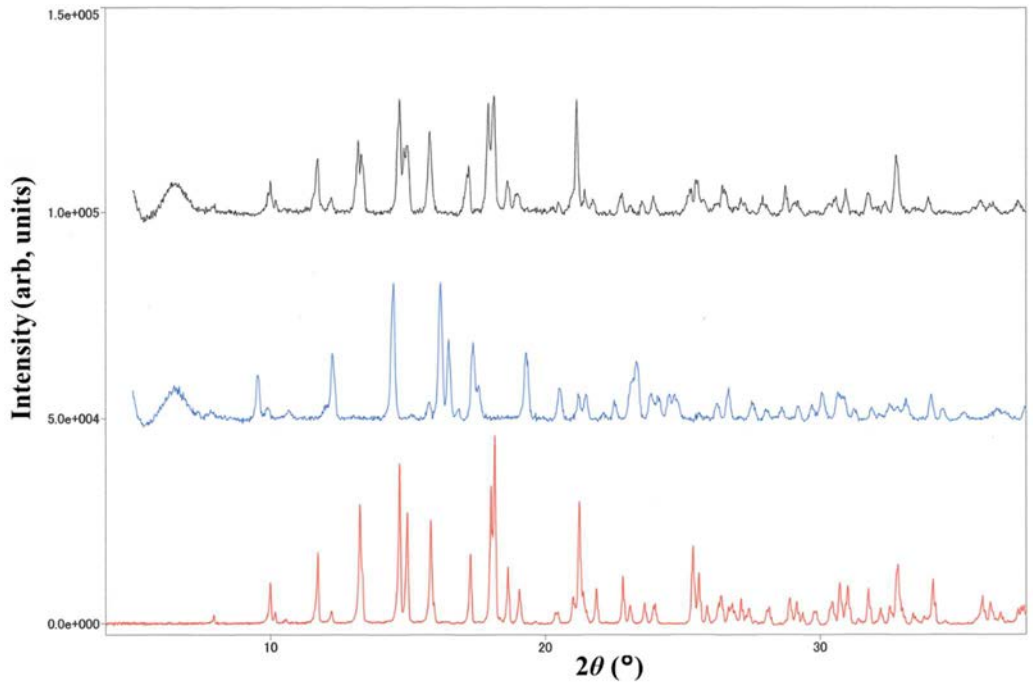

Figure 3-11 XRD patterns of TAZ, anhydrate (black), hemihydrate (blue) and dehydrated sample stored in 75%RH desiccator (red).

The phase transformations of SPE, MEPM, ACR, PIPM, ENO (sesquihydrate and trihydrate), PIPC, CEF, AMO, TAZ and NF in dehydration processes were further investigated by XRD/DSC measurements (**Figure 3-12** - **Figure 3-13**).

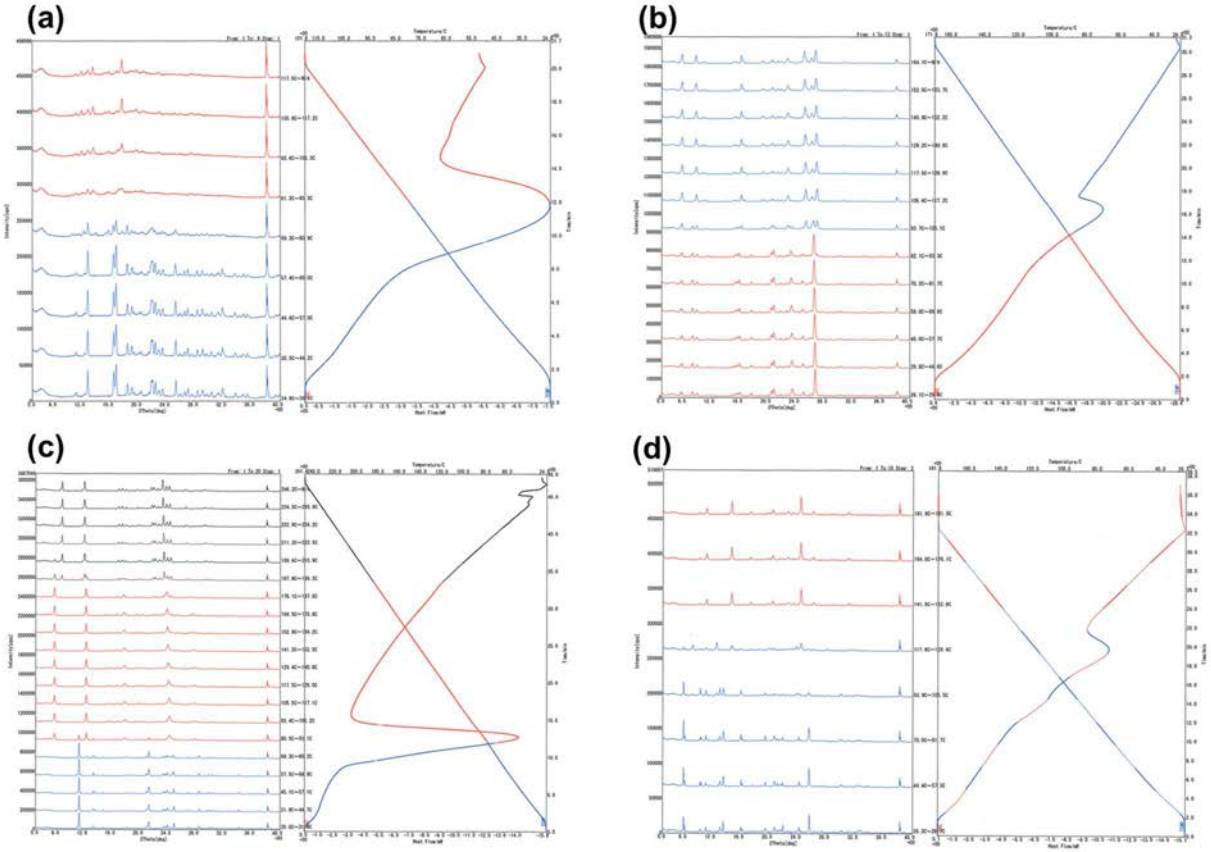

Figure 3-12 XRD/DSC results of (a)MEPM trihydrate, (b)ACR trihydrate, (c)PIPM trihydrate and (d)ENO sesquihydrate. Blue, red and black pattern indicates hydrate, anhydrate and anhydrate II, respectively.

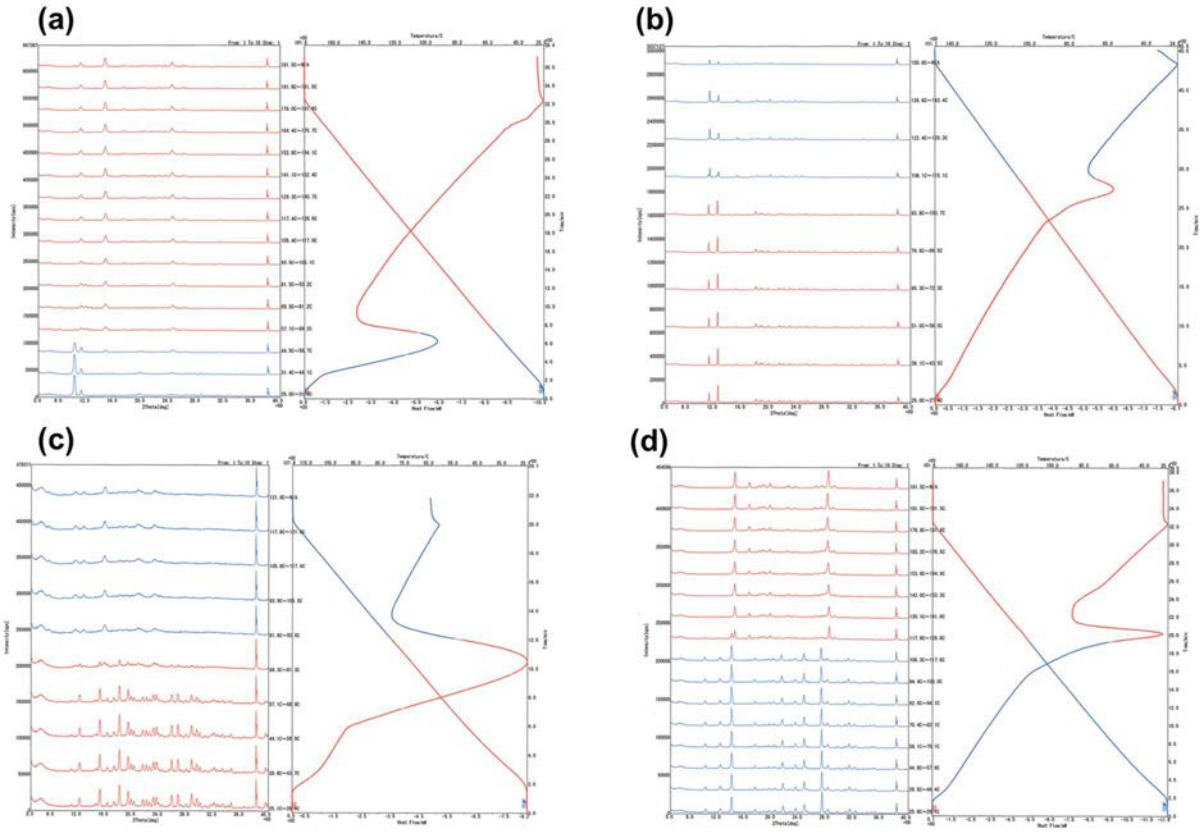

Figure 3-13 XRD/DSC results of (a)ENO trihydrate, (b)PIPC monohydrate, (c)AMO trihydrate and (d)NF monohydrate. Blue or red pattern indicates hydrate and anhydrate, respectively.

Variable temperature XRD patterns of SPE, CEF and TAZ were shown in **Figure 3-14** -**Figure 3-16**. There were significant changes of XRD patterns of SPE pentahydrate at around 341K and 402K, and they indicate the phase transformations from pentahydrate to dihydrate and from dihydrate to anhydrate, respectively. Additionally, the anhydride form was suggested to be an amorphous phase according to its XRD halo pattern. The significant changes in XRD patterns were also observed in CEF and TAZ. The phase transition temperature from heptahydrate to anhydrate was estimated to be around 353K in CEF, and that from hemihydrate to anhydrate was estimated to be around 390K in TAZ. From their XRD patterns, anhydride forms of CEF and TAZ were suggested to be an amorphous form and a new crystal form, respectively. The schematic diagram of phase transformation of SPE, CEF and TAZ showed in **Figure 3-17** indicate dehydration and rehydration pathways.

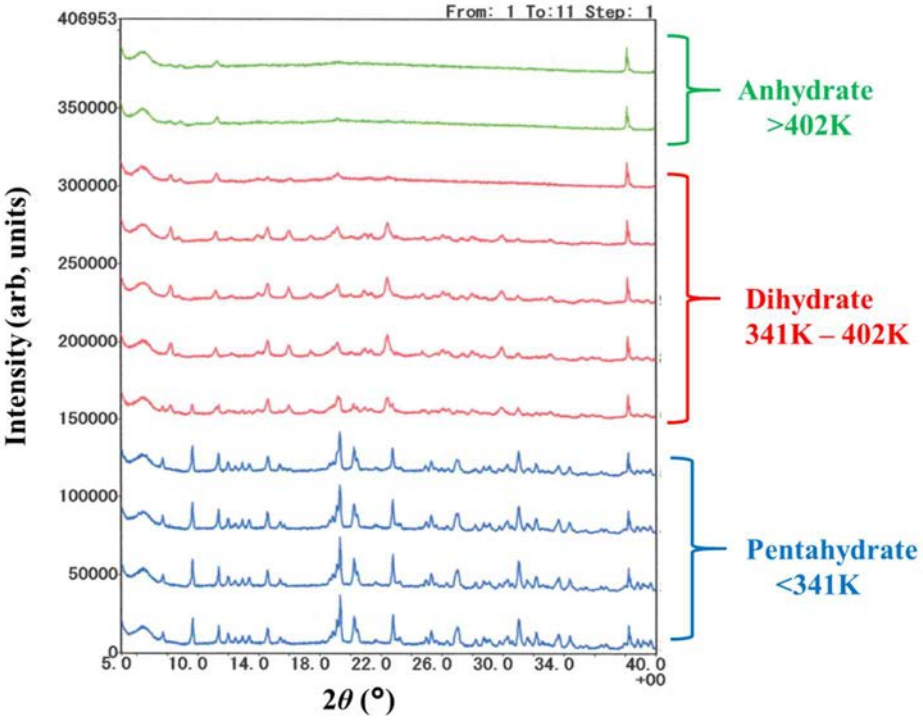

Figure 3-14 XRD patterns of SPE pentahydrate at variable temperature by XRD/DSC measurement, pentahydrate (blue), dihydrate (red) and anhydrate (green).

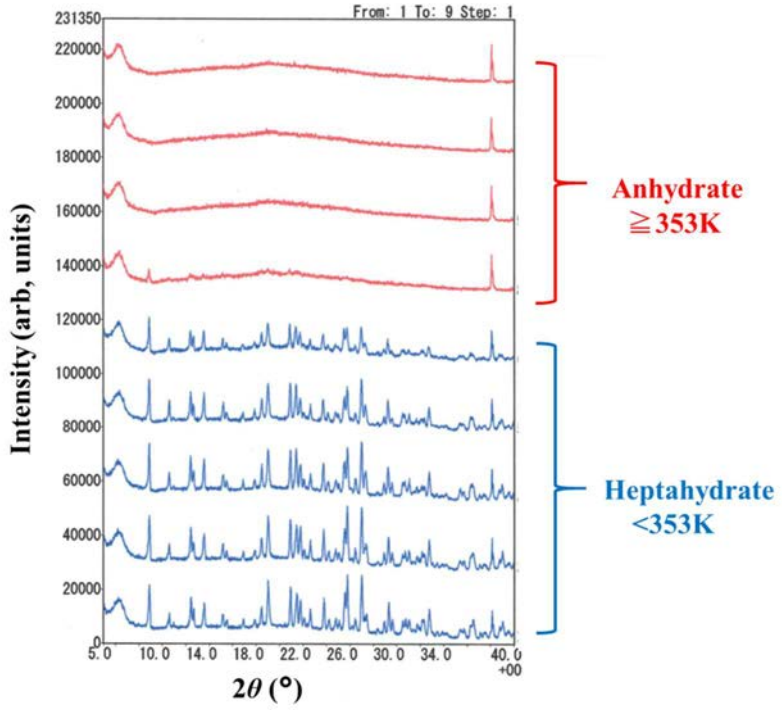

Figure 3-15 XRD patterns of CEF heptahydrate at variable temperature by XRD/DSC measurement, heptahydrate (blue) and anhydrate (red).

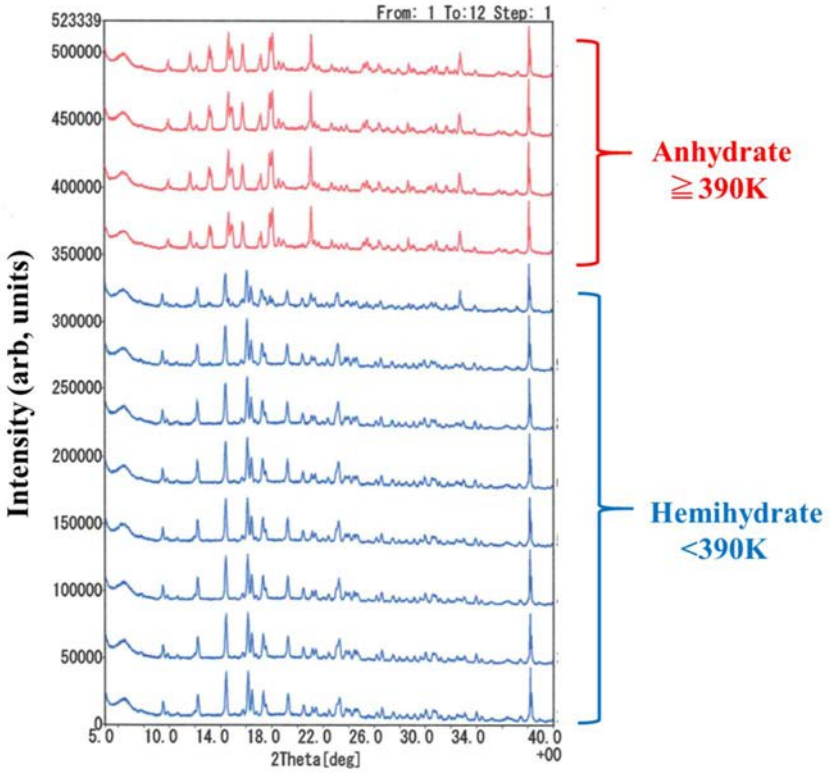

Figure 3-16 XRD patterns of TAZ hemihydrate at variable temperature by XRD/DSC measurement, hemihydrate (blue) and anhydrate (red).

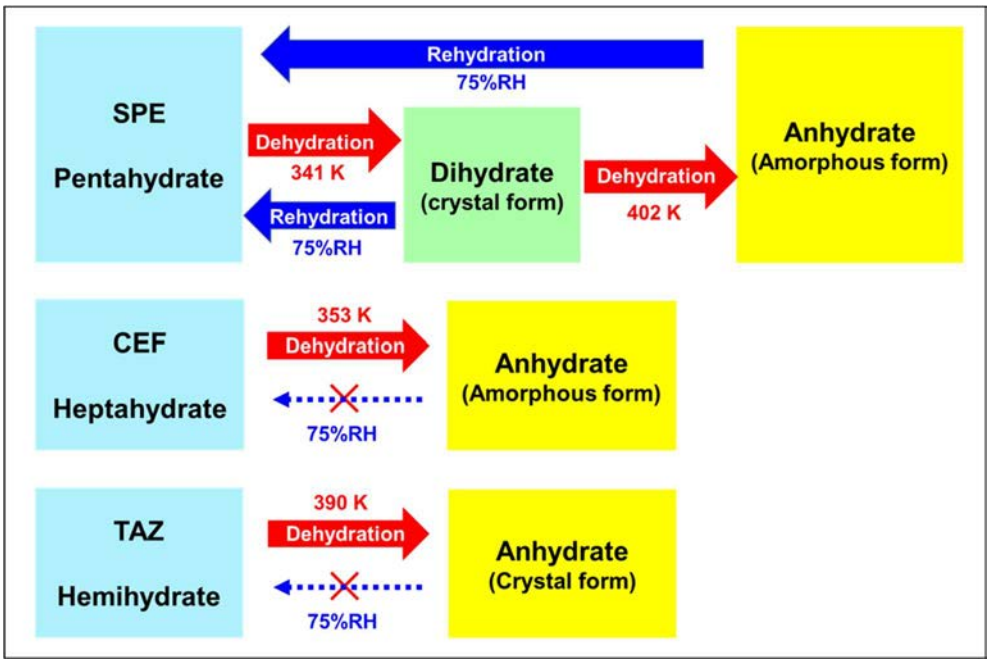

Figure 3-17 Schematic diagram of phase transformation of SPE, CEF and TAZ.

MEPM, PIPC, ENO, ACR and PIPM formed anhydrides after dehydration, but upon rehydration recovered to the original hydrates like SPE (**Figure 3-18**).

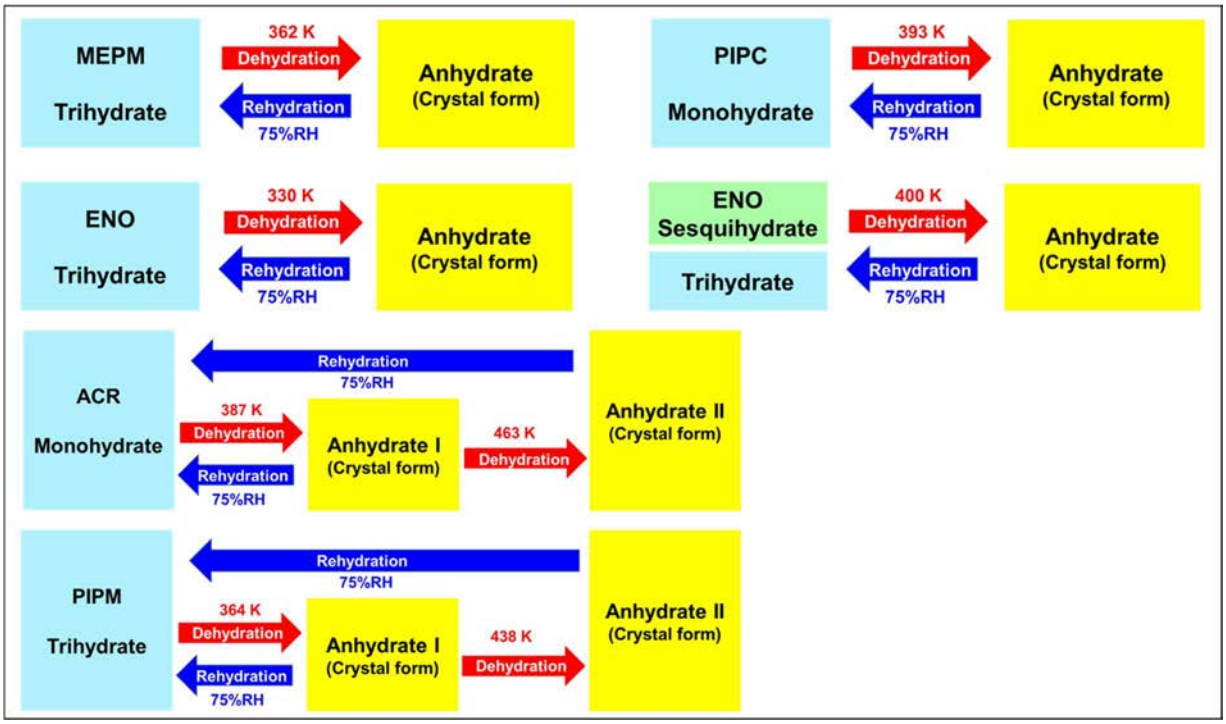

Figure 3-18 Schematic diagram of phase transformation of MEPM, PIPC, ENO, ACR and PIPM.

AMO formed an amorphous anhydride after dehydration and did not recover to the original hydrate like CEF. NF formed crystal anhydride after dehydration and did not recover to the original hydrate like TAZ (**Figure 3-19**).

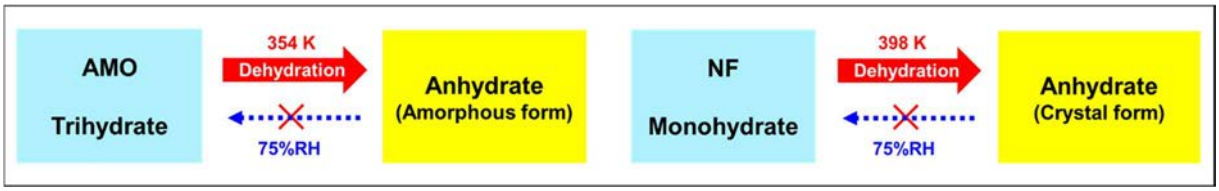

Figure 3-19 Schematic diagram of phase transformation of AMO and NF.

The dehydration and rehydration behavior of eleven hydrate crystals revealed three types of transition behaviors: (I) dehydration - anhydride crystal - rehydration (recovery), (II) dehydration – amorphization – no rehydration, and (III) dehydration - anhydride crystal - no rehydration.

3.3.2. Noniso-thermal E_a for dehydration

The values of dehydration E_a of PIPC monohydrate, ACR monohydrate, PIPM trihydrate, ENO trihydrate, ENO sesquihydrate, AMO trihydrate and NF monohydrate were also obtained by conducting in the same manner as described in 2.3.2. In order to check the precision of the data of dehydration E_a, all measurements were carried out three times, and the average values and relative standard deviations of all samples were given in **Table 3-2**. The relative standard deviations were from 0.2 to 9.2% in the hydrate samples used in this study and they could be used as measurement errors of dehydration E_a. The values of dehydration E_a of TAZ and NF were twice as high as those of SPE, MEPM, PIPC, ACR, PIPM, AMO, CEF, ENO trihydrate, and the sesquihydrate. The difference of E_a of them was more than 67 kJ/mol, and the magnitude of this difference was greater than the measurement errors.

Table 3-2 The noniso-thermal dehydration E_a obtained through triplicate measurement and statistic parameters.

Hydrate sample	Hydrate type	Dehydration Ea (kJ/mol)				RSD (%)
		1	2	3	av.	
SPE	Penta	71.1	68.3	68.2	69.0	2.4
	Di	90.2	89.8	90.5	90.0	0.4
MEPM	Tri	71.6	72.2	71.6	71.8	0.5
PIPC	Mono	81.2	75.5	76.9	77.9	3.8
ACR	Mono	79.2	79.3	79.0	79.2	0.2
PIPM	Tri	91.8	89.9	90.1	90.6	1.1
ENO	Tri	68.0	65.0	67.3	66.8	2.4
ENO	Sesqui	90.4	91.5	84.9	89.0	4.0
AMO	Tri	63.2	62.1	65.4	63.5	2.6
CEF	Hepta	78.2	84.6	79.5	80.8	4.2
TAZ	Hemi	158.2	156.3	157.4	157.3	0.6
NF	Mono	156.7	174.2	188.4	173.1	9.2

Form these results, in the dehydration E_a assessment using the noniso-thermal method, it was possible to classify into two groups, and the high energy group had twice the energy of the low energy group.

3.3.3. Rehydration E_a

Further, to explore insights on rehydration propensities converting from the dehydrated form to the hydrate form, kinetic data were obtained in the isothermal mode at 25, 30 or 35°C by monitoring the rehydration process from dehydrated samples to its hydrate form with DVS experiments. The rehydration curve of PIPM at 25°C in controlled 95%RH air were shown in **Figure 3-20**.

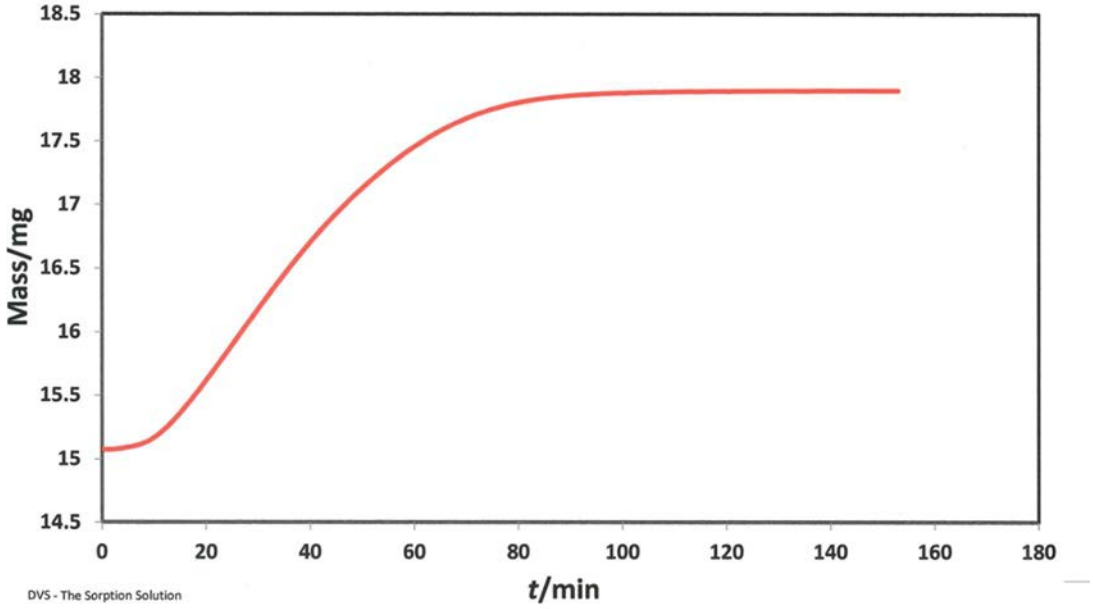

Figure 3-20 Rehydration curve of dehydrated PIPM at 25°C/95%RH.

To obtain quantitative values from the kinetics data, it is important to choose the appropriate mathematical model describing the rehydration mechanism. The values in the range of 0.1-0.9 fraction rehydrated (α) were fitted to the Hancock-Sharp equation to determine the rehydration mechanism, and m was calculated to be 2.1 from the slope of the line (**Figure 3-21**).

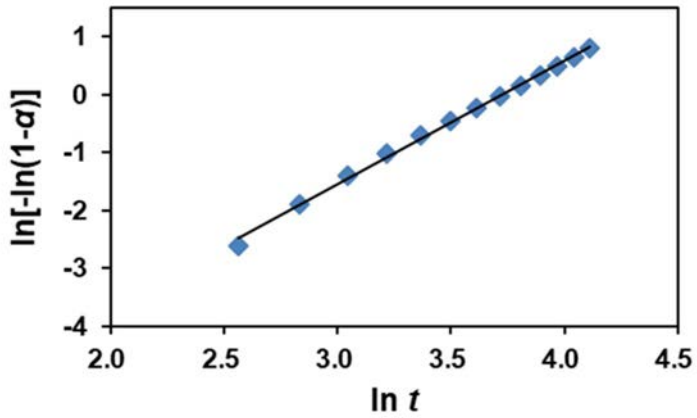

Figure 3-21 Hancock-Sharp plot for rehydration of PIPM at 25°C/95%RH.

The value of m allowed us to predict that the rehydration mechanism of PIPM was Avrami-Erofe'ev A2 model by referring to m for solid-state reaction rate equations (**Table 3-3**). The slightly higher correlation coefficient R (0.9964) obtained using A2 model as compared to that using Avrami-Erofe'ev A3 model (0.9963), suggested the better suitability of A2 model for describing the rehydration mechanism of PIPM.

Table 3-3 Value of m for solid-state reaction rate equations.[9,10]

Model	*m*	Equation
1-D diffusion (D1)	0.62	$\alpha^2 = kt$
2-D diffusion (D2)	0.57	$[(1-\alpha)\ln(1-\alpha)]+\alpha = kt$
3-D diffusion-Jander eqn. (D3)	0.54	$[1-(1-\alpha)^{1/3}]^2 = kt$
Ginstling-Brounshtein (D4)	0.57	$1-(2\alpha/3)-(1-\alpha)^{2/3} = kt$
First-order (F1)	1.00	$-\ln(1-\alpha) = kt$
Contracting area (R2)	1.11	$1-(1-\alpha)^{1/2} = kt$
Contracting volume (R3)	1.07	$1-(1-\alpha)^{1/3} = kt$
Zero-order (F0)	1.24	$\alpha = kt$
Avrami-Erofe'ev (A2)	2.00	$[-\ln(1-\alpha)]^{1/2} = kt$
Avrami-Erofe'ev (A3)	3.00	$[-\ln(1-\alpha)]^{1/3} = kt$

The rehydration rate constant was evaluated using A2 model for identification of the best fit model. A2 model fitting at 25°C/95%RH was shown in **Figure 3-22**. Rehydration rate constants were calculated using the slope obtained from $[-\ln(1-\alpha)]^{1/2}$ - t graph.

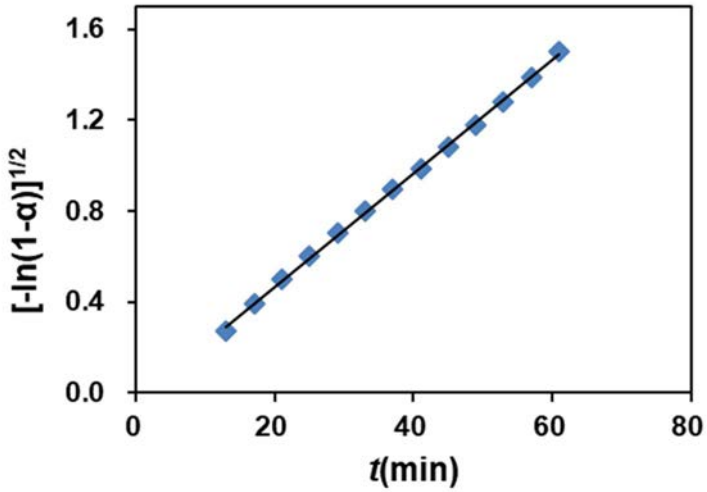

Figure 3-22 Avrami – Erofe'ev A2 model fitting of PIPM at 25°C/95%RH.

The calculated results monitored at 25°C/95%RH, 30°C/95%RH and 35°C/95%RH were given in **Table 3-4**. It was seen that the rehydration rate constant increased by increasing temperature.

Table 3-4 Rehydration rate constants of PIPM at 25 °C /95%RH, 30 °C /95%RH and 35 °C /95%RH.

Rehydration temperature (°C)	Rehydration rate constant (min^{-1})
25	0.0249
30	0.0295
35	0.0368

The Arrhenius plot was shown in **Figure 3-23**, and the rehydration E_a of PIPM was estimated to be 32.5 kJ/mol from the slope of the line.

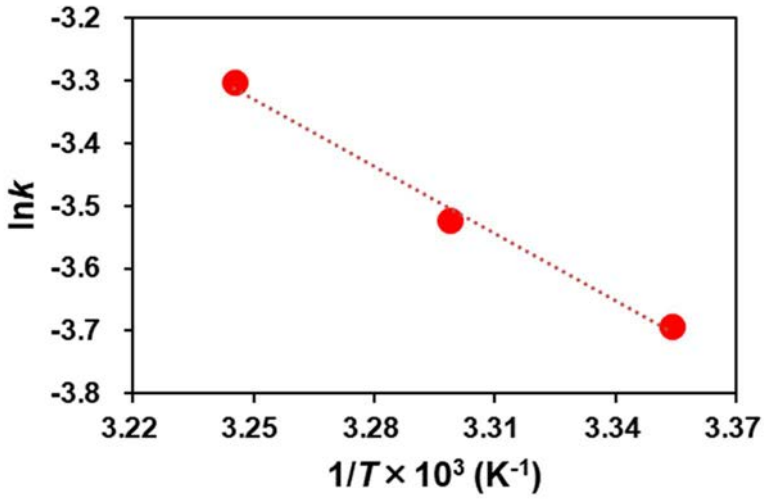

Figure 3-23 Arrhenius plot obtained by plotting ln*k* as a function of 1/*T* for PIPM.

Forming PIPM trihydrate was confirmed at the end of rehydration study at 25°C/95%RH from PXRD measurements (**Figure 3-24**).

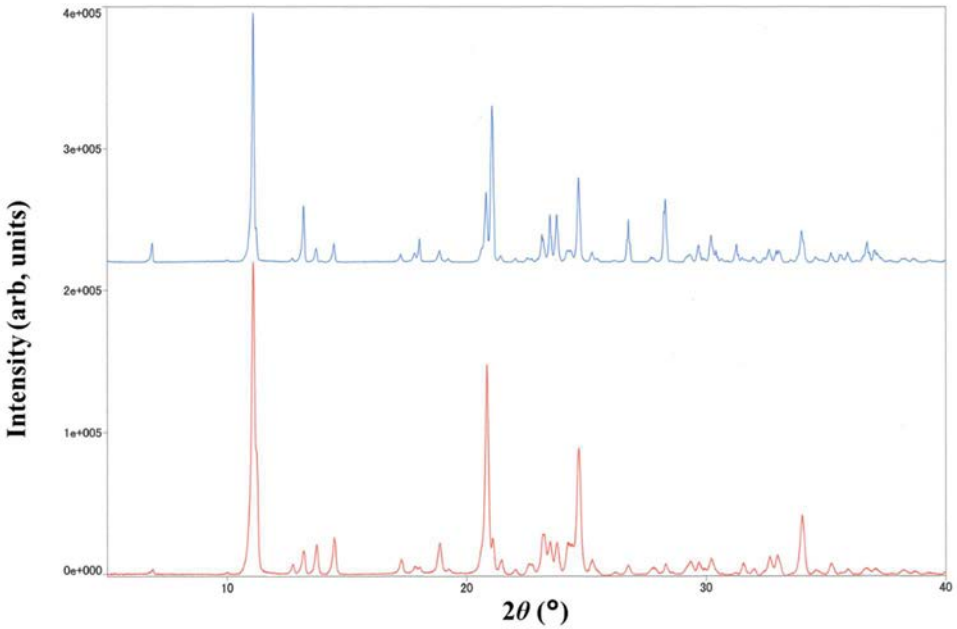

Figure 3-24 XRD patterns of PIPM, trihydrate (red) and after rehydration study at 25°C /95%RH (blue).

E_a gave values within ±5 kJ/mol, or about 15 % based on confidence limit which was equal to the relative standard deviation obtained by triplicate measurement. Since the transition behavior during the rehydration process of ENO and SPE were clear, the rehydration process from anhydrate to trihydrate was monitored for ENO sesquihydrate and from dihydrate to pentahydrate for SPE pentahydrate. Rehydration kinetic analysis of CEF, AMO, TAZ and NF were not conducted, because they were not reverted to initial hydrate forms in the dehydration-rehydration cycling study. The rehydration kinetics parameters of SPE, MEPM, PIPC, ACR, PIPM, ENO trihydrate and sesquihydrate were summarized in **Table 3-5**. For the samples used in this study, the rehydration E_a was estimated to be between 18.5 and 70.6 kJ/mol.

Table 3-5 Rehydration kinetics parameters. Rehydration E_a of PIPM is average value.

Hydrate sample	Rehydation E_a (kJ/mol)	Fraction rehydrated α	Relative humidity (%)	Mathematical model[13]	Kinetic equation[42]
SPE	32.8	0.2 - 0.7	80	F0	$\alpha = kt$
MEPM	18.5	0.0 - 0.5	50	A2	$[-\ln(1-\alpha)]^{1/2} = kt$
PIPC	18.8	0.4 - 0.8	50	F1	$-\ln(1-\alpha) = kt$
ACR	35.0	0.2 - 0.7	50	A2	$[-\ln(1-\alpha)]^{1/2} = kt$
PIPM	29.9	0.1 - 0.9	95	A2	$[-\ln(1-\alpha)]^{1/2} = kt$
ENO tri	70.6	0.1 - 0.9	95	A2	$[-\ln(1-\alpha)]^{1/2} = kt$
ENO sesqui	25.4	0.1 - 0.9	95	A2	$[-\ln(1-\alpha)]^{1/2} = kt$

As described above, in the rehydration (recovery) group (I), the weight change rate of the rehydration process was analyzed kinetically to calculate rehydration E_a.

3.3.4. Potential Energy Profile

Two hydrate crystals of "Class 1", MEPM trihydrate and SPE pentahydrate, were selected and energetic schemes were shown in **Figure 3-25** and **Figure 3-26**, respectively, based on rehydration E_a (**Table 3-5**) and dehydration E_a (**Table 2-10**) by the iso-thermal method. E_a of them are tabulated in **Table 3-6**. The hydrate crystals of "Class 2" and "Class 3" were not discussed here because they did not occur rehydration.

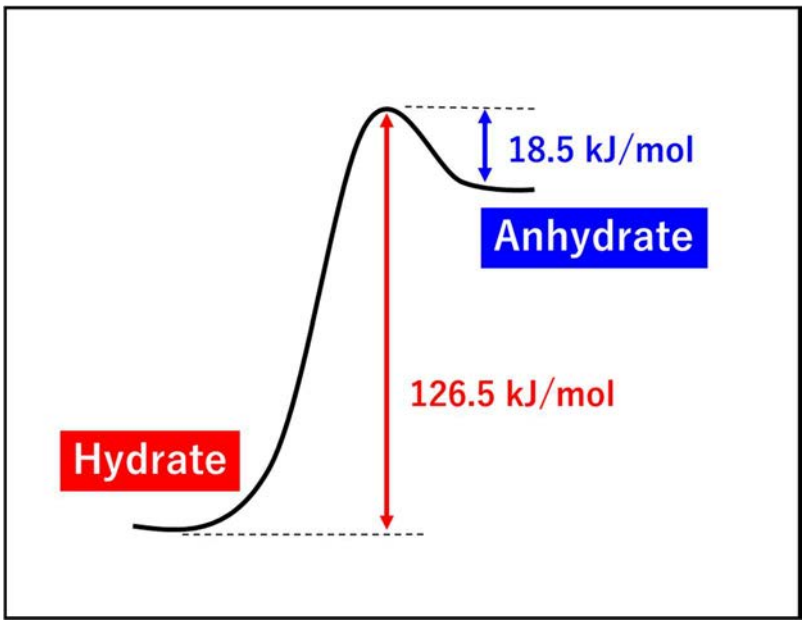

Figure 3-25 Schematic potential diagram of MEPM along the path of transformation. Red and blue arrows indicate dehydration E_a and rehydration E_a, respectively.

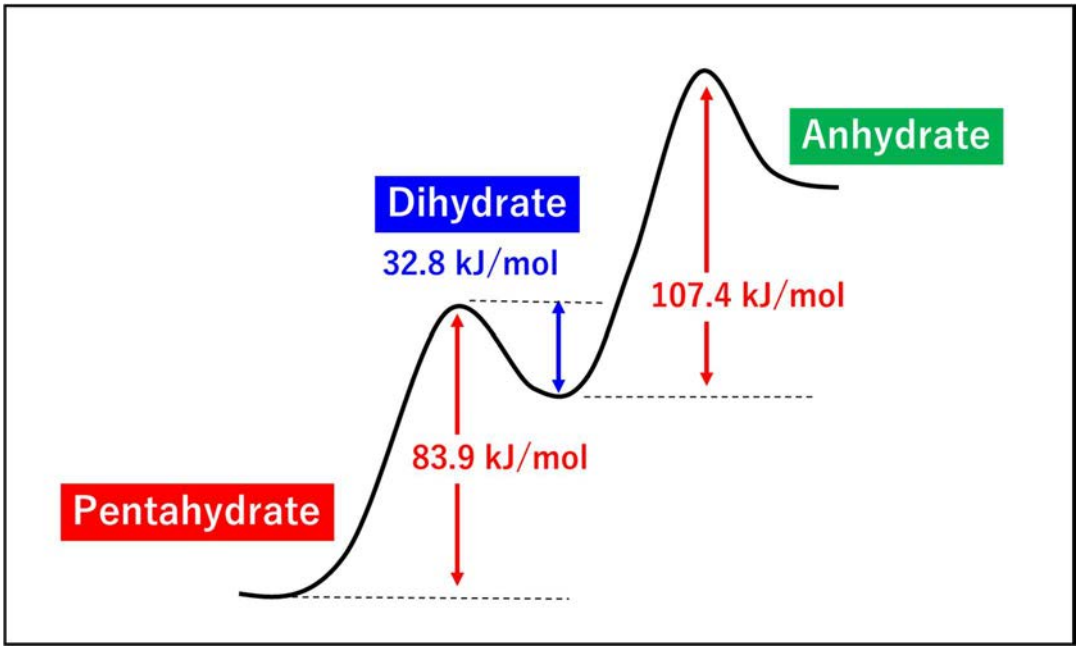

Figure 3-26 Schematic potential diagram of SPE along the path of transformation. Red and blue arrows indicate dehydration E_a and rehydration E_a, respectively.

Table 3-6 Dehydration E_a and rehydration E_a of SPE and MEPM.

Hydrate sample	Hydrate type	Dehydration		Rehydration	
		Model	E_a (kJ/mol)	Model	E_a (kJ/mol)
SPE	Penta	A2	83.9	-	-
	Di	A2	107.4	F0	32.8
MEPM	Tri	R2	126.5	A2	18.5

As far as MEPM, the rehydration E_a, 18.5 kJ/mol, was approximately one-seventh of dehydration E_a, 126.5 kJ/mol, and the energy required for rehydration was less than that required for dehydration. This means that the hydrate form can exist more stable state than anhydrate form under ambient temperature and humidity.

As far as SPE, schematic potential diagram consisted of two steps. The rehydration E_a from dihydrate to pentahydrate, 32.8 kJ/mol, was around one-third of dehydration E_a, 83.9 kJ/mol. The rehydration E_a from anhydrate to dihydrate could not be obtained because anhydrate directly transformed into pentahydrate without proceeding through dihydrate in the rehydration process. Besides, the dehydration E_a of the second step, 107.4 kJ/mol, is higher than the first one, 83.9 kJ/mol. It is very likely that the second step requires more energy to collapse completely followed to form amorphous phase. Note that the ratio of E_a of the first step dehydration to the second step dehydration was the same for both the noniso-thermal and the iso-thermal methods. The dehydrated E_a in the noniso-thermal method was 69.0 kJ/mol in the first step and 90.0 kJ/mol in the second step, and the ratio was 1.3. In the iso-thermal method, the dehydrated E_a was 83.9 kJ/mol in the first step and 107.4 kJ/mol in the second step, and the ratio was 1.3. So, the ratio of both were 1.3 and the same.

From the above, it seems reasonable to conclude that potential profiles give the propensities of dehydration and rehydration from energy point of view.

3.3.5. Classification of Hydrates

A classification rule of hydrates has not been reported because of the lack of specific comparison parameters. This problem may be overcome by using dehydration and rehydration activation energies and rehydration propensity. The classification of pharmaceutical hydrates was shown in **Figure 3-27**.

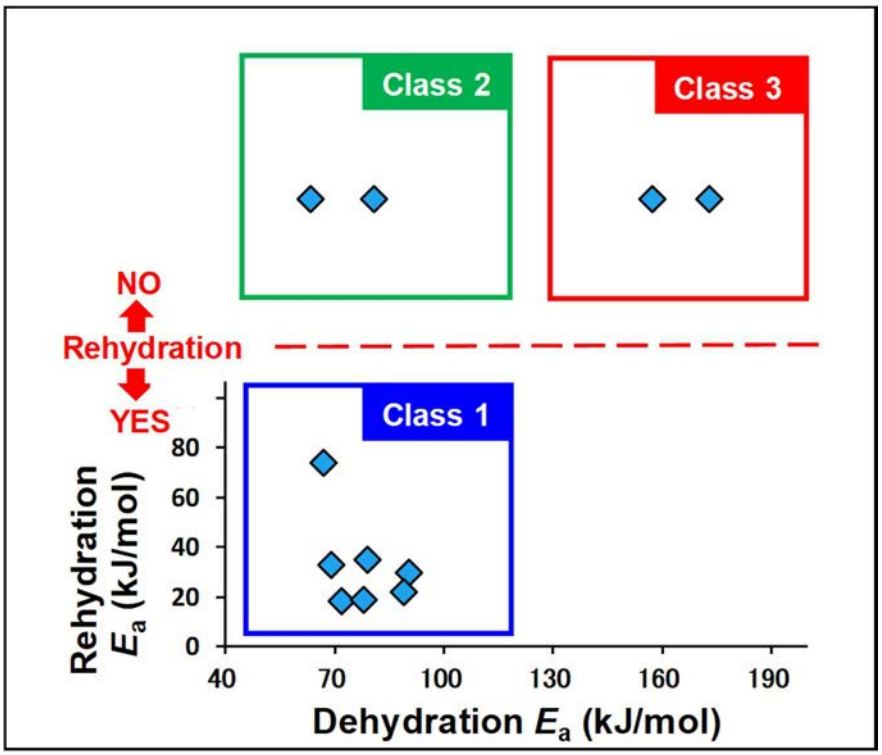

Figure 3-27 Classification of pharmaceutical hydrates used in this study. Diamonds indicate the relation between dehydration E_a, rehydration E_a and rehydration propensity on each hydrate. Rehydration "YES" and "NO" indicate reverting to its hydrate form or not, respectively. Squares indicate the energetic areas of Class 1 (blue), Class 2 (green), and Class 3 (red).

Eleven pharmaceutical hydrates used in this study were classified into three classes by mapping dehydration E_a of **Table 3-2**, rehydration E_a of **Table 3-5** and rehydration propensities obtained in section 3.3.1. For this classification, dehydration E_a obtained in transforming from dihydrate to anhydrate for SPE and rehydration E_a obtained in transforming from anhydrate to trihydrate for ENO sesquihydrate were used. SPE, MEPM, PIPC, ACR, PIPM, ENO trihydrate, ENO sesquihydrate were categorized in Class 1, which had low dehydration Ea, 67 - 91 kJ/mol, and they reasily rehydrated to revert to its hydrate form when the relative humidity of the environment was increased. AMO and CEF were categorized in Class 2, which also had low dehydration Ea, 64 - 81 kJ/mol. Still, they did not revert to its original hydrate due to the destruction of its crystal structure in the dehydration process following to form the amorphous phase. TAZ and NF were categorized in Class 3, which had high dehydration Ea, 157 - 173 kJ/mol, and did

not revert to its original hydrate in order to recrystallize into a new anhydrous form.

The values of dehydration E_a of TAZ and NF were twice as high as those of SPE, MEPM, PIPC, ACR, PIPM, ENO trihydrate, ENO sesquihydrate, AMO and CEF, indicating that Class 3 had higher dehydration E_a compared to Class 1 or Class2. The results showed that the hydrates categorized in class 1 and class 2 exhibited easier dehydration. The threshold for dehydration E_a between Class 1/Classs2 and Class 3 was estimated to be approximately 120-130 kJ/mol with a range of 3 kJ/mol, the mean RSD, on the median calculated from 90.6, the highest value of dehydration E_a in class 1, and 157.3, the lowest value of dehydration E_a in class 3. The distinguishing between Class 1 and Class 2 is also necessary in determining whether to revert to the original hydrate, which allows us to predict rehydration propensity.

As for hydrates of Class 1, since information about the ease of rehydration has been obtained in advance, a wet granulation method, in which water is added, is a candidate formulation procedure to avoid transformation into an anhydrate. As for hydrates of Class 2, the possibility of amorphization with the removal of water molecules becomes apparent in advance, which makes us aware of the need to optimize drying conditions in order to prevent the transition to an amorphous form that is less chemically stable than the crystal form. As for hydrates of Class 3, as we know that they are less likely to dehydrate in advance, the utmost attention to drying condition is not required. The classification of hydrates may provide crucial information about whether the hydrate readily dehydrates and whether the anhydrate reverts to the original hydrate without difficulty.

From the above results, eleven kinds of hydrates were classified into three classes. Class1 was a small dehydrated E_a and rehydrated group, Class2 was a small dehydrated E_a but not rehydrated group, and Class3 was a very large dehydrated E_a and not rehydrated group.

3.4. Concluding Remarks

Thermal analysis, moisture absorption equilibrium, and X-ray powder diffraction methods were used to observe dehydration and rehydration behaviors of eleven pharmaceutical hydrates, and three types of transition behaviors were revealed.

In addition, the dehydration E_a using the non-isothermal method were classified into two groups based on thresholds of 120 to 130 kJ/mol.

The E_a of rehydration was also calculated by kinetic analysis of the weight change rate of the hydration process.

From the above results, eleven kinds of hydrates were classified into three classes, Class1 was a group in which dehydration E_a was small and rehydrated, Class2 was a group in which dehydration E_a was small but not rehydrated, and Class3 was a group in which dehydration E_a was very large and not rehydrated.

Furthermore, potential profiles consisted of the iso-thermal E_a of dehydration and rehydration gave the propensities of taking in or taking out of water molecules in hydrate crystals from an energetic perspective.

4. Correlation between Crystal Structure and Classification

4.1. Introduction

Water can be incorporated into the crystal structure in some ways. Historically, the hydrate crystals have been classified into three types by their structures, isolated site hydrate, channel hydrates, and ion associated hydrates.[58-60] They are primarily classified by the type of bonding of water molecules in the crystal structure. Crystal structures of three types of hydrate were shown in **Figure 4-1**.[61] Crystallographic considerations by single crystal X-ray structure analysis are considered to be useful for visually understanding the incorporation of water molecules in crystals.

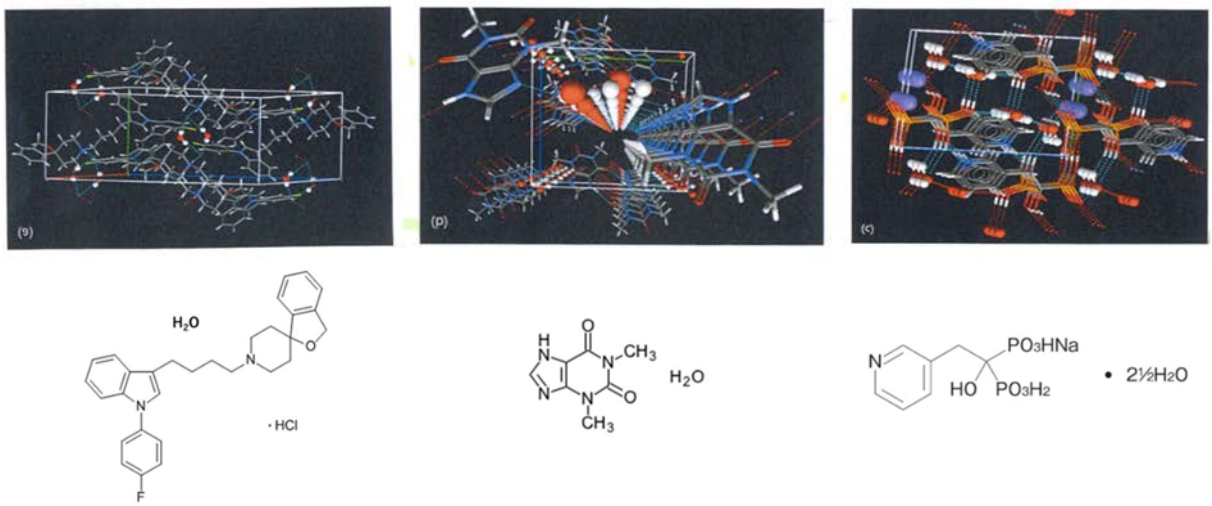

Figure 4-1 Crystal structures and chemical structures of three types of hydrate. Isolated site hydrate: siramesine hydrochloride (left), channel hydrate: theophylline monohydrate (middle), ion associated hydrate: risedronate sodium dihydrate (right).[61]

Besides, these classifications are predominantly based on analytical techniques by thermal analysis. Differential scanning calorimetry (DSC) and thermogravimetric analysis thermograms (TGA) for an example of three hydrates were shown in **Figure 4-2** - **Figure 4-4**. The isolated site hydrate shows sharp DSC endotherm, narrow TGA weight loss, and relatively high dehydration

temperature (**Figure 4-2**). The channel hydrate shows early onset of dehydration, rather wide TGA weight loss, broad DSC endotherm and dehydration temperature is usually lower than that of isolated site hydrate (**Figure 4-3**). The ion associated hydrate contains ion coordinated water and it typically shows high dehydration temperature (**Figure 4-4**).[58] Herein, the DSC thermogram shows a large broad endotherm and a smaller endotherm through two dehydration steps, which are associated with loss of eight moles and two moles of water. As the heating continues, a sharper endotherm is seen at high temperature region, which corresponds to four moles of water directly associated with calcium ion.

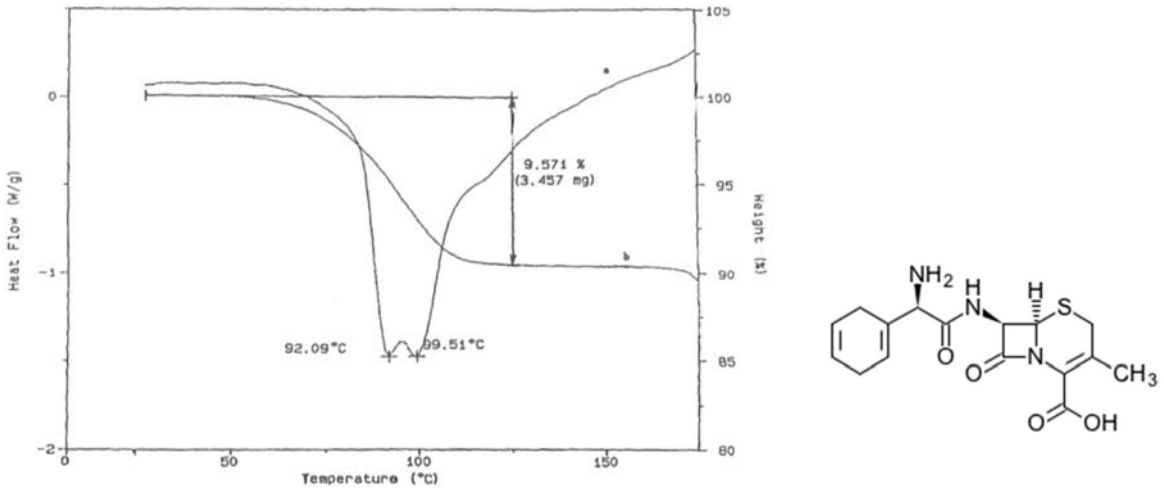

Figure 4-2 DSC and TGA for cephradine dihydrate (isolated site hydrate) and chemical structure of cephradine.[58]

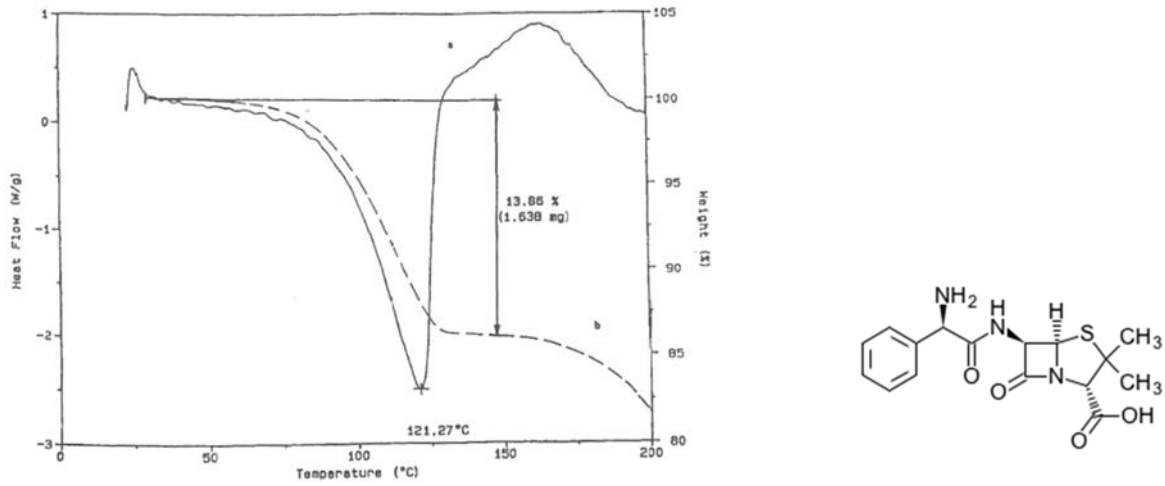

Figure 4-3 DSC and TGA for ampicillin trihydrate (channel hydrate) and chemical structure of ampicillin.[58]

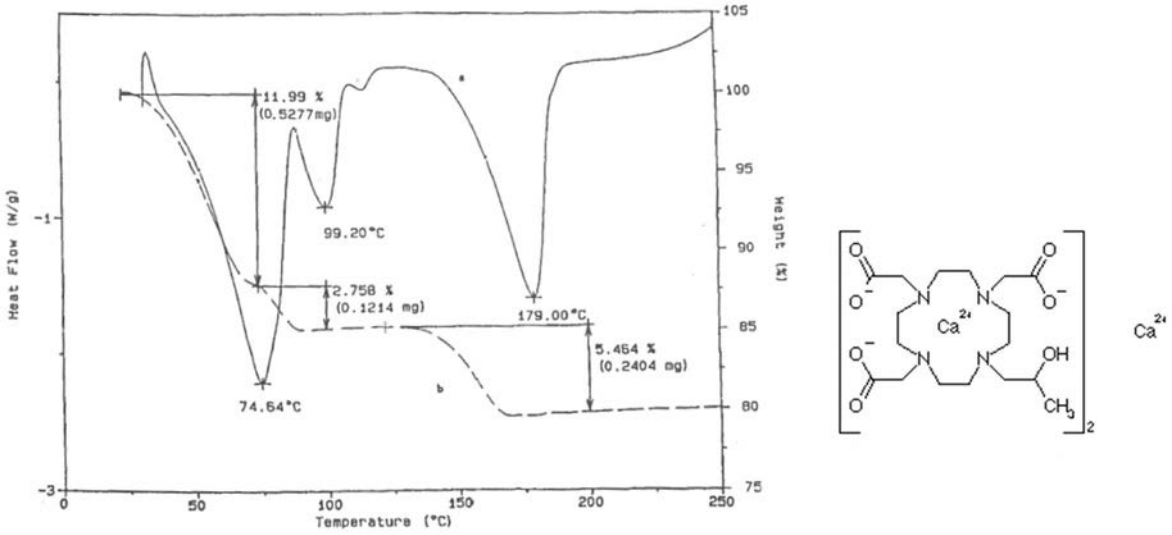

Figure 4-4 DSC and TGA for calteridol calcium tetradecahydrate (ion associated hydrate) and chemical structure of calteridol calcium.[58]

The physical treatment on drug substances in the formulation process makes effects on dehydration of medicine. The relationship between the physical manipulation like tabletting and the dehydration temperature of pharmaceutical hydrate is also not an exception. There was a relation between compression stress and dehydration temperature of the compressed cephalexin monohydrate. The dehydration temperature decreased with increasing compression stress.[62]

In the past, dehydration temperatures have been used favorably in both drug substances handling hydrate crystals alone and in the tableting process of formulation as described above. The easiness of the crystal water to escape form crystal lattice has been conventionally estimated by the dehydration temperature.

The aim of this study was to investigate the relation of classified hydrates with their crystal structure characteristics, especially for water packing in crystal. The crystal structures of spectinomycin dihydrochloride petahydrate, cefminox heptahydrate, and tazobactam hemihydrate were analyzed by single X-ray diffraction method. Among them, the crystal structure of tazobactam hemihydrate is reported first time. Furthermore, by comparing dehydration temperature and dehydration E_a of various hydrate crystals, we examine which of them gave the

useful knowledge on the dehydration easiness in the pharmaceutical production site.

4.2. Experimental

4.2.1. Material

Spectinomycin dihydrochloride (SPE) pentahydrate, meropenem (MEPM) trihydrate, piperacillin (PIPC) hydrate, acrinol (ACR) monohydrate, pipemidic acid (PIPM) trihydrate, enoxacin (ENO) trihydrate, enoxacin (ENO) sesquihydrate, amoxicillin (AMO) trihydrate cefminox sodium (CEF) heptahydrate, tazobactam (TAZ) anhydrate and nitrofurantoin (NF) monohydrate were used. Herein, NF monohydrate and ENO trihydrate which were obtained in section 3.2.2 were used in this study.

Other solvents and chemicals were acetone of guaranteed grade and concentrated hydrochloric acid.

4.2.2. Preparation of Single Crystal Hydrates

Single crystals of TAZ hemihydrate were obtained by dissolving TAZ anhydrate powder in water and adjusting pH of the aqueous solution 1.7 adding 17% w/w hydrochloric acid solution prepared by diluting concentrated hydrochloric acid with water, followed by cooling in the refrigerator (2-8°C).

Single crystals of CEF heptahydrate were obtained by dissolving CEF heptahydrate powder in water, followed by cooling in the refrigerator (2-8°C).

Single crystals of SPE pentahydrate were obtained by dissolving SPE pentahydrate powder in acetone-water solution (volume ratio 1:1), followed by evaporating at room temperature.

4.2.3. Fourier Transform - Infrared spectroscopy analysis (FT-IR)

FT-IR spectra of SPE pentahydrate, dihydrate and anhydrate were measured at ambient temperature using IRAffinity-1S with GladiATR 10 (Shimdzu) via attenuated total reflection method at 4 cm^{-1} resolution. Herein, dihydrate and anhydrate were obtained by heating pentahydrate to remove three molecules and five molecules of water, respectively.

4.2.4. Single Crystal X-Ray Diffraction (SC-XRD)

Single crystal X-ray diffraction data of using single crystals of SPE pentahydrate, CEF heptahydrate and TAZ hemihydrate were collected in ω-scan

mode using an R-AXIS RAPID Imaging plate camera (Rigaku) with Mo Kα radiation (λ = 0.71075 Å) obtained from a rotating anode source with a graphite monochromator while spraying liquid nitrogen. The integrated and scaled data were empirically corrected for absorption effects using ABSCOR.31. The initial structures were solved by using direct methods with SHELXT and refined with SHELXL. All the non-hydrogen atoms were refined anisotropically. All hydrogen atoms were found in the difference Fourier map; however, they were placed by geometrical calculations and treated using a riding model during the refinement.

4.3. Results and Discussion

4.3.1. Single Crystal X-Ray Diffraction Analysis

In order to address if there was any correlation between crystal structures, dehydration E_a and rehydration propensities, SPE pentahydrate, CEF heptahydrate and TAZ hemihydrate were selected as representative hydrates for Class 1, Class 2 and Class3, respectively. The crystal data of these hydrates were analyzed based on the single crystal X-ray diffraction data obtained in this study (**Table 4-1**). These crystal structures have not been reported in any international journals or in Cambridge Structural Database, which contains more than one million structures obtained from X-ray and neutron diffraction analyses. Furthermore, that of TAZ hemihydrate has not been clarified so far.

Table 4-1 Crystal data of SPE pentahydrate, CEF heptahydrate and TAZ hemihydrate obtained in this study, and that of TAZ anhydrate collected from literature.[63]

	SPE	CEF	TAZ	
Molecular formula	$C_{14}H_{24}N_2O_7$-2HCl-5H_2O	$C_{16}H_{20}N_7O_7S_3Na$-7H_2O	$C_{10}H_{12}N_4O_5S$-0.5H_2O	$C_{10}H_{12}N_4O_5S$-0H_2O
Crystal system	Orthorhombic	Triclinic	Monoclinic	Orthorhombic
Space groupe	$P2_12_12_1$	P_1	$P2_1$	$P2_12_12_1$
a (Å)	8.0604(4)	8.4579(3)	9.9008(5)	10.230(2)
b (Å)	14.7852(7)	8.6984(4)	12.2025(6)	14.396(2)
c (Å)	18.3307(10)	10.3862(4)	12.0204(5)	17.291(2)
α (deg)	90	75.5471(12)	90	90
β (deg)	90	75.0894(10)	111.4777(14)	90
γ (deg)	90	74.5575(12)	90	90
V (Å^3)	2184.56(19)	698.15(5)	1351.41(11)	2546.5
Z	4	1	2	8
R-factor (%)	3.67	4.94	4.55	3.3

For the other hydrates, the parameters for the crystal structure were collected from the literature.[63-72] Crystal structures of MEPM trihydrate, PIPC monohydrate, ACR monohydrate, PIPM trihydrate, ENO trihydrate, ENO sesquihydrate, AMO trihydrate and NF monohydrate were confirmed from good agreements between

powder X-ray diffractions obtained in this study and simulation patterns of single crystal X-ray diffractions obtained from literatures[64-71] (**Figure 4-5 and Figure 4-6**).

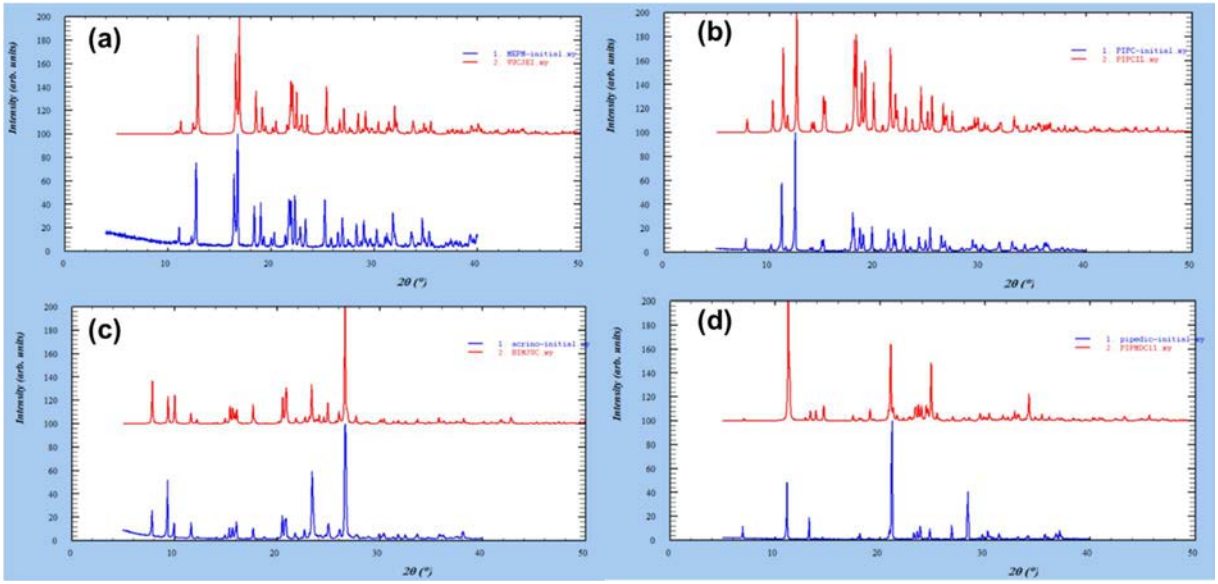

Figure 4-5 Experimental powder X-ray diffraction pattern (blue) and simulation pattern of single crystal X-ray diffraction (red). (a); MEPM trihydrate, (b); PIPC monohydrate, (c); ACR monohydrate, (d); PIPM trihydrate.

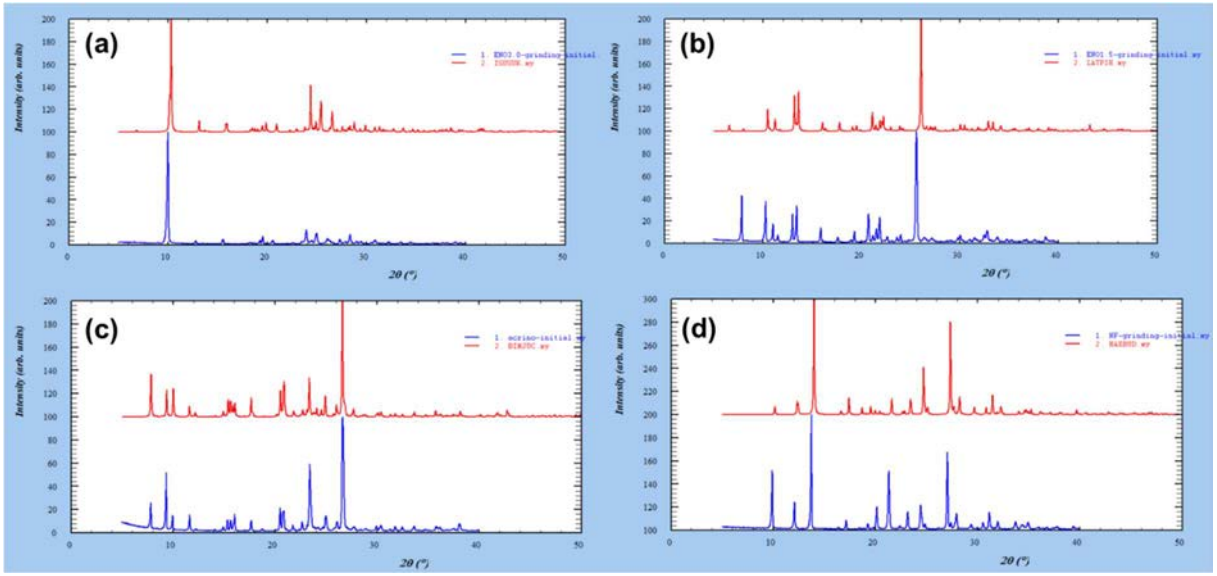

Figure 4-6 Experimental powder X-ray diffraction pattern (blue) and simulation pattern of single crystal X-ray diffraction (red). (a); ENO

trihydrate, (b); ENO sesquihydrate, (c); AMO trihydrate, (d); NF monohydrate.

Regarding NF monohydrate, it has two hydrate forms, I and II,[71] and the hydrate sample obtained in this study was clarified to be form II.

Regarding Class 1, the crystal structure of SPE pentahydrate was shown in **Figure 4-7** and hydrogen bonds and weak interactions were tabulated in **Table 4-2**. Hydrogen atoms were omitted for clarity, one of the water molecules in SPE pentahydrate existed as a ketone hydrate. The oxygen atom in the water molecule and ketone hydrate were shown as a red ball-and-stick model. There were hydrogen bonds between three water molecules; O9-H2…O12 with a distance (D…A) of 3.038 Å and O11-H18…O12 with a distance of 2.696 Å. The other water molecules and two chloride ions showed weak O…Cl interactions; O10-H15…Cl1 with a distance of 3.237 Å, O4-H13…Cl1 with a distance of 3.152 Å and O6-H6A…Cl2 with a distance of 3.138 Å.

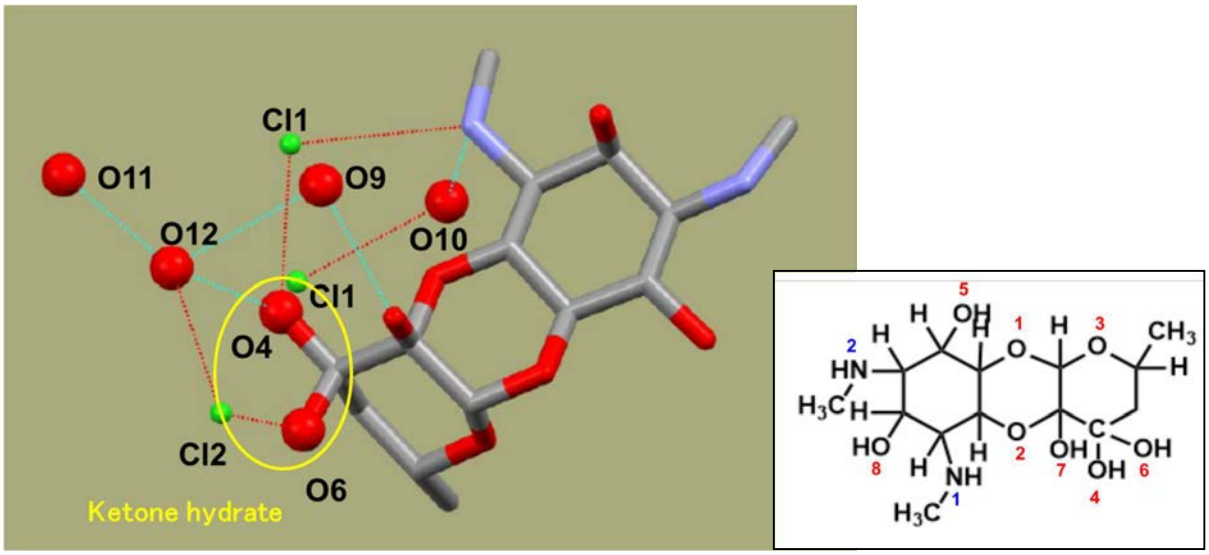

Figure 4-7 Crystal structure of SPE pentahydrate, hydrogens bond (blue dashed lines), weak interaction (red dashed line). Hydrogen atoms are omitted for clarity. Oxygen in the water molecule is shown as a red ball-and-stick model, O4 or O6 is a water molecule existed as a ketone hydrate.

Table 4-2 Bonds and weak interactions in the crystal structure of SPE pentahydrate.

D-H...A	D...A (Å)	D-H...A	D...A (Å)
Bonding interacted to water molecule		Bonding between host molecules	
O9-H2...O12	3.038	N2-H20...O3	2.933
O11-H18...O12	2.696		
O4-H13...Cl1	3.152	Bonding between host molecule and chloride ion	
O6-H6A...Cl2	3.138		
O10-H15...Cl1	3.237	N1-H30...Cl1	3.224
O9-H3...Cl1	3.157	O5-H17...Cl2	3.032
O7-H7A...O9	2.652		
O8-H8A...O11	2.705		
O11-H16...O7	2.877		
O12-H12D...Cl2	3.201		
O12-H4...O4	2.791		
N1-H30...O10	3.053		

The positions of hydrogen atoms were introduced at calculated positions, and the packing motif of SPE pentahydrate was shown in **Figure 4-8**. The water molecules and chloride ions space accessible to a probing sphere of radius 1.2 Å and a grid size of 0.5 Å was indicated in blue. Water molecules and chloride ions were laid along a-axis in the channel of the host framework. It can be inferred that only empty channels remained in the crystal by the loss of water molecules by dehydration. The existence of channel structures could play an important role in reverting to an original hydrate by rehydration.

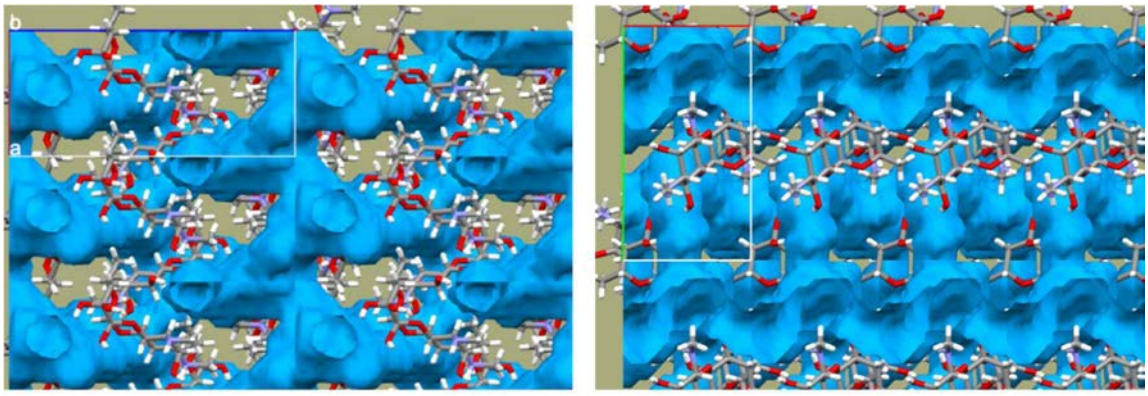

Figure 4-8 Packing motif of SPE pentahydrate. Blue spheres indicate channel which consists of water molecules and chloride ions.

In MEPM trihydrate, PIPC monohydrate, ACR monohydrate, PIPM trihydrate, ENO trihydrate and ENO sesquihydrate which were categorized in Class 1, water molecules acted as fillers in channel of hydrate structure. They could be removed from hydrate structure easily. MEPM trihydrate, PIPC monohydrate, ACR monohydrate, PIPM trihydrate had channels along the c-axis, ENO trihydrate had channels along the b-axis and ENO sesquihydrate had channels along the a-axis in each crystal structure.

In order to identify the remaining water molecules removed by the first dehydration step of SPE pentahydrate, its dihydrate crystal structure was tried solving. However, the structure of dihydrate has not been solved yet, since single crystal of dihydrate suitable for crystal analysis was not obtained. It was only found that one of two water molecules involved dihydrate form existed as a ketone hydrate, because carbonyl band at 1736 cm^{-1} was absent in dihydrate from FT-IR spectra (**Figure 4-9**).

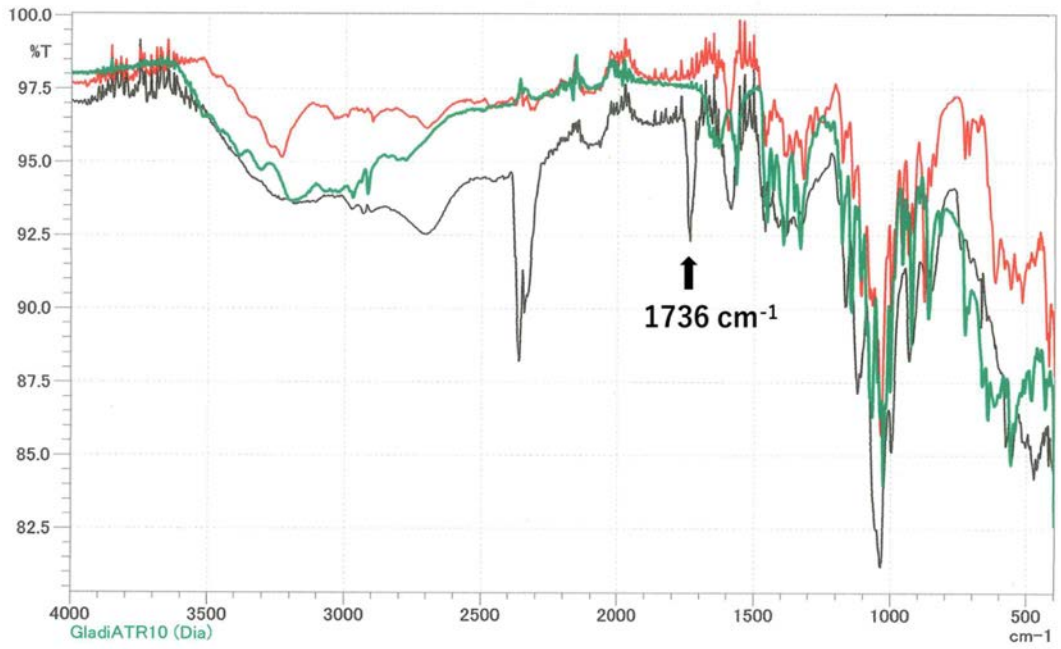

Figure 4-9 FT-IR spectra of SPE pentahydrate (green), dihydrate (red) and anhydrate (black).

From the above results, water molecules of hydrates in Class 1 were considered to form channel structures, and the crystal structure is hardly considered to be changed even if the channel water was removed.

Regarding Class 2, the crystal structure of the CEF heptahydrate was shown in **Figure 4-10** and hydrogen bonds were tabulated in **Table 4-3**. A sodium ion forms a 6-coordinated octahedral structure by coordinating four water molecules (O8, O9, O10 and O14), a carbonyl (O1) of lactam ring and a nitrogen of a tetrazole ring. Host molecules were connected along the a-axis via sodium ions. There were hydrogen bonds between three water molecules; O8-H8…O12 with a distance (D…A) of 2.689 Å and O12-H7…O13 with a distance of 2.777 Å. The other water molecule interacts with a carbonyl (O4) of cephalosporin skeleton; O11-H11D…O4 with a distance of 2.772 Å.

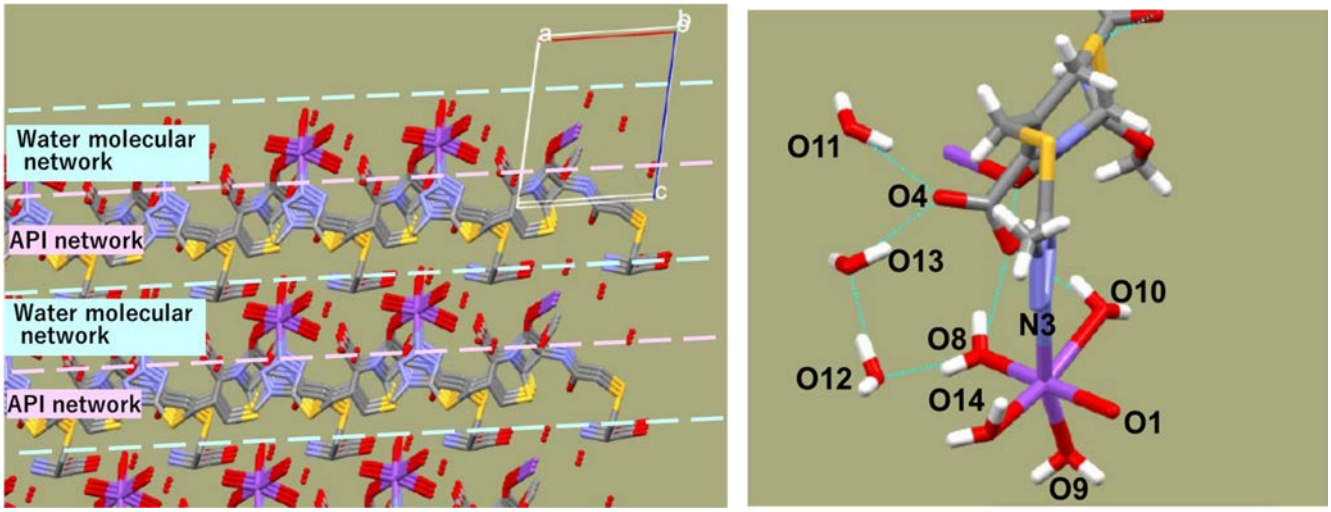

Figure 4-10 Crystal structure of CEF heptahydrate.

Table 4-3 Hydrogen bonds in the crystal structure of CEF heptahydrate.

D-H...A	D...A (Å)
Hydrogen bonding between water and water molecules	
O12-H7...O13	2.777
O8-H8...O12	2.689
Hydrogen bonding between water and host molecule	
O13-H4...O4	2.745
O11-H11D...O4	2.772

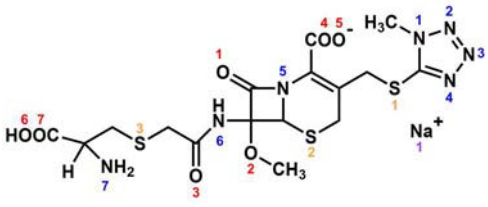

A packing motif of CEF pentahydrate was shown in **Figure 4-11**. The water molecules space accessible to a probing sphere of radius 1.2 Å and a grid size of 0.5 Å was indicated in blue. Water molecules and host molecules formed a two-dimensional network on the ab-plane, respectively, and they were alternately stacked along the c-axis. Here, the aggregate region of water molecules formed part of the crystal structure. Interlayer hydrogen bonding between host molecules and water molecules played a critical role in their structural stability and formation. The host molecule itself could not form a three-dimensional network without water molecules. Consequently, the pentahydrate form was collapsed completely upon water removal. It resulted in forming an amorphous which had no ability to revert to its initial hydrate form.

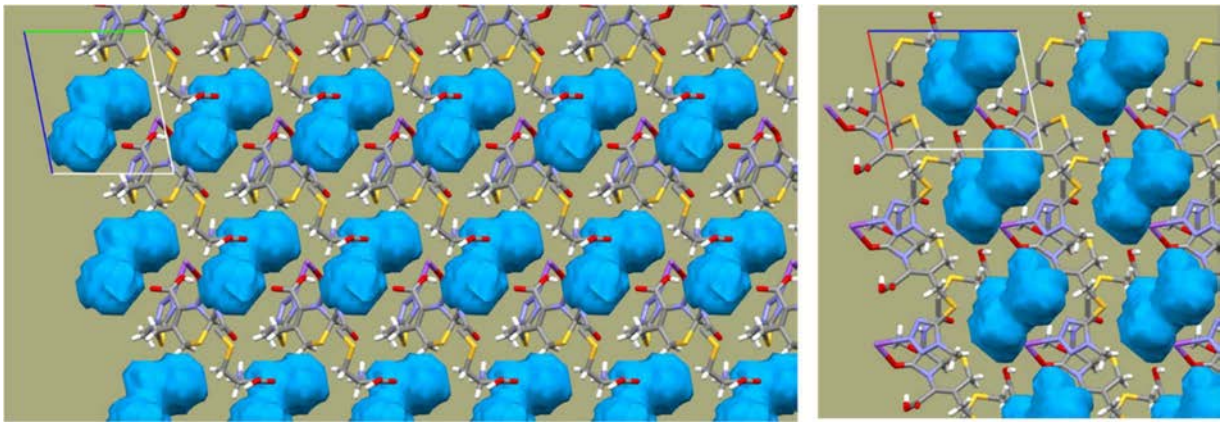

Figure 4-11 Packing motif of CEF heptahydrate. Blue spheres indicate water molecules. Two-dimensional network stacks along c-axis.

AMO trihydrate which was also categorized in Class 2 had layer-like water packing, which was formed by expanding along the ac-plane in the unit cell. The host molecules gathered around the water molecules and formed a layered structure. As a result, the aggregate region of water molecules in the ac-plane was extended. Since AMO trihydrate also had the aggregate region of water molecules formed part of the crystal structure, removing water molecules caused the destruction of the crystal lattice. From the above results, water molecules of hydrates in Class 2 were considered to form a layer-like structure.

Volume parameters and porosities of representative hydrates of each class were summarized in **Table 4-4**. Volume parameters were calculated using the Mercury 4.00 program – radius 1.2 Å, grid 0.5 Å, and the void volume and porosity of SPE were calculated based on three water molecules; O9, O11 and O12 of **Figure 4-7**. A porosity indicates the ratio of void volume to cell volume when water molecules

are excluded from the crystal structure. The porosity of CEF heptahydrate was estimated to be 11.7%, which was larger than those of SPE pentahydrate, 5.2%, and TAZ hemihydrate, 1.4%. In the case of CEF heptahydrate, the removal of water molecules from the crystal lattice was considered to have provided the driving force for their converting to an amorphous solid, since its porosity was large enough to cause the structural destruction.

Table 4-4 Volume parameters and porosities of hydrate samples. The void volume and porosity of SPE was calculated on the basis three water molecules; O9, O11 and O12 of Figure 4-7.

Hydrate sample	Void volume ($Å^3$)	Cell volume ($Å^3$)	Porosity (%)
SPE	113.11	2184.56	5.2
CEF	81.81	698.15	11.7
TAZ	19.46	1351.41	1.4

Regarding Class 3, the crystal structures of TAZ hemihydrate and anhydrate were shown in **Figure 4-12** and hydrogen bonds were tabulated in **Table 4-5**. A nitrogen of triazole ring and a hydrogen of carboxylic acid were connected via hydrogen bond in both hemihydrate and anhydrate crystal lattice. A Water molecule of hemihydrate was hydrogen bonded to three host molecules through, triazole, carboxylic acid and sulfonyl group, with a distance (D…A) of 2.770 Å, 2.594 Å and 2.735 Å, respectively, without contacting with other water molecules in its crystal lattice.

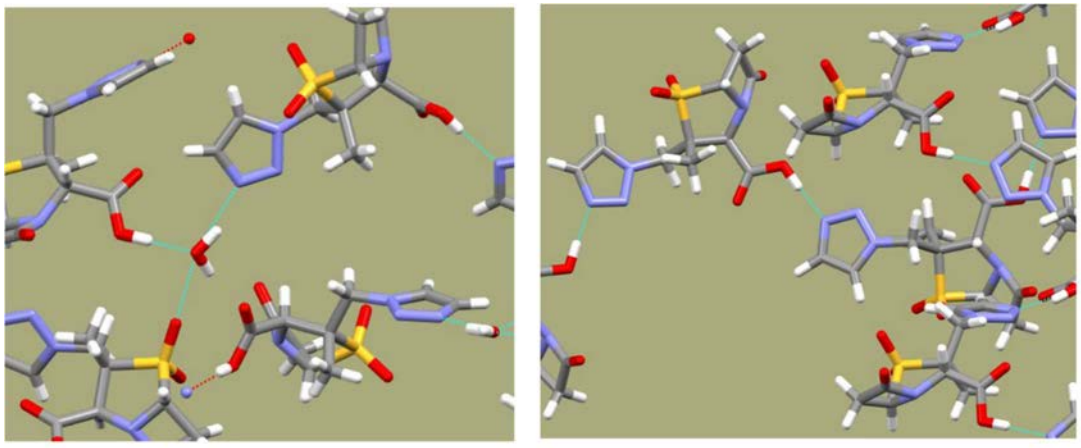

Figure 4-12 Crystal structure of TAZ hemihydrate (left side) and anhydrate (right side).

Table 4-5 Hydrogen bonds in the crystal structure of TAZ hemihydrate and anhydrate.

Sample D-H...A	TAZ hemihydrate D...A (Å)	TAZ anhydrate[63] D...A (Å)
Hydrogen bonding between water and host molecule		
O47-H4...O38	2.735	
O47-H3...N7	2.770	
O26-H6...O47	2.594	
Hydrogen bonding between host molecules		
O5-H5...N55	2.588	2.666

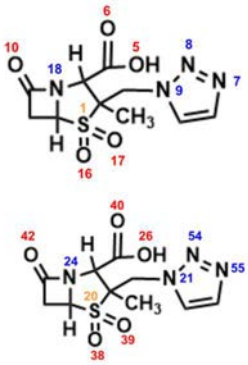

A packing motif of TAZ hemihydrate and anhydrate were shown in **Figure 4-13**, that of anhydrate was calculated using previously reported crystal data.[11] The water molecules space accessible to a probing sphere of radius 1.2 Å and a grid size of 0.5 Å was indicated in blue. Water molecules were isolated and kept from contact with other water molecules in the TAZ hemihydrate crystal structure. This hydrate presented dehydration associated with larger structural changes in the crystal lattice in order to arrange into new anhydrous form. As a result, no packing features of the hydrate seemed to be transferred to the anhydrous form upon dehydration.

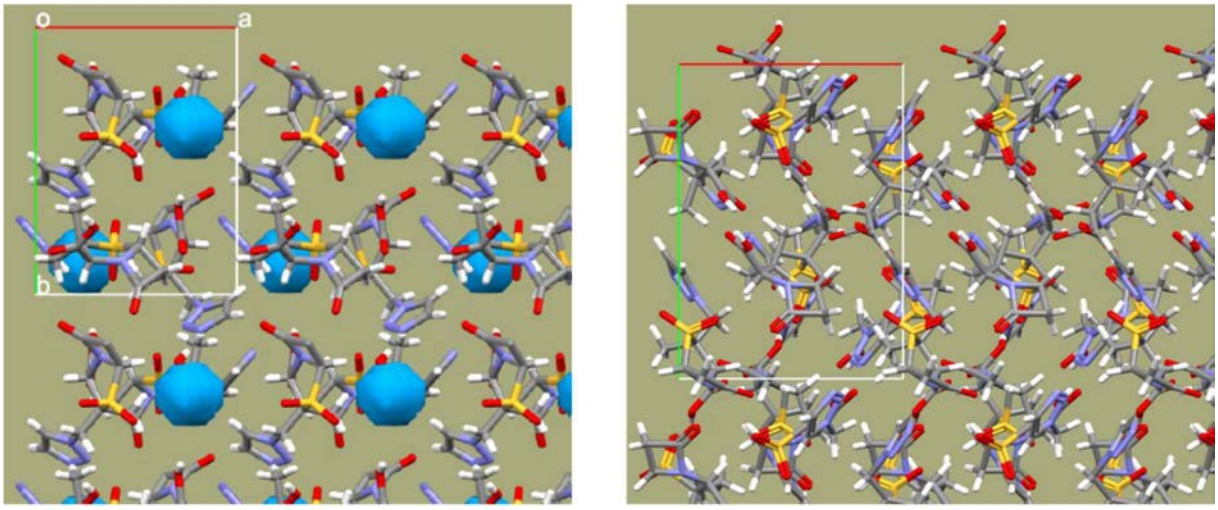

Figure 4-13 . Packing motif of TAZ hemihydrate (left side) and anhydrate (right side). Blue spheres indicate water molecules.

The dehydration of NF monohydrate which was categorized in Class 3 was also accompanied by a significant structural change and its water molecules resided in isolated lattice site by calculation using of previously reported crystal data.[71,72] The water molecules of hydrates of Class 3 were considered to form isolated structures. They are not reverted to initial hydrate form, because the dehydration can result in conversion to a crystalline form with different structures, which means the lattice structure is completely altered. Since transformation from hydrates of this class requires energy both to remove water molecules and to rearrange into a new crystal form, they are considered to need much higher dehydration E_a than hydrates of Class 1 and Class 2.

The above results indicate that the water molecule accommodation in the host structure was different in each class. Specifically, water molecules were arranged one-dimensionally in the crystal structure as channel hydrates in Class 1, two-dimensionally as layer hydrates in Class 2, without contact to each other as isolated sites hydrates in Class 3. Furthermore, the dehydration-rehydration cycling study and rehydration kinetic analysis indicate that rehydration propensities such as reverting to its original hydrate form are specified in each class. Therefore, dehydration E_a and rehydration propensities are closely related to the packing of water molecules in the crystal lattice, and it can be said that there is a correlation between structures and activation energy. Thus, the hydrates of the respective Class had a characteristic crystal structure, and the thermodynamic classification and the classification by the crystal structure were combined successfully.

4.3.2. Comparing Dehydration E_a with Dehydration Temperature

The dehydration E_a (average value) and dehydration temperature which was estimated from endothermic peak temperature at 10K/min were summarized in **Table 4-6**. The relationship of dehydration E_a to dehydration temperature was shown in **Figure 4-14**. The dehydration E_a and the dehydration temperature for each class were shown in **Figure 4-15**.

Table 4-6 The average value of dehydration E_a and dehydration temperature estimated from endothermic peak of DSC at 10°C/min. Hydration number indicates number of water molecules per formula unit. Two values of SPE indicate the result by monitoring the dehydration process from pentahydrate to dihydrate a) and from dihydrate to anhydrate b).

Class	Hydrate sample	Hydration number	Dehydration E_a (kJ/mol)	Dehydration temp. (K)
1	SPE	5	69.0[a], 90.0[b]	361[a], 403[b]
	MEPM	3	71.8	362
	PIPC	1	77.9	393
	ACR	1	79.2	387
	PIPM	3	90.6	364
	ENO	3	66.8	330
	ENO	1.5	89.0	400
2	AMO	3	63.5	354
	CEF	5	80.8	361
3	TAZ	0.5	157.3	393
	NF	1	173.1	398

In the hydrates assigned to the three classes, there were no significant differences in dehydration temperatures between the classes; from 330 K to 400 K in Class 1, from 354 K to 361 K in Class 2 and from 393 K to 398 K in Class 3. The dehydration temperature that have traditionally been important as a measure of the ease of dehydration was in the range of 330 to 400K, and there was no correlation with the dehydration E_a according to **Figure 4-14**. On the other hand, if these results were shown for each class, there was a distinctive difference in dehydration E_a according to **Figure 4-15**. The dehydration E_a of Class 1 were 66.8 kJ/mol to 90.6 kJ/mol, those of Class 2 were 63.5 kJ/mol to 80.8 kJ/mol and those of Class 3 were 157.3 kJ/mol to 173.1 kJ/mol. Class 3 hydrates had higher E_a in comparison to Class 1/Class 2, and difficult to dehydrate crystals were clearly differentiated.

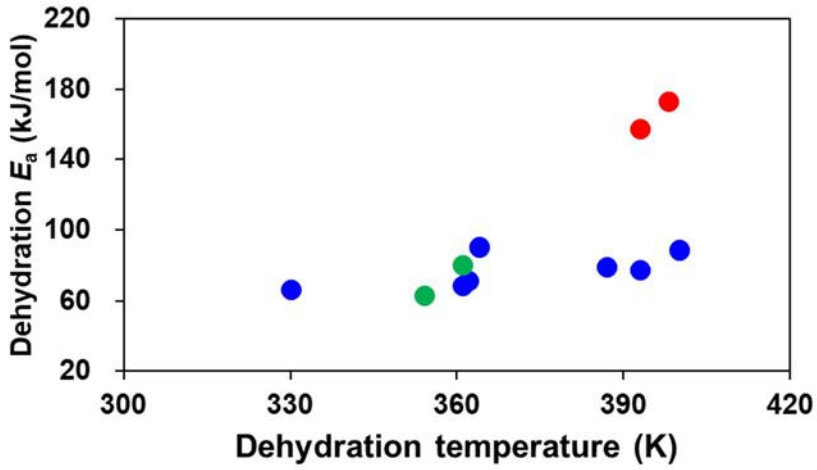

Figure 4-14 The relationship of dehydration E_a to dehydration temperature, Class 1 (blue), Class 2 (green), Class 3 (red).

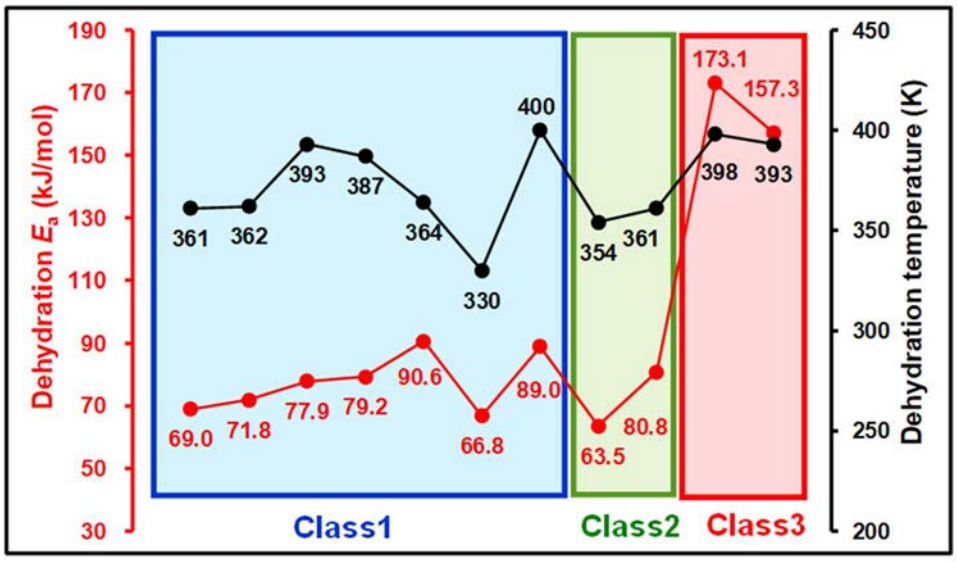

Figure 4-15 The dehydration E_a (red circle) and the dehydration temperature (black circle) estimated from endothermic peak of DSC at 10°C/min for each Class. Square indicates the area of Class 1 (blue), Class 2 (green), and Class 3 (red). The values of SPE indicate the result by monitoring the dehydration process from pentahydrate to dihydrate.

Hence, the relation between dehydration E_a versus hydrate "Class" brought the interesting insight that E_a could be a quantitative comparison parameter to

evaluate the strength of the intermolecular interactions between water molecules and the host molecules in the crystal lattice. In addition, it is notable that E_a was not affected by either number of water molecules per formula unit (hydration number) or complicated dehydration processes originated from a great diversity in the strength of intermolecular interaction.

Heretofore, although the tendency of dehydration has been classified mainly by the dehydration temperature, it is not dehydration temperature but dehydration E_a can quantitatively differentiate dehydration propensities in pharmaceutical hydrates from the results of this study.

In the isothermal method, E_a cannot be estimated unless the rate constant is obtained, but in the non-isothermal method, E_a can be directly obtained without performing rate constant calculation. Therefore, in order to consider what the noniso-thermal E_a suggests, the dehydration rate constants were compared between hydrates which have the same dehydration temperature. MEPM as Class 1 hydrate and CEF as Class 2 hydrate were selected, and dehydration rate constants at 323K and the noniso-thermal E_a of both hydrates were shown in **Table 4-7**. The dehydration rate constant of CEF, 0.0150 min^{-1}, with dehydration E_a of 80.8kJ/mol was 1.6 times that of MEPM, 0.0095 min^{-1}, with dehydration E_a of 71.8kJ/mol.

Table 4-7 Dehydration rate constants and noniso-thermal E_a of MEPM and CEF.

Class	Hydrate	Dehydration temperature (K)	Dehydrationrate constant at 323K (min^{-1})	Noniso-thermal E_a (kJ/mol)
1	MEPM	362K	0.0095	71.8
2	CEF	361K	0.0150	80.8

PIPC as Class 1 hydrate and TAZ as Class 3 hydrate were selected, and the dehydration rate constants and the non-isothermal E_a at 373K of both hydrates were shown in **Table 4-8**. The dehydration rate constant of PIPC, 0.1592 min^{-1}, with dehydration E_a of 77.9kJ/mol was 12 times that of TAZ, 0.0132 min^{-1}, with dehydration E_a of 157.3kJ/mol.

Table 4-8 Dehydration rate constants and noniso-thermal E_a of PIPC and TAZ.

Class	Hydrate	Dehydration temperature (K)	Dehydrationrate constant at 373K (min^{-1})	Noniso-thermal E_a (kJ/mol)
1	PIPC	393K	0.1592	77.9
3	TAZ	393K	0.0132	157.3

These results indicate that the dehydration rate of hydrates that have almost the same E_a was almost the same, and the dehydration rate of hydrates that have a low E_a was fast, confirming that the noniso-thermal E_a correlates with the dehydration rate constant. In other words, the smaller noniso-thermal E_a of the hydrate has the faster dehydration rate at the same temperature. From a practical point of view, it means that attention must be paid not only to the dehydration temperature but also to the dehydration rate of the hydrate that has a low dehydration E_a.

Thus, knowledge of the rate which was not obtained from the dehydration temperature could be obtained from the dehydration E_a. From the above, it was very likely that the noniso-thermal E_a indirectly indicated the dehydration rate, even though the calculation process of the rate constant was not performed.

4.4. Concluding Remarks

Single crystal X-ray structure analysis was carried out for one compound from each Class. Furthermore, the packing motif of water molecules of all hydrate crystals were confirmed from the crystal structure data. As a result, the water molecules in the crystals form one-dimensionally like channels in the Class1, form a two-dimensional networks like layers in the Class2, and exist in isolation without contact to another water molecule in the Class3. From this, it was considered that Class1 and Class2 can be easily dehydrated through the area of aggregation of water molecules, so that less E_a is required, and Class3 requires more E_a because the crystal structures are greatly changed in dehydration. From the above, the hydrate of the Class has a characteristic crystal structure, and the thermodynamic classification and the classification by the crystal structure were combined successfully.

Heretofore, the tendency of dehydration has been classified by the dehydration temperature. Therefore, the dehydration temperature and dehydration E_a of each hydrate crystal were compared. As a result, there is a variability in dehydration temperature from compound to compound in any of the crystals and there was no correlation with the dehydration energy. On the other hand, E_a greatly differentiated from Class1/Class2 to Class3 and crystals difficult to dehydrate were clearly differentiated.

Comparison of the dehydration rate constant between hydrates which have the same dehydration temperature confirmed that the noniso-thermal E_a correlated with the dehydration rate constant. Therefore, it points that the noniso-thermal E_a indirectly suggested the dehydration rate without calculation process of the rate constant.

5. Conclusion

One-third of drug substances have been developed as hydrates, but it is essential to investigate the thermal behavior of hydrate crystals in the developing and manufacturing process to ensure the stability of the drug substance and drug product. Indeed, in the manufacturing of drug substance, formulation, and marketing processes, there is the possibility of dehydration and rehydration as a result of environmental changes. In order to prevent such risks, it is crucial to quantitatively evaluate the tendency of dehydration and rehydration. In the past, the easiness of dehydration has been identified mainly by the dehydration temperature, but there is no method for quantitatively classifying the easiness of dehydration and rehydration of various hydrate crystals by the same standard. Therefore, this study focuses on dehydration and rehydration activation energy (E_a), which can realize quantitative evaluation, as the specific comparison parameters of classification rule, and aims to examine the correlation between the classification of hydrate crystals, which is categorized by E_a, and their crystal structures.

In the first of this study, the application of the noniso-thermal method to calculate E_a from the endothermic peak temperature of DSC was examined as the iso-thermal method which is conventionally used in the past. Noniso-thermal method utilizes a model-independent relationship in which the logarithm of the ratio between the heating rate and the square of the peak temperature is proportional to the reciprocal of the temperature. Comparison of E_a obtained from this measurement with the value obtained by the conventional iso-thermal method revealed that there was a certain correlation between both. Furthermore, in the iso-thermal method, there were many approximations in the process of obtaining E_a, and it can be inferred that the E_a variation became large. The noniso-thermal method in which the E_a variation was reduced by the minimum approximation should be used for comparison of E_a among various hydrate crystals. As an influencing factor used for the thermal measurement, the possibility that the particle diameter of the sample crystal influences E_a has been pointed out in the past. Therefore, agglomerated samples, samples of various particle size, samples obtained by changing the grinding method and samples which had different dehydration history were prepared. When E_a measurements for their samples were

performed by the noniso-thermal method, agglomeration in the range of 75 - 212 μm and sample size in the range of 10 - 100 μm did not affect E_a, but E_a depended on only dehydration history. Therefore, intact samples should be used for the classification of hydrates. From the above, it was clarified that E_a using a non-isothermal method should be used instead of the conventional method in order to uniformly evaluate a plurality of hydrate crystals with different dehydration mechanisms.

In the second of this study, thermal analysis, moisture absorption equilibrium, and X-ray powder diffraction methods were used to observe dehydration and rehydration behaviors of eleven pharmaceutical hydrates, and three types of transition behaviors were revealed. In addition, the dehydration E_a using the non-isothermal method were classified into two groups based on thresholds of 120 to 130 kJ/mol. The rehydration E_a was also calculated by kinetic analysis of the weight change rate of the hydration reaction process. From the above results, eleven kinds of hydrates were classified into three Classes, and Class1 was a group in which dehydration E_a was small and rehydrated, Class2 was a group in which dehydration E_a was small but not rehydrated, and Class3 was a group in which dehydration E_a was very large and not rehydrated. Furthermore, potential profiles consisted of the iso-thermal E_a of dehydration and rehydration gave the propensities of taking in or taking out of water molecules in hydrate crystals from an energetic perspective.

In the third of this study, single crystal X-ray structure analysis was carried out for one compound from each Class. Furthermore, the packing motif of water molecules of all hydrate crystals were confirmed from the crystal structure data. As a result, the water molecules in the crystals form one-dimensionally like channels in the Class1, form a two-dimensional networks like layers in the Class2, and exist in isolation without contact to another water molecule in the Class3. As seen from the results, it can be inferred that Class1 and Class2 can be easily dehydrated through the area of aggregation of water molecules, so that less E_a is required, and Class3 requires more E_a because the crystal structures are greatly changed in dehydration. From the above, the hydrate of the Class has a characteristic crystal structure, and the thermodynamic classification and the classification by the crystal structure were combined successfully. Heretofore, the tendency of dehydration has been classified by the dehydration temperature.

Therefore, the dehydration temperature and dehydration E_a of each hydrate crystal were compared. As a result, there is a variability in dehydration temperature from compound to compound in any of the crystals and there was no correlation between the dehydration temperature and the dehydration E_a. On the other hand, E_a greatly differentiated from Class1/Class2 to Class3, and hydrate crystals difficult to dehydrate were clearly differentiate by E_a. Furthermore, the noniso-thermal E_a correlated with the dehydration rate constant by comparing the dehydration rate constant between hydrates which have the same dehydration temperature. It was very likely that the noniso-thermal E_a indirectly indicated the dehydration rate, even though the calculation process of the rate constant was not performed.

In summary, E_a obtained by the non-isothermal method showed smaller variation than that obtained by the conventional isothermal method. Moreover, the peak top temperature used in the non-isothermal method was a value unique to each hydrate obtained under constant conditions, and E_a could be directly calculated by applying them to the Kissinger equation. For these reasons, it was suggested that the non-isothermal method is more suitable for comparing dehydration E_a between hydrates. By establishing an activation energy evaluation system by the noniso-thermal method for pharmaceutical hydrated crystals, it was possible to quantitatively evaluate dehydration for various kinds of crystals, and it was possible to classify hydrate crystals into three groups. Furthermore, from the correlation with the crystal structure, the classification of hydrates and the packing of the characteristic water in the crystal were combined and interpreted successfully. We have not found any other examples of this approach applied for the classification of pharmaceutical hydrates. We convince that activation energy offers a useful measure to specify a variety of dehydration states and provides suitable information in selecting proper form of the drug substance which shows thermodynamically stable solid. Also, by obtaining such prior information about dehydration ease in a manufacturing process, this may be helpful to supply pharmaceutical products of high quality and stability to the medical field.

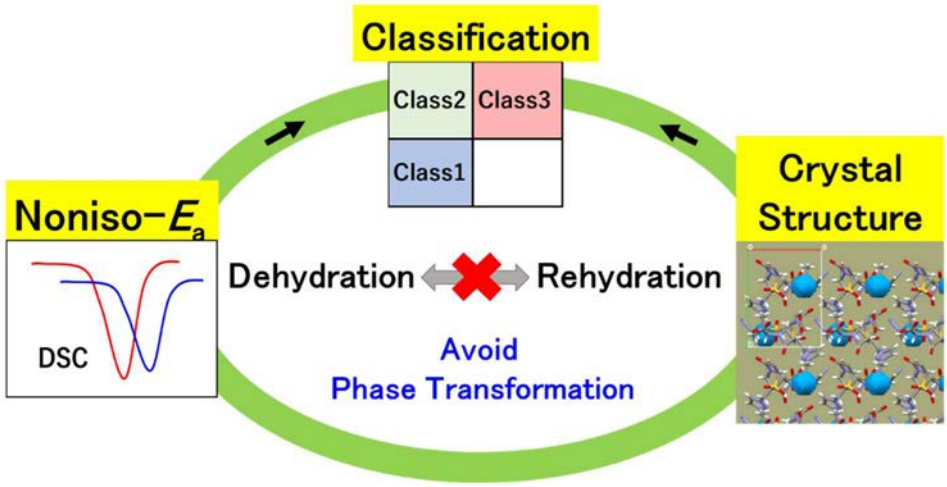

Figure 5-1 Schematic diagram of summary

By adding crystallographic considerations on the incorporation of water molecules in the crystal structure to the quantitative evaluation of activation energy, we discovered a new classification of pharmaceutical hydrates (**Figure 5-1**). This study proposes a new method to evaluate the dehydration and rehydration process of hydrates, and the knowledge useful for avoiding the risk of phase transformation that may occur in the manufacturing and distribution processes of pharmaceutical products was obtained.

6. Reference

1. J. Han, R. Suryanarayanan. Influence of environmental condition on the kinetics and mechanism of dehydration of carbamazepine dihydrate. *Pharmaceutical development and technology.* 1998;3;587-596
2. M. Falk, O. Knop. Water in stoichiometric hydrates. *In:F. Franks ed. Water*. 1973;55-113
3. G. P. Stahly. Diversity in single- and multiple-component crystal. The search for and prevalence of polymorphs and cocrystals. *Cryst. Growth Des.* 2007;7;1007-1026.
4. R. K. Khankari, D. J. W. Grant. Pharmaceutical hydrates. *Thermochim Acta.* 1995;248;61-79
5. B. G. Pereira, F. D. Fonte-Boa, J. A. L. C. Resende, C. B. Pinheiro, N. G. Fernandes, M. I. Yoshida, C. D. Vianna-Soares. Pseudopolymorphs and intrinsic dissolution of nevirapine. *Cryst. Growth Des.* 2007;7;2016-2023
6. Y. Kobayashi, S. Ito, S. Itai, K. Yamamoto. Physicochemical properties and bioavailability of carbamazepine polymorphs and dihydrate. *Int. J. Pharm.* 2000;193;137-146
7. H. Nakgawa, T. Miyata, I. Sugimoto. The effect of water of crystallization of berberine chloride on disintegration and dissolution behaviors of the tablet. *YAKUGAKU ZASSHI*. 1978;98;1305-1310
8. S. Miyazaki, M. Nakano, T. Arita. Effect of crystal forms on the dissolution behavior and bioavailability of tetracycline, chlortetracycline, and oxytetracycline bases. *J. Pharm. Sci*. 1975;23;552-558
9. J. W. Poole, C. K. Bahal. Dissolution behavior and solubility of anhydraous and trihydrate forms of ampicillin. *J. Pharm. Sci*. 1968;57;1945-1948
10. A. A. Ali, A. Farouk. Comparative studies on the bioavailability of ampicillin anhydrate and trihydrate. *Int. J. Pharm.* 1981;9;239-243
11. R. F. Falk, T. W. Randolph. Process variacble implications for residual solvent removal and polymer morphology in the formation of gentamycin-loaded poly (L-lactide) microparticles. *Pharm. Res.* 1998;15;1233-1237

12. V. R. Kallakunta, H. Patil, R. Tiwari, X. Ye, S. Upadhye, R. S. Vladyka, S. Sarabu, D. W. Kim, S. Bandari, M. A. Repka. Exploratory studies in heat-assisted continuous twin-screw dry granulation: A novel alternative technique to conventional dry granulation. *Int. J. Pharm.* 2019;555;380-393

13. J. P. Reddy, J. W. Jones, Patrick S. Wray, Andrew B. Dennis, Jonathan B, Peter T. Monitoring of multiple solvent induced form changes during high shear wet granulation and drying processes using online Raman spectroscopy. *Int. J. Pharm.* 2018;541;253-260

14. M. K. Yeboah, Z. Rahman, D. Shah, A. Mohammad, S. Wu, A.Siddiqui, M. A. Khan. Impact of formulation and process variables on solid-state stability of theophylline in controlled release formulations. *Int. J. Pharm.* 2016;499;20-28

15. T. Niskanen, T. Jouko, M. Niskanen. Validation of the drying process in a production scale tray drier. *Boll. Chim. Farmaceutico*. 1995;134;629-633

16. S. H. M. Gibson, R. C. Rowe, E. F. T. White. The mechanical peoperties of pigmented tablet coating formulations and their resistance to cracking II. Dynamic mechanical measurement. *Int. J. Pharm*. 1989;50;163-173

17. K. Cheng. Determining crystallization kinetics parameters of Li2O-Al2O3-SiO2 glass from derivative differential thermal analysis curves. *Materials Science and Engineering*. 1999;B60;194-199

18. M. Avrami. Kinetics of phase change. II Transformation-time relations for randome distribution of muclei. *J. Chem. Phys.* 1940;8;212-224

19. H.E. Kissinger. Reaction kinetics in differential thermal analysis. *Anal. Chem*. 1957;29;1702-1706

20. J. Sheng, G. M. Venkatesh, S. P. Duddu, D. J. W. Grant. Dehydration behavior of eprosartan mesylate dihydrate. *J. Pharm. Sci.* 1999;88;1021-1029

21. A. J. Aguiar, J. KRC, A. W. Kinkel, H. C. Samyn. Effect of polymorphism on the absorption of chloramphenicol from chloramphenicol palmitate. J. *Pharm. Sci.* 1967;56;847-853

22. R. M. Atkinson, C. Bedford, K. J. Child, E. G. Tomich. Effect of particle size on blood griseofulvin-level in man. *Nature*. 1962;10;588-589

23 B. Olsson, P. Backman. Mouth-throath models for realistic in vitro testing:A proposal for debate. *Respiratory Drug Delivery*. 2014;1;287-293

24. C. I. Grainger, M. Saunders, F. Buttin, R. Telford, I. L. Merolla, G. P. Martin, S. A. Jones, B. Foebes. Critical characteristic for corticosteroid solution metered dose inhaler bioequivalence. *Mol. Pharmaceutics.* 2012;9;563-569

25. X. J. H. Pepin, T. R. Flanagan, D. J. Holt, A. Eidelman, D. Treacy, C. E. Rowlings. Justification of drug product dissolution rate and drug substance particle size specifications based on absorption PBPK modeling for lesinurad immediate release tablets. *Mol. Pharmaceutics.* 2016;13;3256-3269

26. J. G Weers, D. P. Miller. Formulation design of dry powders for inhalation. *J. Pharm. Sci*. 2015;104;3259-3288

27. C. O. Agbada, P. York. Dehydration of theophylline monohydrate powder-effects of particle size and sample weight. *Int. J. Pharm.* 1994;106;33-40

28. A. Joseph, C. E. S. Bernardes, A. S. Viana, M. F. M. Piedade, M. E. M. da Piedade. Kinetics and mechanism of the thermal dehydration of a robust and yet metasrable hemihydrate of 4-hydroxynicoyinic acid. *Cryst. Growth Des.* 2015;15;3511-3524.

29. A. Berzins, A. Actins. Dehydration of mildronate dihydrate: a study of structural reansformations and kinetics. *CrystEngComm*. 2014;16;3926-393

30. M. Otsuka, N. Kaneniwa. Effect of grinding on the degree of crystallinity of cephalexin powder. *Chem. Pharm. Bull*. 1983;31;4489-4495

31. Z. Qiu, J. G. Stowell, W. Cao, K. R. Morris, S. R. Byrn, M. T. Carvajal. Effect of illing and compression on the solid-state maillard reaction. *J. Pharm. Sci.* 2005;94;2568-25808

32. H. Steckel, N. Rasenack, B. W. Muller. In-situ-micronization of disodium cromoglycate for pulmonary delivery. European *Journal of Pharmaceutics and Biopharamceutics.* 2003;55;173-180

33. K. Knenari, T. Ozawa. Thermal conductivity of the filler-containing epoxy resin. *Netsu Bussei* 1989;3;106-111

34. D. M. Bigg. Mechanical, thermal, and electrical properties of metal firber-filled polymaer composites. *Polym. Eng. Sci*. 1979;19;1188-1192

35. Y. Agari, A. Ueda, S. Nagai. Thermal conductivity of a polymer composite. *J. Appl. Polymer. Sci*. 1993;49;1625-1634

36. H. Fricke. A mathematical treatment of the electric conductivity and capacity of disperse systems. *Phys. Rev*. 1924;24;575-587

37. A. Tanaka, H. Kitaura, K. Nishikawa, N. Nishiki. High thermal conductivity composit material with graphite. *Journal of network polymer, Japan.* 2014;35;65-68

38. N. Vlachos, I. T. H. Chang. Graphical and statistical comparison of various size distribution measurement systems using metal powders of a range of sizes and shapes. *Powder metallurgy.* 2011;54;497-506

39. N. N. Dufour, L. Bougeard, M. F. Devaux, D. Bertrand, F.L. D. D. Monredon. Comparison of sieving and laser diffraction for the particle size measurement of raw materials used in foodstuff. *Powder Technol.* 1993;76;191-200

40. C. Andres, P. Rrginault, M. H. Rochat, B. Chailot, Y. Pourcelot. Paticle-size distribution of a powder: comparison of three analytical techniques. *Int. J. Pharm.* 1996;144;141-146

41. J. D. Hancock, J. H. Sharp. Method of comparing solid-state kinetic data and its application to the decomposition of kaolinite, brucite, and BaCO3. *J. Amer. Ceram. Soc.* 1972;55;74-77

42. K. Ammar, D. R. Flanagan. Basics and applications of solid-state kinetics: A pharmaceutical perspective. *J. Pharm. Sci.* 2006;95;472-498

43. E. Shefter, H. Fung, O. Mok. Dehydration of crystalline theophylline monohydrate and ampicillin trihydrate. *J. Pharm. Sci.* 1973;62;791-794

44. J. Gong, D. Zhang, Y. Ran, K. Zhang, S. Du. Solvates and polymorphs of clindamycin phosphate: structural, thermal stability and moisture stability studies. *Font. Chem. Sci. Eng.* 2017;11;220-230

45. X. Zhang, Q. Yin, W. Du, J. Gong, Y. Bao, M. Zhang, B. Hou, H. Hao. Phase transformation between anhydrate and monohydrate of sodium dehydroacetate. *Industrial and Engineering Chemistry Research.* 2015;54;3438-3444

46. B. R. Jali, J. B. Baruah. Polymorphs and solvates of 2-(1,4-dihydro-1,4-dioxonaphthalen-3-ylthio)benzoic acid. *Cryst. Growth Des.* 2012;12;3114-3122

47. A. Zimermann, B. Frostrup, A. D. Bond. Polymorphs of pridopidine hydrochloride. *Cryst. Growth Des.* 2012;12;2961-2968

48. A. Shevchenko, D. D. Belle, S. Tiittanen, A. Karjalainen, A. Tolvanen, V. P. Tanninen, J. Haarala, M. Makela, J. Yliruusi, I. Miroshnyk. Coupling polymorphism/solvatomorphism and physical stability evaluation with early salt synthesis optimization of an investigational drug. *Organic Process Research and Development*. 2011;14;666-672

49. V. Koradia, H. L. de Diego, M. R. Elema, J. Rantanen. Integrated approach to study the dehydration kinetics of nitrofurantoin monohydrate. *J. Pharm. Sci.* 2010;99;3966-3976

50. L. Malaj, R. Censi, P. D. Martino. Mechanisms for dehydration of three sodium naproxen hydrates. *Cryst. Growth Des.* 2009;9;2128-2136

51. P. Chakravarty, R. T. Berendt, E. J. Munson, V. G. Young, R. Govindarajan, R. Suryanarayanan. Insight into the dehydration behavior of thiamine hydrochloride (vitamin B1) hydrates:Part II. *J. Pharm. Sci.* 2010;99;1882-1895

52. D. E. Braun, T. Gelbrich, V. Kahlenberg, R. Tessadri, J. Wieser, U. J. Griesser. Stability of solvates and packing systematics of nine crystal forms of the antipsychotic drug aripiprazole. *Cryst. Growth Des.* 2009;9;1054-1065

53. D. E. Braun, T. Gelbrich, R. K. R. Jetti, V. Kahlenberg, S. L. Price, U. J. Griesser. Colored polymorphs: Themochemical and structural features of N-Picryl-p-toluidine polymorphs and solvates. *Cryst. Growth Des.* 2008;8;1977-1989

54. F. Kang, F. G. Vogt, J. Brum, R. Forcino, R. C. B. Copley, G. Williams, R. Carlton. Effect of particle size and morphology on the dehydration mechanism of a non-stoichiometric hydrate. *Cryst. Growth Des.* 2012;12;60-74

55. F. G. Vogt, J. Brum, L. M. Katrincic, A. Flach, J. M. Socha, R. M. Goodman, R. C. Haltiwanger. Physical crystallographic and spectroscopic characterization of a crystalline pharmaceutical hydrate: Understanding the role of water. *Cryst. Growth Des.* 2006;6;2333-2354

56. A. Zimmermann, F. Tian, H. L. de Diego, K. Frydenvang, J. Rantanen, M. R. Elema, L. Hovgaard. Structural characterization and dehydration behavior of siramesine hydrochloride. *J. Pharm. Sci.* 2009;98;3596-3607

57. E. A. Schmitt, D. Law, G. G. Z. Zhang. Nucleation and crystallization kinetics of hydrate amorphous lactose above the glass transition temperature. *J. Pharm. Sci.* 1999;88;291-296

58. K. R. Morris. Structural aspects of hydrates and solvates. *In:Harry G. Brittain ed. Polymorphism in Phamaceutical Solids.* 1999;125-181

59. K. R. Morris, N. R. Hornedo. Hydrates. *In: James S, James C. Boylan eds. Encyclopaedia of Phamaceutical Technology.* 1993;393-440

60. W. L. Gossman, S. R. Wilson, E. Oldfield. Three hydrates of the bisphosphonate risedronate, consisting of one molecular and two ionic structures. *Acta Crystallogr., Sect C:Cryst.Struct.Commun.* 2003;C59;m33-m36

61. F. Tian, H. Qu, A. Zimmermann, T. Munk, A. C. Jorgensen, J. Rantanen. Factors affecting crystallization of hydrates. *Journal of Pharmacy and Pharmacology*. 2010;62;1534-1546

62. N. Kaneniwa, K. Imagawa, M. Otsuka. Effect of tableting on the degree of crystallinity and on the dehydration and decomposition points of cephalexin crystalline powder. *Chem. Pharm. Bull.* 1985;33;802-809

63. C. A. Toomer, C. H. Schwalbe, N. S. Ringan, P. A. Lambert, P. R. Lowe, V. J Lee. Structural studies on tazobactam. *J. Med. Chem.* 1991;34;1944-1947

64. K. Yanagi, Y. Takeuchi, M. Sunagawa. Structure of a novel carbapenem antibiotic, meropenem. *Acta Cryst.* 1992;C48;1737-1739

65. F. M. Lovell, N. A. Perkinson. [2S-[2α,5α,6β(S)]]-6[[[[(4-ethyl-2,3-dioxo-1-piperazinyl)carbonyl]amino]phenylacetyl]amino]-3,3-dimethyl-7-oxo-4-thia-1-azabicyclo[3.2.0]heptane-2-carboxylic acid, hydrate, $C_{23}H_{27}N_5O_7S$ H_2O. *Cryst. Struct. Comm.* 1978;7;7-14

66. S. Neidle, A. Aggarwal. Nuclei acid binding drugs. VI. The structure of 3,9-diamino-7-rthoxyacridine (Rivanol) as the lactate monohydrate salt. *Acta. Cryst.* 1982;B38;2420-2424

67. I. Fonseca, S. M. Carrera, S. G. Blanco. Structure of pipemidic acid. *Acta Cryst.* 1986;C42;1618-1621

68. P. Masood, A. Saeed, S. Najima, Z. S. Ahsan. Enoxacin trihydrate. *Acta Crystallogr., Sect C:Cryst.Struct.Commun.* 2004;C60;o281-o283

69. J. J. Holstein, C. B. Hubschle, D. Birger. Electrostatic properties of nine fluoroquinoline antibiotics derived directly from their crystal structure refinements. *CrystEngComm.* 2012;14;2520-2531

70. M. O. Boles, R. J. Girven, P. A. C. Gane. The structure of amoxycillin t rihydrate and a comparison with the structures of ampicillin. *Acta Cryst* 1978;B34;461-466

71. E. W. Pienaar, M. R. Caira, A. P. Lotter. Polymorphs of nitrofurantoin. I. Preparation and X-ray crystal structures of two monohydrated forms of nitrofurantoin. *J. Crystallogr. Spectrosc. Res.* 1993;23;739-744

72. E. W. Pienaar, M. R. Caira, A. P. Lotter. Polymorphs of nitrofurantoin. 2. Preparation and X-ray crystal structures of two anhydrous forms of nitrofurantoin. *J. Crystallogr. Spectrosc. Res.* 1993;23;785-790